NOAA TECHNICAL MEMORANDUM NWS CR-96

DEPARTMENT OF COMMERCE · UNITED STATES OF AMERICA

A CASE STUDY EVALUATION OF SATELLITE-DERIVED RAINFALL ESTIMATES AND THEIR APPLICATION TO NUMERICAL MODEL PRECIPITATION FORECAST VERIFICATION

Glenn A. Field
National Weather Service Forecast Office
Milwaukee, Wisconsin

MAY 1989

U.S. DEPARTMENT OF COMMERCE / National Oceanic and Atmospheric Administration / National Weather Service

Table of Contents

A CASE STUDY EVALUATION OF SATELLITE-DERIVED RAINFALL ESTIMATES AND THEIR APPLICATION TO NUMERICAL MODEL PRECIPITATION FORECAST VERIFICATION[1]

Glenn A. Field
National Weather Service Forecast Office
Milwaukee, Wisconsin

ABSTRACT. Satellite-derived precipitation estimates are computed and then evaluated using a dense network of cooperative observer rain gauge reports as the verification. The feasibility of using these satellite rainfall estimates to evaluate numerical model precipitation forecasts is investigated. The correspondence between the numerical model forecast and the observations also is assessed.

The satellite rainfall estimates are produced every half hour for the 24-hour period starting 1200 GMT, July 20, 1981. They are computed using the operational Scofield-Oliver Convective Rainfall Estimation Technique on the University of Wisconsin's Man-Computer Interactive Data Access System (McIDAS) (Suomi et al., 1983). A severe weather outbreak occurred over parts of the southern Midwest during this period and significant rainfall amounts were observed. More than 300 cooperative observer rain gauge observations made during the same time period as the estimates are compiled. The McIDAS analysis procedure provides estimate values assigned to grid points spaced 22 km apart. The rainfall observations, however, are at irregularly located positions. In order to be able to objectively evaluate the estimates, the observations are interpolated to the same grid points as the estimates using a minimum of smoothing. Difference fields then are evaluated.

The numerical model evaluated is an Australian mesoscale model referred to as the Subsynoptic Scale Model (SSM). Its 24-hour precipitation forecast is examined for the same time period as the satellite estimates and ground-based observations. The horizontal resolution (134 km) and map projection of the SSM are much different than for the estimates and observations. A regridding and interpolation scheme is employed, which allows the SSM model to be objectively evaluated on a common grid with the estimates and observations.

The results show that the satellite estimates compare very favorably with the observations, especially with regard to

---

1 This is a reprint of Mr. Fields' Master Thesis from the University of Wisconsin-Madison which was supervised by Professor David D. Houghton.

location of rainfall maxima. It is shown that the orientation of the maxima and minima axes in the contoured estimate field is in good agreement with the observations and radar reports. As would be expected, this agreement improves with higher amounts of smoothing. There are many apparent overestimates, for which several plausible explanations are given. Some displacement errors are observed and it is shown how small location errors can lead to large errors in a gridded difference field.

By using satellite estimates as part of the SSM model verification, this study suggests a new application for the use of the Scofield-Oliver technique. Unfortunately, the SSM model fails to accurately predict convective precipitation in this case study. It's forecast precipitation area is too far to the north and the amounts are much too small. Nevertheless, the feasibility of using satellite estimates to verify the model is demonstrated. It is shown that the potential exists for operational numerical (mesoscale) modeling to benefit by having such satellite verification information for precipitation which can be produced in near real-time.

I. INTRODUCTION

One of the newest and most exciting topics within the field of satellite meteorology is precipitation estimation. Since 1978, the Synoptic Analysis Branch (SAB) of the National Environmental Satellite, Data, and Information Service (NESDIS) has been responsible for providing the National Weather Service (NWS) and other users with real-time estimates and short-range forecasts of precipitation from satellite pictures. The operational estimates are computed for individual counties using the improved Scofield-Oliver Convective Rainfall Estimation Technique, with the help of IFFA, the Interactive Flash Flood Analyzer. These estimates, when used in conjunction with local radars, provide timely rainfall information and are instrumental in the issuance of flash flood watches and warnings, which save lives and property. Throughout this paper, one should not lose sight of the fact that satellite precipitation estimation is truly amazing, considering that information from satellite pictures taken more than 22,000 miles in space is being used to make rainfall estimates for areas as small as an individual county.

Because the Scofield-Oliver technique is designed specifically for convective events, its application is most appropriate for what are termed "mesoscale" (or sub-synoptic scale) systems. These could range from a large mesoscale convective complex (MCC) covering a few states to individual thunderstorm clusters. Much attention has focused on problems of the mesoscale in the past decade, yet a comprehensive theory regarding the nature of mesoscale phenomena is still lacking. This is mainly because there is an "inadequate understanding of the physical and dynamical processes associated with the phenomena...and because a suitable observational system does not exist" (Ray, 1986). In an effort to gain an understanding of what actually occurs on the mesoscale, numerous field research experiments have been conducted (such as AVE, COOPE, CYCLES, SESAME, and STORM). Many of these experiments collected much needed data with a better temporal and spatial resolution than is normally available. Similarly, as new empirical evidence regarding mesoscale systems has been gained from satellite imagery, the original Scofield-Oliver Convective Rainfall Estimation Technique, developed in 1977, has undergone several modifications. For example, the original technique was designed for tropical-type systems with high tropopauses and high precipitable water values. However, it was noticed that some heavy rainfall events went unestimated because they had relatively warm tops in the enhanced infrared GOES imagery. In 1982, the technique was modified by Spayd and Scofield to include heavy localized rainfall from "warm-top" events in the satellite imagery (Spayd, 1982). Other empirical correction factors, such as for overshooting tops, thunderstorm cluster or line mergers, stationary storms, mean environmental relative humidity, and precipitable water have been developed recently and are discussed further in Chapter III.

Although not discussed in this paper, it should be noted that microwave frequencies also have been used to estimate precipitation from satellites. (However, they are not as yet used in an operational mode.) According to Spencer et al. (1983b), "Microwave methods are more direct [than Visible/IR methods] because the microwave radiation upwelling from the earth is affected more by rain drops than by cloud droplets." For more information on microwave satellite precipitation estimation, see reference list for articles by: Weinman and Guetter, Spencer, Spencer et al., Hood and Spencer, and Ferraro et al.

The first main goal of this paper is to demonstrate the use of the NESDIS Operational Scofield-Oliver Convective Rainfall Estimation Technique by computing estimates for a convective event that occurred over the southern Midwest in July, 1981. Forty-eight grids of half-hourly precipitation estimates are added together to make a 24-hour total.

The next major section of this paper presents the verification of these satellite-derived estimates. Because of the often short-lived and localized nature of convective storms, verification of satellite rainfall estimates is a difficult task (Field, 1985a). Observations from exactly the same time period and location as the estimate are very rare. Also, heavy warm-season precipitation is usually a mesoscale event and it is highly unlikely that the maximum reported values will be representative of the local maximum amount that actually falls. The maximum rainfall usually falls between the rain gauges! Recently, a verification system which attempted to minimize these temporal and spatial problems was developed and used to verify NESDIS' Synoptic Analysis Branch's operational estimates for the 1984 convective season. Results showed that the satellite estimates were accurate to within about 30 percent in magnitude and 10-20 miles in location (Field, 1985b). Although the verification method used in this paper differs from the NESDIS method, many of the same factors (such as sparsity of observations) were important. For this paper, the verification procedure involved the collection of more than 300 cooperative observer rain gauge reports corresponding (as well as possible) to the same time period as the estimates. The observations then were interpolated to the same grid points as the estimates. The resulting contoured difference fields will be presented and discussed. Similarities and differences between the NESDIS method and this method will be mentioned.

Evaluation of a mesoscale model precipitation forecast is the subject of the third part of this paper. As Anthes (1983) and Lindstrom (1984) have pointed out, crucial improvements are still needed in the parameterization of many processes related to precipitation forecasts, such as planetary boundary layer processes and moist convection. While mesoscale models are used mainly for research at present, it is conceivable that they will eventually be used in an operational mode. Until that time in the future, however, it is important that the state of the art in mesoscale precipitation modeling improve. This paper provides an evaluation of model forecasts for the case of July 20-21, 1981. The Australian Subsynoptic Scale Model's (SSM) 24-hour precipitation forecast is examined using two data sets. The first was from cooperative observer reports smoothed to a degree that allowed a fair comparison to be made with the resolution of the model output. Contoured gridded difference fields are presented in Chapter VII. Although it was possible to use such a dense network of rainfall observations for this research, this normally would not be available to mesoscale modelers on a real-time, operational basis. Some NWS cooperative observers report only every week and it is months before their reports are published in a climatological journal. The second data set was derived from satellite imagery. Such estimates could be used to verify numerical model forecasts in a timely manner and to supplement other data, especially where there are gaps in the observed data. In fact, the Heavy Precipitation Unit (HPU) of the National Meteorological Center (NMC) currently tries to incorporate estimates from NESDIS' Synoptic Analysis Branch, along with radar and rain gauge reports when verifying their operational products. This paper used a smoothed satellite-derived estimate field as the verification for the SSM's convective precipitation forecast. Contoured difference fields are presented in Chapter VII. Although the SSM failed to accurately predict convective precipitation in this case study, this paper presents both the idea of and an example method for using estimates to verify a numerical model.

A description of the synoptic setting and important dynamics on July 20-21, 1981 is given in Chapter II. Much work has been done (see Uccellini and Petersen) using VAS soundings for this severe weather outbreak and some of this work is shown.

Satellite precipitation estimation is discussed in Chapter III. First, the Scofield-Oliver Convective Rainfall Estimation Technique is explained in detail. This is followed by a description of the physical set-up of the University of Wisconsin's Man-Computer Interactive Data Access System (McIDAS) and a summary of the procedure used in computing estimates for this paper. A comparison is then made between the author's estimation scheme and the current NESDIS operational Precipitation Estimation Program, which is performed in Washington, D.C. by Synoptic Analysis Branch meteorologists using the Interactive Flash Flood Analyzer.

Chapter IV explains how the observed rainfall data were compiled and what were the sources of the data.

Chapter V gives a description of the Subsynoptic Scale Model and a summary of the particular model run used for this study.

In Chapter VI, the topic of smoothing is addressed. The smoothing factors used for inter-comparisons between the estimates, observations, and model are explained.

The results of this research are presented in Chapter VII. Comparisons are made between: (a) the estimates and the observations, (b) the observations and the model, and (c) the estimates and the model. These comparisons are evaluated with regard to magnitude errors, location errors, orientation of maximum/minimum axes, etc. A statistical skill score that was able to be objectively calculated is cited.

A summary and conclusion is given in Chapter VIII.

A complete list of references follows the conclusions.

The Appendices show the VAS data that is mentioned earlier in Chapter II and the actual cooperative observer rain gauge reports for each state in both plotted and tabular form.

II. THE SYNOPTIC SETTING

During the afternoon on July 20, 1981, a 500 mb short wave trough was advancing through the Mississippi Valley and strong cold advection was entering Nebraska behind this trough. At the surface, a cold front trailing from a low pressure center in Ontario extended southwestward through northern Ohio, central Missouri, and the Oklahoma Panhandle. This front separated very hot, moist air to the south from warm, but drier air to the north. At 2100 GMT the temperature was 97°F with a dew point of 77°F in southeast Missouri (Figure 1).

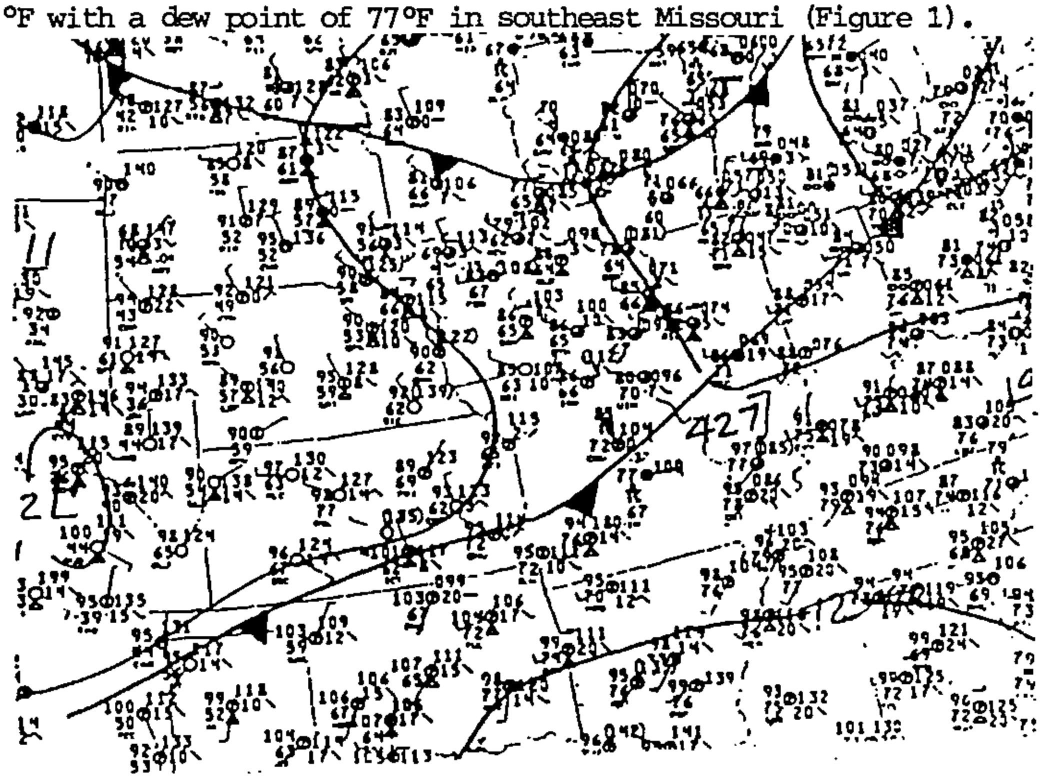

Figure 1. Surface Analysis from 2100 GMT, July 20, 1981 for the Central United States region.

From early in the day, the atmosphere was unstable in the southern Midwest. Figure 2 shows the McIDAS-derived Lifted Index, Total Totals Index, precipitable water, and the Severe Weather Threat (SWEAT) Index for radiosonde stations across the Midwest at 1200 GMT, July 20. The maximum negative Lifted Index was -8 from Oklahoma to southwest Missouri. The SWEAT Index was also a pronounced maximum of 318 over southwestern Missouri. Total Totals Indices were in the unstable mid-50's over the same area. (For each of these indices, the larger the magnitude (absolute value) of the index, the more unstable it is.) Precipitable water values were highest in Oklahoma and Arkansas.

During the afternoon, a mid-level dry air intrusion approached and overtook the low-level moisture that existed ahead of the front. At 1930 GMT a cluster of severe thunderstorms developed in central Missouri and swept southeastward during the day. Tornadoes were reported near Columbia, Missouri. A few hours later, a second area of thunderstorms developed across Oklahoma, where surface temperatures had reached 107°F with dew points in the 60's. The 2235 GMT radar chart shows these two areas of thunderstorms (Figure 3).

Recently, meteorologists have been able to use VAS (Visible and Infrared Spin Scan Radiometer Atmospheric Sounder) satellite data to continuously monitor changes in atmospheric stability. Using VAS data, the development of the two main areas of storms on this day has been found to be closely related to the onset of the mid-level dry air intrusion at these locations (Petersen et al., 1983a). By using a method known as the "split-window" technique to identify areas of low-level moisture (Chesters et al., 1983) and then overlaying regions of mid-level dryness, Petersen et al. were able to identify areas of strong (and severe) convective potential in real-time. This helped lead to the prompt issuance of tornado watches that afternoon by the Severe Storms Forecast Center in Kansas City and may, in part, be the reason that no persons were killed in Missouri, despite numerous severe reports. Table 1 shows a listing from Storm Data reports for Missouri on July 20, 1981. Further details about the use of VAS satellite data on this day are given in Appendix A.

By early the next morning, Arkansas was receiving heavy rainfall, as shown on the 0935 GMT radar chart (Figure 4). Throughout the period of concern in this case study, precipitable water values (Figure 5) were high (greater than 1.5") ahead of the cold front. Observed 24-hour (1200-1200 GMT) rainfall totals of 1.5" were common from northwest and central Arkansas northeastward to southern Illinois and western Kentucky, with more than 2.5" in parts of Missouri and Arkansas.

Further synoptic and radar maps for this July 20 case can be found in Petersen et al (1983b, c).

III. SATELLITE PRECIPITATION ESTIMATION

A. Characteristics and Scales of Satellite-Observed Heavy Convective Rainfall Systems

Before the meteorologist can attempt to compute a quantitative satellite precipitation estimate, it is important for him/her to be able to recognize the type of convective system that is occurring. This can help in making more

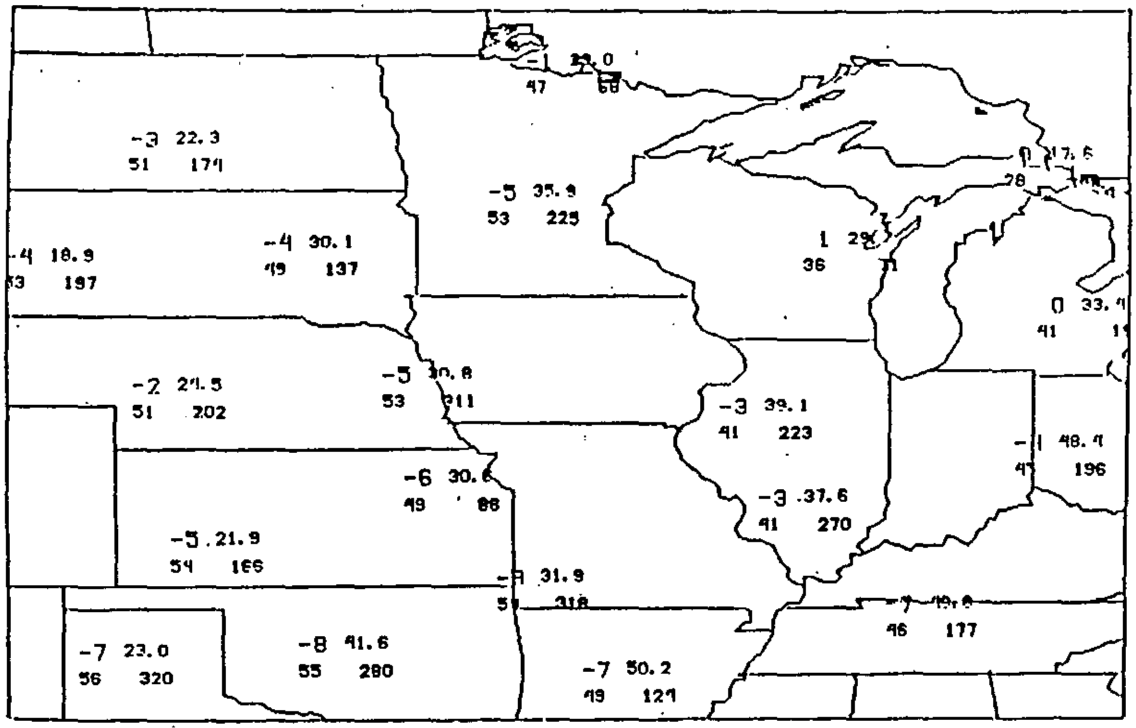

Figure 2. Lifted Index (upper left), Total Totals Index (lower left), Severe Weather Threat Index (lower right), and Precipitable Water (upper right, in mm. of water) at 1200 GMT, July 20, 1981

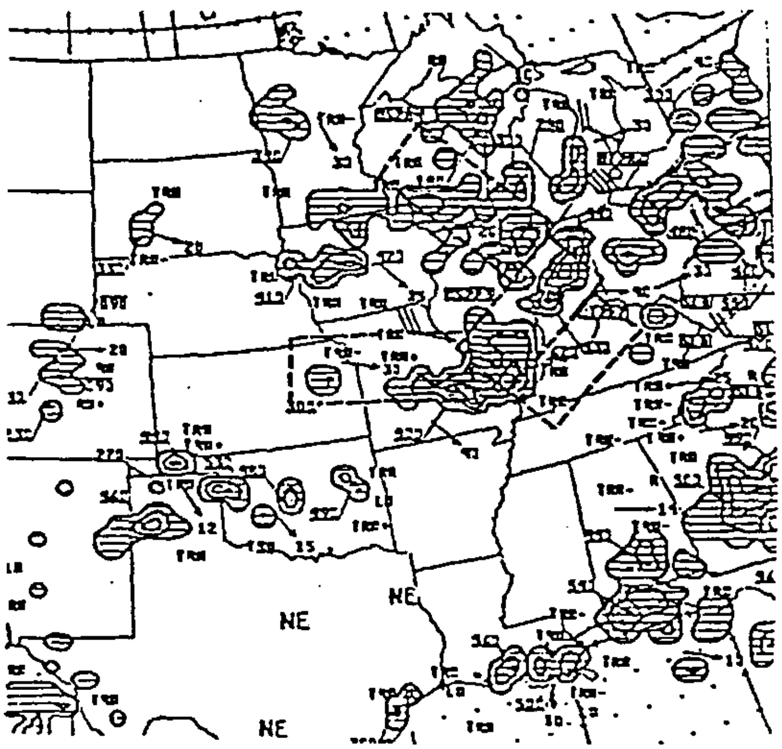

Figure 3. 2235 GMT radar summary on July 20, 1981.

PLACE	DATE	TIME - LOCAL STANDARD	LENGTH OF PATH (MILES)	WIDTH OF PATH (YARDS)	NO. OF PERSONS KILLED	NO. OF PERSONS INJURED	ESTIMATED DAMAGE PROPERTY	ESTIMATED DAMAGE CROPS	CHARACTER OF STORM
MISSOURI									
St. Charles	20	3.35 PM			0	8	5	?	Damaging Wind
	A particularly violent storm hit Weldon Springs and did much damage to the T/K Mobile Home Park. Five mobile homes were completely destroyed and a number of other were damaged. Two of the injuries were serious. The storm also contributed to a private school bus accident. There were reports of damage to trees and power lines. A police officer reported he went to survey the damage and found out a tree had been dropped on his car. This line of thunderstorms produced scattered damage throughout the county until around 4 PM. A meteorologist saw tires on fire on a parked car while heading for work. A late report of golf ball size hail was also received. Reports of a possible tornado were never confirmed.								
Jefferson	20	3.48 PM	1	50	0	0	3	0	Tornado (F0)
	A tornado dipped down briefly 5 miles north of Hillsboro. It damaged trees and produced minor structural damage to homes.								
St. Louis	20	4.02 PM			0	0	3	0	Damaging Wind
	Minor damage was reported to have occured to parked aircraft at the Spirit of St. Louis Airport located in the western part of the county.								
St. Louis City and St. Louis County	20	4 to 4.30 PM			0	0	6	?	Damaging Wind
	A line of severe thunderstorms produced widespread scattered damage throughout the area. Trees were uprooted and power lines were downed. Some fences were blown over. The most significant damage was the serious damage to the radar antenna at Jefferson Barracks. Damage there was reported at $300,000.00								
Crawford	20	4 to 420 PM			0	0	?	?	Large Hail Strong Wind
	Large hail and wind to 55 mph at Bourbon. No size given on hail.								
Bollinger and Cape Girardeau Counties	20	530 PM			0	0	3	0	Damaging Wind
	High winds downed trees in the area.								

PLACE	DATE	TIME - LOCAL STANDARD	LENGTH OF PATH (MILES)	WIDTH OF PATH (YARDS)	NO. OF PERSONS KILLED	NO. OF PERSONS INJURED	ESTIMATED DAMAGE PROPERTY	ESTIMATED DAMAGE CROPS	CHARACTER OF STORM
MISSOURI									
..Central..									
........A line of severe thunderstorms moved through central Missouri on the afternoon of July 20 between 155 and 630 PM. This is the same line of thunderstorms that did the damage to eastern Missouri earlier in the report. The number of storms and various delayed reports make it hard to ascertain the exact times of each damage occurrence. There were a number of reports of possible tornadoes but radar and storm surveys indicate that this was straight line wind damage. The exception seems to be High Hill in the eastern portion of Montgomery County. The below storm reports give the times of a number of occurrences. These are followed by a number of reports that came in after the initial reports and the times are not given but are assumed to have occurred about the time of the earlier reports.									
Boone	20	155 PM			0	0	4	0	Damaging Wind
	Several small trees uprooted and numerous houses sustained minor roof damage. This about 5 miles north of Columbia.								
Boone	20	157 PM			0	0	3	0	Damaging Wind
	Trees down on east side of Columbia.								
Cooper	20	2 PM			0	0	4	0	Damaging Wind
	A radio tower was blown down and trees downed 6 miles north of Boonville.								
Boone	20	2 PM			0	0	4	0	Damaging Wind
	A sundeck was ripped off a home a a roof was torn off a home 4 miles northeast of Columbia.								
Boone	20	215 PM			0	0	3	0	Damaging Wind
	Glass was strewn over a parking lot at a shopping center in Columbia. This was due to broken auto windows.								
Montgomery	20	307 PM	1	50	0	0	4	0	Tornado (F2)
	A tornado touched down at High Hill in the eastern portion of the County. One home was demolished.								
Boone	20	345 PM			0	0	3	0	Damaging Wind
	A late report of winds to 70 MPH and downed trees just north of Columbia.								
	20	455 PM							Damaging Wind
	The following reports are all delayed and all occurred much before the 455 PM time.								
Boone					0	35	6	?	
	Civil Defense reported winds to 77 MPH at Columbia. The county received winds generally in the 60 to 80 MPH range. Widespread structural damage was reported throughout the area to homes and businesses. The damage ranged from minor to heavy. There were also a number of reports of damage to sheds, trees, fences and cars. A number of trees and power lines were also downed. The injuries were minor except for one women. She was hospitalized and was reported in fair condition.								
Howard					0	0	4	0	
	A barn blown down and a tower blown over.								
Callaway					0	0	4	0	
	Numerous trees down and many homes with roof damage.								

Table 1. Partial listing of storm reports for Missouri during the afternoon of July 20, 1981.

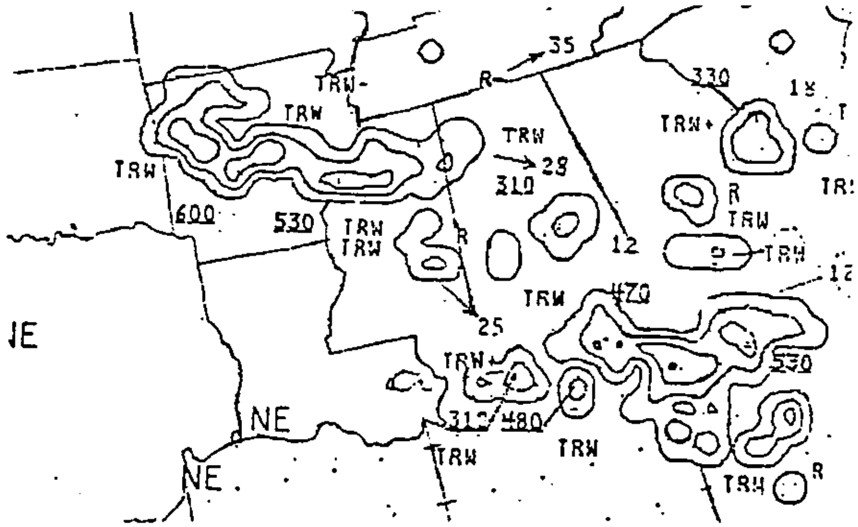

Figure 4. 0935 GMT radar summary on July 21, 1981.

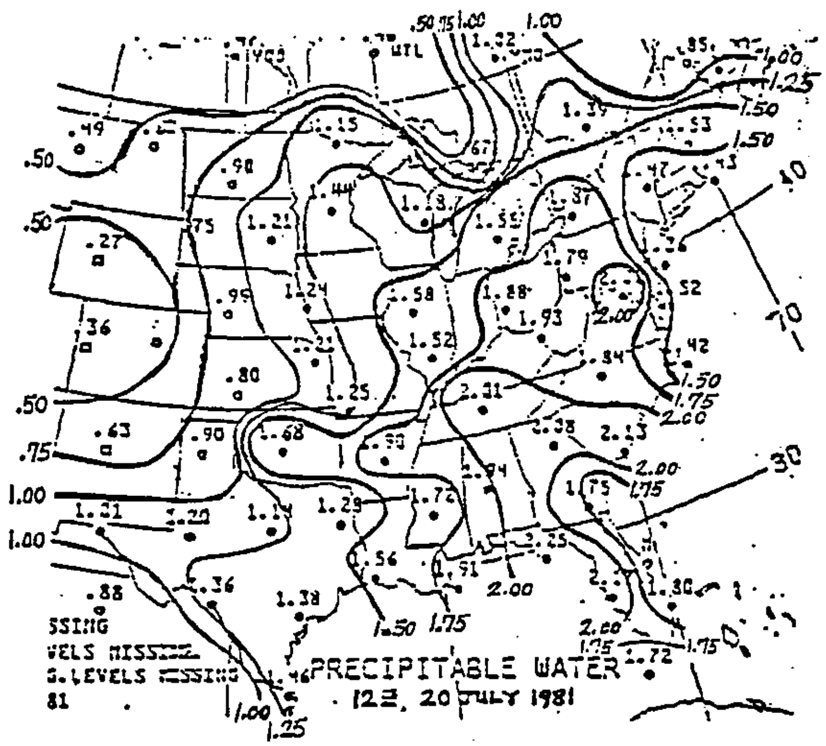

Figure 5. Precipitable water (in.) at 1200 GMT, July 20, 1981.

prudent decisions regarding the intensity and duration of the storms. For example, certain systems become more efficient rainfall producers hours after initial development, such as the Mesoscale Convective Complex (MCC), while others, such as Single-Clustered systems, have short-lived heavy rainfall. After years of viewing satellite imagery and studying the signatures of mesoscale systems, the NESDIS Satellite Applications Laboratory in Washington, D.C. has developed a classification scheme for several convective systems. These include Tropical, Linear, Single-Clustered, Multi-Clustered, Synoptic Scale, Overrunning, and Regenerative systems. There are several sub-categories within each of these classifications. For example, "Tropical" systems include remnants of pure tropical cyclones as well as mesoscale quasi-tropical systems (such as the MCC), which possess a large circular or oval anticyclonic cirrus outflow. The "Linear" category consists of both squall lines and deep large-scale convective wedges. "Multi-clustered" systems can be either circular or wedge-shaped, depending on the velocity of the upper level flow. As will be shown in sections 2 and 3 of this chapter, the determination of the areas of heaviest rainfall (from a satellite picture) for this latter category is highly dependent on knowledge of the upper level wind pattern. Table 2 shows the characteristics of satellite-observed heavy convective rainfall systems. It describes the location and appearance of these systems in satellite data, conventional data, and radar data (Spayd and Scofield, 1984a). Since the operational meteorologist usually has access to local radar observations, the radar signatures listed in Table 2 provide valuable insight into the correct diagnosis and classification of a convective system.

Table 2. Characteristics of Satellite-Observed Heavy Convective Rainfall Systems

		CHARACTERISTICS OF SATELLITE-OBSERVED HEAVY CONVECTIVE RAINFALL SYSTEMS		
TYPES	DIURNAL VARIATIONS	SATELLITE DATA	CONVENTIONAL DATA	RADAR DATA
Ia. TROPICAL SYNOPTIC SCALE TROPICAL	"Peripheral thunderstorms" develop in the afternoon in response to surface heating away from the circulation center. At night, boundary layer stabilizes and "core thunderstorms" develop at circulation center due to maximum moisture convergence. "Core thunderstorms" may form a MCC type system.	Cold tops, readily identifiable, persistent anticyclonic outflow aloft which causes cloud top growth to become quasi-constant. Weak jets in westerlies can cause elliptical elongation in outflow and convection. When system becomes extra-tropical the pattern may resemble that of an occluded frontal cloud structure and the maximum rainfall shifts north and east away from the center of the system. Outer rainbands and in dissipating stages the entire system may become warm-topped.	Remnant of Hurricane, Tropical Storm, or Tropical Depresson; initially-persistant forward motion and cyclone symmetry; occurs in extremely moist air mass (PW≥ 2"), low to mid-level cyclonic vorticity focuses rainfall.	Outer curved rainbands may have a combination of convective and stratiform Z-R rain rates. Large persistent area of VIP 1-3, embedded but non-persistent VIP 4-6. New echoes may reappear hours after previous echos dissipate. Echoes may appear on periphery of circulation center during afternoon and reappear near circulation center at night. Echo movement is a combination of movement along the spiral band, propagation of spiral band around circulation center, propagation of circulation center.
Ib. TROPICAL MESOSCALE QUASI-TROPICAL (MESOSCALE CONVECTIVE COMPLEX -MCC)	Strong maximum in early evening to early morning; strong minimum in mid-morning.	Cold tops, overshooting tops, and numerous cell mergers observed. Large circular or oval anticyclonic outflow. Speed of movement of coldest tops most important for heaviest rainfall. Intensifying if coldest tops moves to central location in cloud pattern and cirrus outflow becomes increasingly anticyclonic in one or more quadrants. Most efficient precipitation producer 4 to 10 hours after initial convection develops, due to large area of light precipitation saturating the surrounding air mass. Usually produces mid-level cyclonic circulations and upper level mesoscale jet streaks which will alter surrounding and future convection.	Triggered by shortwave trough moving through upper level ridge and focused by low level axis of maximum winds overriding low level boundaries. Vertical circulation similar to Synoptic Scale Tropical system. Cyclonic vorticity in low to mid troposphere couples with anticyclonic outflow aloft. Winds veer strongly with height.	Large, persistent, trackable area of VIP 1-3 with embedded non-persistent VIP 4-6. Numerous echo mergers are detected. Highest VIP levels usually occur in first 5 hours of development when the precipitation efficiency is lowest.
IIa. LINEAR LARGE SCALE WEDGE	No distinct diurnal variation.	Large 50-90 degree angle pointing into the wind. Southern most cluster may be embedded in a N-S oriented squall line. Shortwaves rotating around longwave trough concentrate the convective outbreaks. Due to persistent low-level southerly inflow convection redevelops after weak shortwave passes and thunderstorms become increasingly efficient rainfall producers. As longwave trough approaches cloud tops may become warmer with time.	Forms where polar front jet and subtropical jet separate. Occurs east of deep 500 mb longwave trough with weak or neutral synoptic scale vorticity advection. Outbreaks concentrated by shortwave troughs. Wedges retard movement of 500 mb pattern. Fueled by strong low level axis of maximum winds over a low level boundary. Winds veer strongly with height.	Large areas of VIP 1 and 2 with embedded VIP 3-6. Echos may redevelop over same area or upwind in surges.

CHARACTERISTICS OF SATELLITE-OBSERVED HEAVY CONVECTIVE RAINFALL SYSTEMS

TYPES	DIURNAL VARIATIONS	SATELLITE DATA	CONVENTIONAL DATA	RADAR DATA
IIb. LINEAR SQUALL LINE	Strong maximum (80%) in late afternoon through evening; minimum in morning.	Cold cloud tops in 75% of cases. Downstream convection may be masked by upstream anvil blowoff. Weakening usually occurs when squall line accelerates away from its initial triggering mechanism (i.e. frontal zone). When convection develops upwind, clusters may pass over the same area if the squall line is slow moving.	Occurs along or ahead of a slow moving cold frontal boundary. Winds veer only 40° with height; winds < 35 knots, PW~1.6", mean RH~80%, triggered by a weak shortwave at 500 mb.	Line Echo Wave Pattern (LEWP) may be observed, an intense line of high VIP 3-6 echos. Echos may suddenly redevelop upwind in surges.
III SINGLE-CLUSTERED	Tied strongly to solar insolation; a strong maximum (80%) in late morning through early evening, and a strong minimum in nighttime and morning.	Very small, round, oval, or carrot shaped. Very rapid growth, stationary, overshooting tops. Usually warm tops. Since tops are so small the actual temperature of the tops may be colder than the resolution of the GOES-IR sensor indicates.	Fueled by solar insolation, anchored by topography, or mesoscale boundaries.	Small, stationary, echo, VIP 3-5.
IVa. MULTI-CLUSTERED CIRCULAR	Eighty percent occur from late afternoon through midnight; minimum in morning.	Warm tops in 70% of cases, round or oval shaped cloud tops, cluser mergers usually evident; usually quasi-stationary. Mergers of separate multi-clustered circular systems may evolve into a MCC-Mesoscale Convective Complex.	Weak upper level flow, develops due to low level forcing.	Quasi-stationary, VIP 3-6, echo mergers may occur.
IVb. MULTI-CLUSTERED LINEAR	Seventy percent occur from late afternoon through evening; weak minimum in morning.	Warm or cold tops, small wedge, carrot or diamond shaped, coldest tops in vertex (enhanced V pattern sometimes observed). Rapid growth and stationary, may build upwind. Much smaller than large scale wedge. The higher the speed shear from mid to high levels the narrower the wedge. Heaviest rain in extreme upwind portion of vertex although thunderstorm cells may stretch linearly from the vertex to the middle of the wedge (in the warmer IR temperatures behind the enhanced V pattern). Existence dependent on jet streak. If jet streak drifts away from wedge in a direction normal to flow, wedge dissipates and new wedges develop where jet subsequently intersects areas with favorable low level conditions. When second wedge develops upstream from the first, the initial wedge is shielded from jet and dissipates unless second wedge induces a mesoscale jet streak that interacts with the first system and intensification results. If another convective system develops upstream and blocks the environmental wind flow (reducing the mid to high level wind shear) the linear multi-clustered system could develop into a MCC.	Upper flow is zonal or weakly diffluent. Strong speed shear from mid to high levels present. May distort upper flow like Mesoscale Convective Complexes - MCC's and produce wind max on northern side. Development due to low level forcing and jet streak aloft.	Individual echo motion may be fast (15-30 knots) but repeated echo development in upwind of cluster may result in slow cluster speed. Persistent VIP 3's are common with embedded non-persistent VIP 4-6. In enhanced V patterns the highest VIP levels are usually at the vertex of the V extending into the warmer temperatures downwind of the vertex.

CHARACTERISTICS OF SATELLITE-OBSERVED HEAVY CONVECTIVE RAINFALL SYSTEMS

TYPES	DIURNAL VARIATIONS	SATELLITE DATA	CONVENTIONAL DATA	RADAR DATA
V. SYNOPTIC SCALE CYCLONIC CIRCULATION	Moderate maximum in the evening into early morning; moderate minimum in mid-morning and afternoon.	Warm tops located in comma head of cyclonic circulation, cyclonic circulation moving E to NE at 2° latitude per 12 hours, rapid cloud growth, overshooting tops, mergers observed, either quasi-stationary or regenerative.	Occurs to north or east of slow moving circular 500 mb vorticity center. Occurs to north of 850 mb low with maximum isodrosotherms rapping around to north of low. Occurs to north and west of 850 mb axis of maximum winds. Occurs north of surface low in cool NE flow. When 500 mb center weak, no surface fronts; when stronger, surface fronts are evident. Winds veer 180° with height; winds ≤ 40 knots. PW=1.3", mean RH~60%. Extremely "wet" when convection is focused along mesoscale surface convergence line.	If quasi-stationary, VIP levels are high, VIP 4-6. If regenerative, echos VIP 3-4.
VI. LARGE/SMALL SCALE OVERRUNNING	Strong maximum in early evening to midnight; strong minimum in early to mid-morning.	Warm tops locted in large anti-cyclonic flow of cirrus. Animation (IR) best for detecting convective bands from cirrus bands. Transverse banding in cirrus appears as textured areas on visible imagery. System doesn't weaken until strong shortwave passes through area.	Cool boundary layer, winds veer over 180° with height, air lifted isentropically until unstable and deep convection is released. Convective bands form perpendicular to 850 mb flow (low level axis of maximum winds), and nearly parallel to 500 mb flow. K index much better than Lifted Index for detection. Extremely moist environments RH ≥ 90%, PW ≥1.5" large area of weak maximum surface moisture convergence values, no defined surface low apparent.	Widespread persistent VIP 1 and 2, occasional VIP 3.
VII. REGENERATIVE	Moderate maximum in late afternoon through mid-evening; weak minimum in mid-morning.	Warm or cold tops. Single-clustered and multi-clustered convective systems develop along the upwind portion of a low-level boundary and transverse the same path downwind along the boundary. Animation is the best tool for detection. No cell mergers usually seen. Outflow from new cells may continually reinforce existing quasi-stationary outflow boundary. If regeneration of cells is very rapid (≥ 1/2 hour) system may resemble a small wedge (linear multi-clustered). Initial thunderstorm cells may saturate the local environment so new thunderstorm cells may be more efficient precipitation producers. The initial thunderstorm cells may also warm the local upper atmosphere causing a lowering (warming) of the equilibrium level; so new thunderstorm cells may have warmer tops. System weakens when triggering shortwave overtakes the quasi-stationary outflow boundary or low level convergence zone. Outflow from new cells may also accelerate existing quasi-stationary outflow boundary away from favored areas of development, so new cells stop regenerating.	Outflow boundary or convergence boundary apparent in surface mesoanalysis. Inflow perpendicular to boundary may be focused by mesolow. Extremely high mesoscale moisture convergence values.	Train echo effect. Individual echos may move at speeds of 15 to 40 knots. New echos may have higher VIP levels than previous echos.

Another way that these systems can be classified is by their scale, as shown in Figure 6 (Spayd, 1985). (Figure 6 is more recent than Table 2 and, while classifications are the same, the terminology is slightly different. "Mesoscale Convective Systems" refer to the "Multi-Clustered" variety previously mentioned. "Convective Wedge" refers to "Linear Large Scale Wedge" and MCC's have been given their own category.) Most convective heavy rainfall events fall within the upper Meso-β and lower Meso-α scales (from approximately 50 to 1500 km). Tropical storms, overrunning, and cyclonic circulation systems are primarily meso-α, while mesoscale convective systems are primarily meso-β. Convective complexes can be Meso-α or Meso-β and single-clustered systems are usually Meso-γ width (from approximately 5 to 20 km).

B. THE SCOFIELD-OLIVER CONVECTIVE RAINFALL ESTIMATION TECHNIQUE

1. Assumptions of the Technique

The Scofield-Oliver Convective Rainfall Estimation Technique (SOCRET) was originally developed in 1977 by Rod Scofield and Vince Oliver of NESDIS in Washington, D.C. (Scofield and Oliver, 1977). It is based on empirical correlations between observed rainfall and satellite imagery. During the past several years, the Technique has become widely accepted and it is the United States' current operational rainfall estimation technique. The SOCRET was developed for deep convection within a moist tropical air mass. Precipitable water values are assumed to be greater than or equal to 1.5 inches. The technique assumes that there are high summer tropopauses, thereby allowing convection to achieve maximum heights (cold tops). Furthermore, the technique does not take into account any orographic effects.

Since 1977, the Technique has undergone many refinements, which have enabled it to be used for a wider range of rainfall events. For example, the improved SOCRET has a "warm-top" modification, which allows an estimate to be computed for convective events in regions with lower tropopauses, such as near a closed upper-level low pressure center during the summer. Also, the new "moisture correction factor" allows estimates to be determined in regions where precipitable water values are lower than 1.5 inches. These and other factors are described in Section 2b.

It should be noted that Rod Scofield and LeRoy Spayd have developed two other rainfall estimation techniques: (1) the Extratropical Cyclone (or "Winter Storm") Technique (Scofield and Spayd, 1984), and (2) the Tropical Cyclone Technique (Spayd and Scofield, 1984b). These should not be confused with the SOCRET.

2. Computation of the satellite rainfall estimate

The computation of an estimated half-hourly rainfall rate requires two enhanced infrared (IR) satellite photos, 1/2-hour apart. The IR enhancement used is the MB-curve, which is shown in Figure 7. The warm end of the MB enhancement table is useful for identifying hot land, low clouds, sea surface

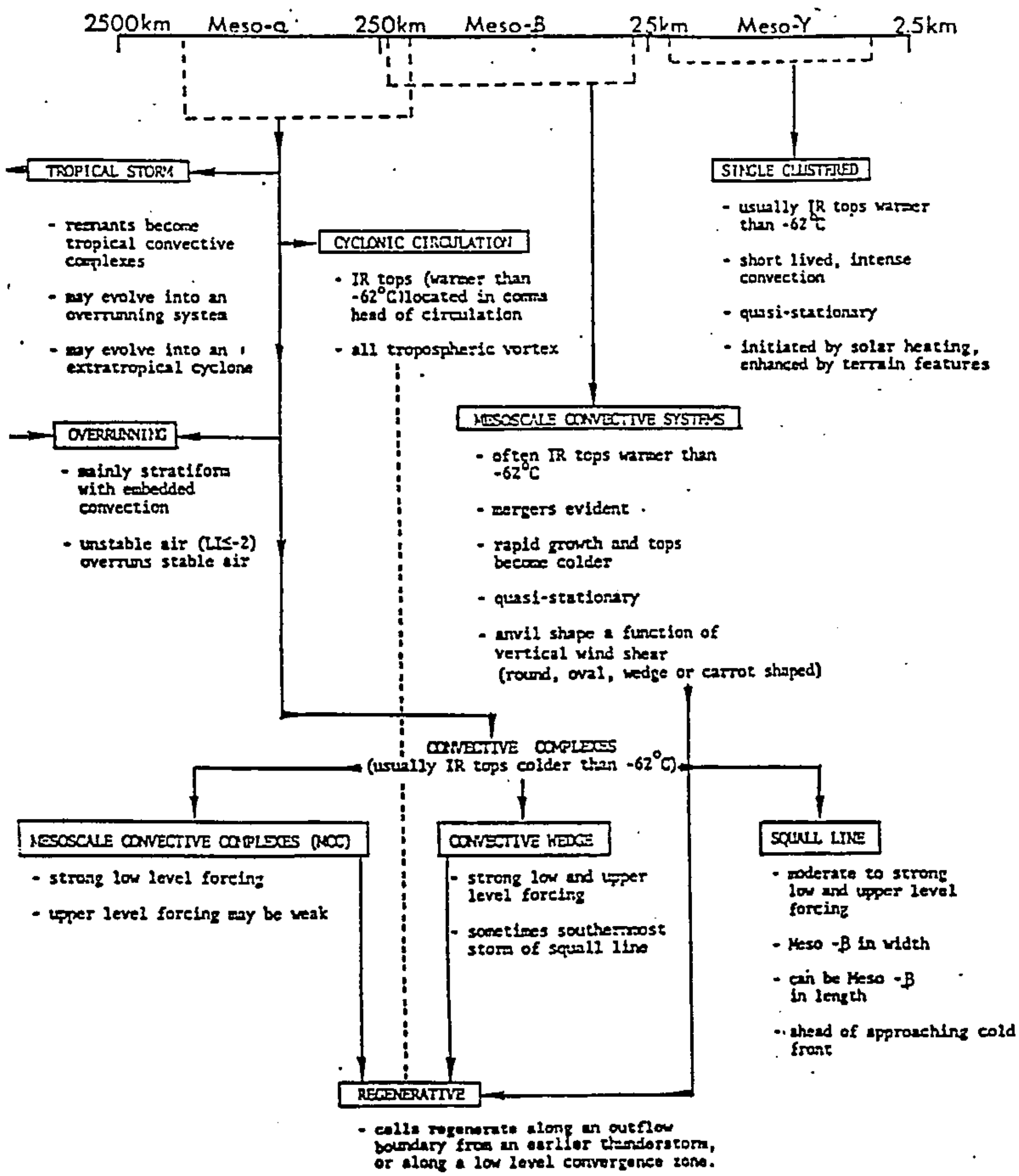

Figure 6. Scales of Satellite-Observed Heavy Convective Rainfall Systems.

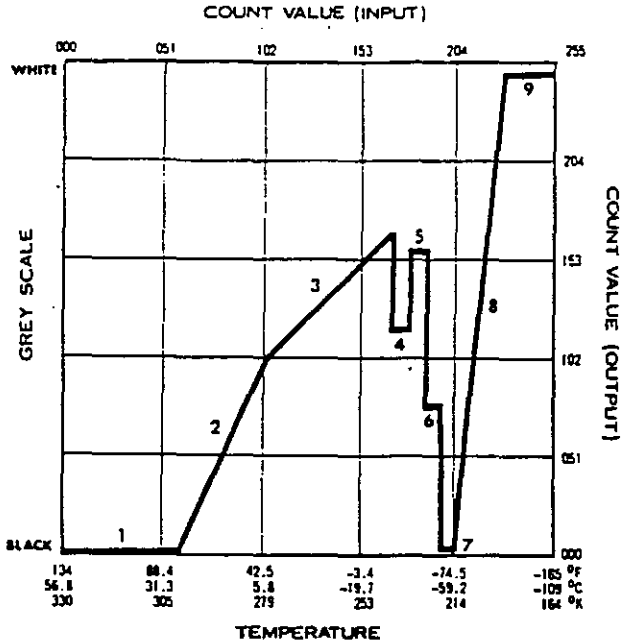

Figure 7. The operational MB-curve for enhancing infrared satellite imagery. (Chart taken from Clark, 1983.)

temperatures, and middle level clouds. However, it is the colder end of the MB-curve (segments 4-9 in Figure 7) which is used for the estimation of precipitation from convective storms. Visible (VIS) images provide additional information and should also be used. The operational SOCRET is shown in Table 3 (Scofield, 1984). Short summaries of each step are given below.

Segment #	Enhancement Color	Temperature (°C)
1,2,3	Unenhanced	greater than -32
4	Medium Gray	-32 to -41
5	Light Gray	-41 to -52
6	Dark Gray	-52 to -58
7	Black	-58 to -62
8	Repeat Gray	-62 to -80
9	White	less than -80

a. Determining the active portion of the thunderstorm system

The first step is to examine the shape of the cloud to determine if it is convective (round, oval, carrot-shaped, or triangular) using both VIS and IR imagery. Then, one determines if the convection is deep by checking whether the cloud top reaches the first or higher level of contoured enhancement using enhanced IR imagery. Once both of these criteria are met, one must determine the active portion of the thunderstorm system, since rainfall estimates are computed only for this region. Step 1 in Table 3 lists several clues for helping to identify the active portion. For example, in moderate to

CONVECTIVE STORM TECHNIQUE

STEP 1

RAINFALL IS COMPUTED ONLY FOR THE <u>ACTIVE</u> PORTION OF THE THUNDERSTORM SYSTEM:

THE FOLLOWING ARE CLUES FOR HELPING TO MAKE THIS DECISION.

- IR TEMPERATURE GRADIENT IS TIGHTEST AROUND STATION END OF ANVIL FOR A THUNDERSTORM SYSTEM WITH VERTICAL WIND SHEAR (IR).
- STATION IS LOCATED NEAR THE CENTER OF THE ANVIL WITH A TIGHT, UNIFORM IR TEMPERATURE GRADIENT AROUND ENTIRE ANVIL FOR A THUNDERSTORM SYSTEM WITH NO VERTICAL WIND SHEAR (IR).
- AN OVERSHOOTING TOP IS OVER THE STATION (VIS AND IR).
- ANVIL IS BRIGHTER AND/OR MORE TEXTURED (VIS).
- FROM COMPARING LAST TWO PICTURES: STATION IS UNDER HALF OF ANVIL BOUNDED BY EDGE WHICH MOVES LEAST (IR).
- STATION IS NEAR 300-MB UPWIND END OF ANVIL (IR, SKIP THIS CLUE IF NO UPPER AIR DATA AVAILABLE).
- STATION IS NEAR THE AREA OF LOW-LEVEL INFLOW (VIS).
- STATION IS LOCATED UNDER A RADAR ECHO.

STEP 2

HALF-HOURLY RAINFALL ESTIMATES IN INCHES ARE COMPUTED FROM THE FOLLOWING FACTORS:

FACTOR 1

CLOUD-TOP TEMPERATURE AND CLOUD GROWTH FACTOR [IR].
DETERMINE AMOUNT THAT THE COLDEST CLOUD TOPS INCREASED WITHIN HALF-HOUR.

	>2/3° LAT	>1/3° ≤2/3° LAT	≤1/3° LAT OR SAME	AREAL DECREASE OF SHADE OR WARMING FROM WHITE TO RPT GRAY OR WITHIN THE RPT GRAY	COLDEST TOPS 1 OR MORE SHADES WARMER
MED GRAY (-32 TO -41°)	0.25	0.15	0.10	0.05	T
LT GRAY (-41 TO -52°)	0.50	0.30	0.15	0.10	↓
DK GRAY (-52 TO -58°)	0.75	0.40	0.20	0.15	
BLACK (-58 TO -62°)	1.00	0.60	0.30	0.20	
RPT GRAY* (-62 TO -80°)	1-2.00	0.60-1.00	0.30-0.60	0.30	
WHITE (BELOW -80°C)	2.00	1.00	0.60	0.40	0.10

*COLDER REPEAT GRAY SHADES SHOULD BE GIVEN HIGHER RAINFALL ESTIMATES.

OR

DIVERGENCE ALOFT FACTOR* [IR AND 200-MB ANALYSIS].

MED GRAY	LT GRAY	DK GRAY	BLACK	RPT GRAY	WHITE
0.15	0.30	0.40	0.60	0.60-1.00	1.00

*IR IMAGERY SHOWS EDGES OF THUNDERSTORM ANVIL ALONG THE UPWIND END FORMING A LARGE ANGLE OF BETWEEN 50-90 DEGREES POINTING INTO THE WIND; 200-MB ANALYSIS OFTEN SHOWS THESE STORMS JUST DOWNWIND FROM WHERE THE POLAR JET AND SUBTROPICAL JET SEPARATE.

FACTOR 2

OVERSHOOTING TOP FACTOR [<u>VIS</u>, IR]. <u>ADD TO THE OVERSHOOTING TOPS*</u>:

MED GRAY	LT GRAY	DK GRAY	BLACK	RPT GRAY	WHITE
0.50	0.45	0.40	0.30	0.30	0.30

*HIGH-RESOLUTION VISIBLE IMAGERY IS THE BEST DATA FOR DETERMINING THIS FACTOR.

FACTOR 3

THUNDERSTORM OR CONVECTIVE CLOUD LINE MERGER FACTOR [<u>IR</u>, <u>VIS</u>]. ADD 0.50 TO THE COLDER TOPS IN THE AREA OF THE MERGER.

FACTOR 4

SATURATED ENVIRONMENT FACTOR [<u>IR</u>, <u>VIS</u>]. ADD TO THE COLDER TOPS STATIONARY FOR A GIVEN AMOUNT OF TIME:

	MED GRAY	LT GRAY	DK GRAY	BLACK	RPT GRAY	WHITE
≥1 HOUR BUT <2 HOURS	0.20	0.20	0.20	0.20	0.30	0.30
≥2 HOURS	0.40	0.40	0.40	0.40	0.50	0.50

FACTOR 5

MOISTURE CORRECTION FACTOR = PRECIPITABLE WATER (SFC-500MB) × RELATIVE HUMIDITY (SFC-500 MB)

STEP 3

FACTORS ARE SUMMED AND MULTIPLIED BY MOISTURE CORRECTION FACTOR:

TOTAL HALF-HOURLY CONVECTIVE RAINFALL ESTIMATES (IN INCHES) =

[(CLOUD-TOP TEMPERATURE AND CLOUD GROWTH FACTOR OR DIVERGENCE ALOFT FACTOR)[1] + OVERSHOOTING TOP FACTOR[2] + MERGER FACTOR[3] + SATURATED ENVIRONMENT FACTOR[4]] × MOISTURE CORRECTION FACTOR[5]

END OF TECHNIQUE

<u>Table 3:</u> The Scofield-Oliver Convective Rainfall Estimation Technique.

strong vertical wind shear environments, the heaviest rain often falls in the upwind-edge of wedge-shaped clusters, where the enhanced IR temperature gradient is the tightest. Comparison of two successive pictures shows the motion of the anvil edge, which is usually greatest in the downwind direction. The heaviest rain is under the part of the anvil which moves the least. Also, the clouds are brightest and sometimes textured at the upwind end. Upper level (300 mb) wind charts can be used for determining the upwind direction. For thunderstorms in an environment that has no vertical wind shear, there often is a uniform IR temperature gradient around the entire anvil and the active area is near the center of the anvil. Active portions also are located under overshooting tops (in VIS imagery). Other clues would be where low-level inflow is indicated in VIS imagery or where there is a radar echo associated with the cloud feature in the satellite picture.

b. Cloud-Top Temperature and Growth Factor

As shown in Factor 1 of Table 3, the half-hourly rate of areal expansion of the coldest tops (measured in degrees of latitude) determines the rainfall rate assigned from this factor. As the coldest tops increase in area, the rainfall rate increases. Note that when the coldest tops begin to warm, estimated rainfall amounts range from only a Trace to .10 inches. The growth is measured along the largest axis of the coldest tops in either picture. An example of this is shown in Figure 8 (Spayd, 1985). Suppose that the 1900 GMT satellite picture consists of an oval-shaped thunderstorm cluster possessing a light gray MB-curve enhancement. Now suppose that by 1930 GMT the light gray area has decreased in size, but there is a small area of dark gray enhancement (even colder tops). The "growth factor" of the SOCRET would assign a rainfall rate of 0.2" per 1/2 hour in the region of these colder tops (see Table 3) because the dark gray has increased from zero areal coverage at 1900 GMT to something less than 1/3° latitude at 1930 GMT.

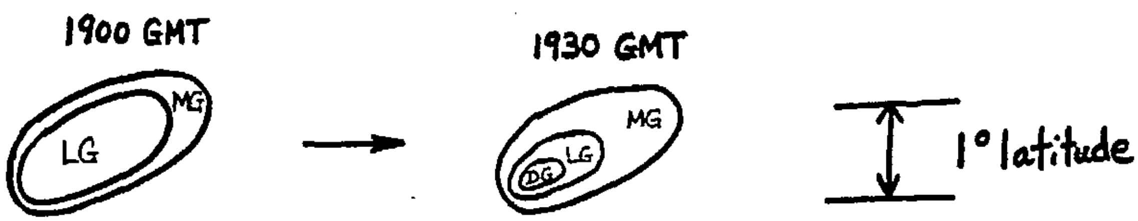

Figure 8. An example of the interpretation of the SOCRET "Cloud Top Temperature and Growth Factor" (MG = medium gray, LG = light gray, DG = dark gray.)

c. Divergence Aloft Factor

This factor should really be named the "Diffluence Aloft Factor." It is used when the IR imagery shows "edges of thunderstorm anvils along the upwind end forming a large angle (between 50-90 degrees) pointing into the wind." These storms often occur just downwind from where the 200-mb polar front jet and the subtropical jet separate. This "Diffluence Factor" assigns to the coldest tops amounts ranging form 0.15 inches to 1.00 inches, depending on the enhancement shade. Note: This factor is only used if there is strong diffluence aloft and the "Diffluence Factor" gives a higher rainfall estimate than the "Cloud Top Temperature and Growth Factor." Only one of these two factors is counted — whichever is greater. "This factor may also be used for MCC's exhibiting pronounced anticyclonic outflow (divergence) aloft" (Scofield, 1984).

d. Overshooting Top Factor

Rainfall is often enhanced underneath overshooting tops, which are more easily recognized in the higher resolution (1 km) VIS pictures than in IR imagery. In VIS imagery, overshooting tops are quite bright and textured; in the IR, they are very small (only a pixel or two wide) and cold (usually colder than -62°C). In the IR, they are often difficult to distinguish from embedded cells in the downwind part of the anvil cirrus or simply from locally higher or denser cirrus clouds. Rainfall rates assigned from this factor range from 0.30 to 0.50 inches per half-hour (see Table 3, Factor 2) and are added only to the regions of the overshooting tops. Note the apparent inconsistency in the values in Table 3, Factor 2. Colder clouds receive less of an addition from this factor than warmer clouds! This is because verification of the original SOCRET showed that the combination of all of the other factors led to overestimates for colder tops and underestimates for warmer tops. Thus, the "Overshooting Top Factor" is strictly an empirical correction factor.

e. Thunderstorm or Convective Cloud Line Merger Factor

When thunderstorm clusters or lines merge, there is an explosive, rapid cooling of tops and there can be a dramatic increase in rainfall rates. This "Merger Factor" adds 0.50 inches per half-hour (see Table 3, Factor 3) to the satellite precipitation estimate for colder tops in the area of the merger, regardless of the enhancement shade of these colder tops.

f. Saturated Environment Factor

This factor assumes that when a thunderstorm cluster remains over the same area for at least one hour, a large area has become saturated to great heights, with dry air no longer entraining into the sides of individual updrafts in the center of the cluster. Storms in the interior of the cluster have rainfall rates much greater than that for isolated storms. Rainfall rates ranging from 0.20 inches to 0.50 inches per half-hour are added to the estimates for the coldest stationary tops (see Table 3, Factor 4). According to Scofield, this factor may also be used for thunderstorms that regenerate at the same location and traverse the same path.

g. Moisture Correction Factor

This factor is used to account for the influence of dry or moist environments on the amount of rainfall produced by thunderstorms. Originally, this factor equalled the current precipitable water (PW), divided by 1.5 inches (the average PW on which the technique was based). Statistically, however, better estimates are obtained by using the current, modified moisture correction factor (see Table 3, Factor 5), which multiplies the PW (sfc-500 mb) by the mean relative humidity (RH) (sfc-500 mb). Thus, a high PW content will not produce as much rain as expected if the RH is very low. If thunderstorms form along a tight gradient of PW and RH, the estimator assumes the low level inflow is from the moist air and uses the higher values of each. It should be noted that since facsimile copies of PW and RH are only available every 12 hours, old charts must be adjusted for moisture advection.

h. The Total Half-Hourly Convective Rainfall Estimate

Rainfall amounts from factors 2-6 above are summed and then multiplied by the Moisture Correction Factor in Section 7 above. This is the official satellite rainfall estimate.

i. An Exception: Warm Top Convection

Quite often, especially in the winter, thunderstorms are capped by a low tropopause or a stable layer below the tropopause. Therefore, the cloud top temperature at the tropopause might only be -46°C (for example), not -70°C. However, even though the thunderstorms possess only a "light gray" enhancement in the satellite imagery, they have realized their thermodynamic potential and are releasing abundant rainfall. The rainfall rate is greater than what would be predicted using values for the standard "light gray" enhancement. The "warm-top" modification for a given location involves the calculation of the equilibrium level (or expected thunderstorm anvil height) from the nearest and most recent sounding (see Figure 9). The temperature corresponding to this equilibrium height is then assigned the rainfall rate of the warmest "repeat gray" level (-62°C to -67°C). This adjusted cloud-top temperature is used for factors 2-6 above.

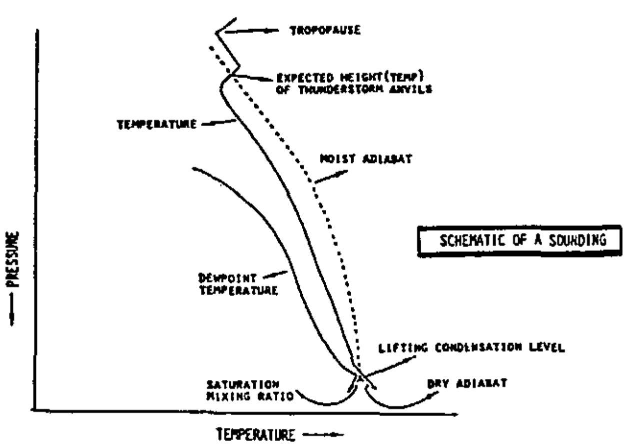

Figure 9. Warm Top Modification to the Convective Technique. (from Scofield, 1984)

3. Limitations of the Satellite Sensor and Implications for the Assignment of Isohyets

When interpreting enhanced IR satellite pictures, the meteorologist must be aware that the satellite sensor cannot respond fast enough to large changes in temperature in the horizontal. The result is that the IR enhancement is often displaced in a downwind direction. (This is different from the downwind displacement discussed earlier which occurs due to strong vertical wind shear.) Also, due to the limitation of the sensor and the fact that the satellite scans from west to east, sometimes the coldest thunderstorm top appears too warm in the enhanced IR picture. These effects are most pronounced in very localized, strong thunderstorm towers, where there can exist a large temperature difference between the warm ground under sunny skies and the cold tower. The displacement effect also can be important in small, wedge-shaped thunderstorm clusters, where the IR temperature gradient is strong (see Brady's Bend Flood case, Scofield, 1981). For circular clusters or MCC's, which often have a weak IR gradient, this effect is not very important. There are obvious implications for the assignment of isohyets. Contours of estimated rainfall must be displaced upwind just a little bit to correct for the downwind displacement and the estimator must carefully evaluate the true height of the coldest tops using upper air and radar charts. The following two examples will illustrate these problems:

<u>EXAMPLE 1</u> (see Figure 10a): Suppose that a small thunderstorm cluster forms with a mean west wind blowing the cirrus downwind to the east. If the thunderstorm cloud tops and the anvil cirrus have a temperature of -70°C and the surrounding warm ground is at +30°C, then the ΔT=100°C. The satellite sensor can respond to a ΔT of only 26°C per pixel. So, it takes four pixels to respond to this ΔT of 100°C. As the satellite scans from west to east, the first two clear pixels are a warm +30°C. The third pixel's average temperature might be only +16°C because a small part of the area had been influenced by the -70°C storm. The next pixel, which is covered entirely by -70°C clouds is only able to register -10°C, since this is 26°C less than the previous pixel. Similarly, the next pixels' temperatures decrease in increments of 26°C until the -70°C is reached. Thus, the resulting IR enhancement is displaced downwind of the coldest tops. The "repeat gray" level is not achieved until four pixels downwind. One image pixel as represented on the McIDAS computer or on a hard-copy satellite photo covers 4 km from east to west and 4 km from north to south at the satellite subpoint. Because the earth is an oblate spheroid, the same size pixel projected onto the earth's surface at 40°N latitude covers roughly 6 km on a side. Thus, a four pixel displacement in the Midwest is on the order of 24 km — this could mean the difference between a flood on one side of town versus the other. In Figure 10a, notice that the enhancement jumps from "medium gray" to "black" without any "light gray" or "dark gray." While this does occasionally occur, it is much more common to have a continuous progression of MB-enhancement shades. The presence of low or middle clouds usually tends to smooth out the temperature gradient somewhat.

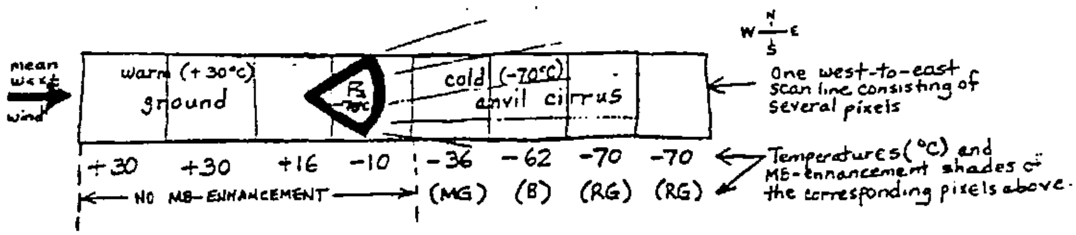

Figure 10a. Depiction of Example 1. Enhancement is displaced downwind (MG = medium gray, B = black, RG = repeat gray) (from Spayd, 1985).

EXAMPLE 2 (see Figure 10b): Given the same situation as in Example 1, except with a mean wind from the south, what will be the result? As the satellite scans from west to east, it measures the warm +30°C ground to the west of the storm. Because of the 26°C ΔT constraint and the narrowness of the storm, the coldest pixel might only reach -10°C (still unenhanced) before warming back up to +30°C to the east of the storm. Thus, the scan line shown in Figure 11 completely failed to capture the -70°C thunderstorm! The only way that -70°C could be accurately depicted in the IR enhancement is if the anvil to the north becomes wide enough to allow the sensor to detect the ΔT of 100°C (four pixels). Thus, if scan lines to the north of the main thunderstorm towers reach the "repeat gray" enhancement, this again represents a displacement of the IR enhancement in a downwind direction.

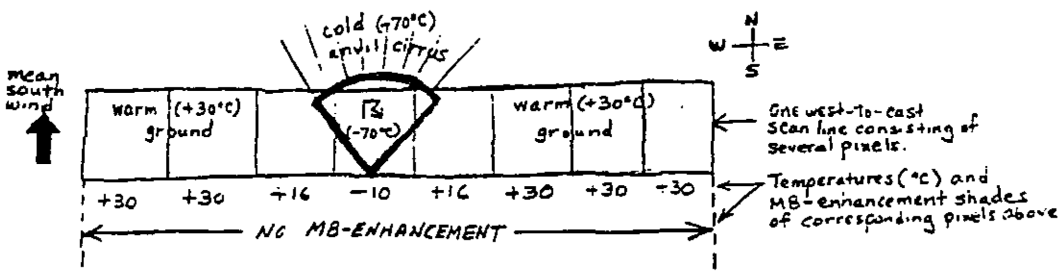

Figure 10b. Depiction of Example 2. Magnitude of narrow thunderstorm tower is -60°C too warm.

Another factor which causes displacement of the colder tops in satellite imagery is parallax. Objects, such as thunderstorms, which are above the earth's surface interfere with the direct "line-of-sight" from the satellite to the earth. Their projection onto the earth's surface is displaced northward (in the Northern Hemisphere) because the GOES satellite is in orbit above the equator. Over the central United States, there also is a westward component to the displacement because the GOES-East satellite (from which data was used in this case study) is geostationary above 75° West longitude. The taller the thunderstorm, the larger the displacement. Figure 11, taken from a NESDIS Satellite Applications Laboratory training exercise, shows the distance and direction a 40,000 ft top must be moved in order to place it in its correct location over the earth's surface. Over Missouri, the parallax error is on the order of 10 km, or roughly two pixels in an infrared image. While parallax is not a limitation of the satellite sensor, it is mentioned here because it does displace colder thunderstorm tops by a small amount.

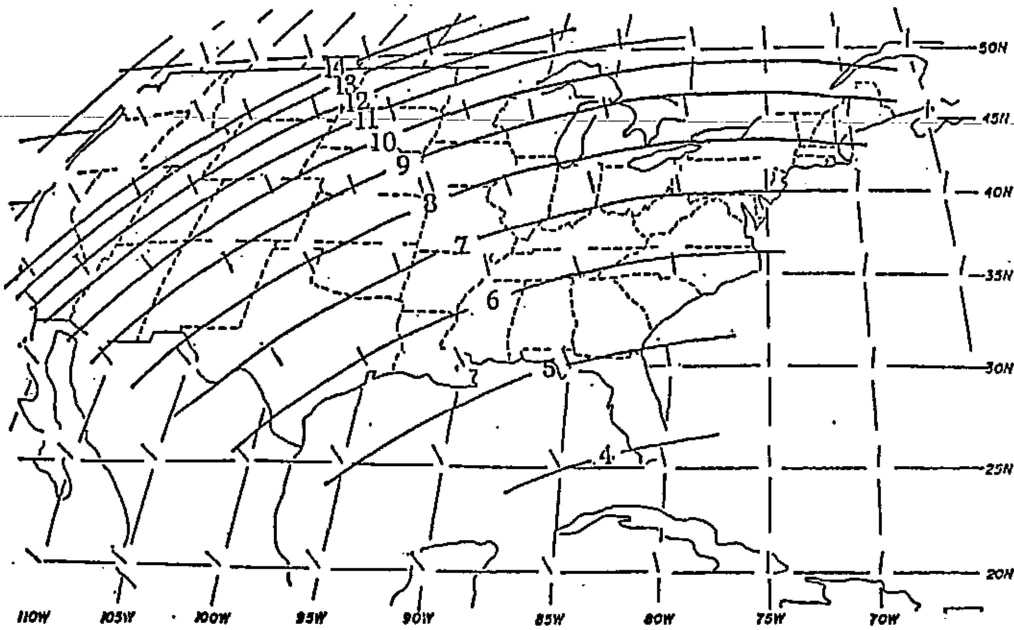

Figure 11. Distance (n mi) and direction at 40,000 ft. top must be moved to place it over earth's surface (for 60,000 ft. tops, add 50%; for 20,000 ft. tops, subtract 50%).

C. McIDAS ANALYSIS PROCEDURE

The physical set-up for the computation of estimates consisted of a computer terminal (keyboard and CRT screen) with a video monitor for displaying satellite imagery and a joystick control for positioning the cursor. This McIDAS system has the ability to digitally store at least eight consecutive visible images and at least eight infrared images. One can easily flicker between VIS and IR images for the same time. The images can be put into motion and the dwell rate can be manually adjusted. In addition, the McIDAS system has the ability to store at least sixteen graphics frames.

The McIDAS system used for this study simulated the capacities of the Interactive Flash Flood Analyzer (IFFA - an earlier version of the current McIDAS) at the Synoptic Analysis Branch of NESDIS in Washington, D.C. The IFFA uses an older Harris computer system, but a new IBM system is used at the University of Wisconsin. Therefore, there were some different commands and the program had to be adjusted a little. The program at Wisconsin was adjusted to:

(1) allow isohyets of estimated precipitation to be drawn. (A closed contour was drawn by connecting a series of short line segments.)

(2) allow values to be assigned to the contours after they were drawn.

(3) assign the specified values to all grid points that lay within the contour. Thus, outer (smaller valued) contours had to be drawn before inner (larger valued) contours.

The spacing between grid points was selected to be 0.2°C of latitude and longitude (22 km or≈14 miles), since this is about the accuracy of current operational estimates (Field, 1985b).

Since it was necessary to create an MB-curve enhancement, the standard McIDAS IR enhancement curve had to be adjusted. A stretching technique was used, whereby detail in the lower brightness (or count) values was sacrificed in order to get more detail in the higher brightnesses (see McIDAS Training Manual). These "stretched" count values then were enhanced with colors that corresponded to the same temperature cutoffs as the MB-curve, used in the Scofield-Oliver Technique. An example of the color enhancement is shown in Figure 12. (For non-colored renditions of this figure... "Medium Gray"=purple; "Light Gray"=red; "Dark Gray"=green; "Black"=blue; "Repeat Gray"=sky blue; "White"=white.) The yellow at the green-red interface in Figure 12 resulted from the color xeroxing process and was not used in the research.

Satellite precipitation estimates were computed each half-hour for a 24-hour period over the southern Midwest from 12Z, July 20 to 12Z, July 21, 1981. A separate grid for each half-hour of estimates was saved. The 48 half-hourly grids of estimates then were added together to make a 24-hour total. The following data sources were used in the computation of estimates: satellite pictures (1 km VIS; 4 km IR that is represented to the equivalent of 1 km resolution), NMC surface, upper air, RH, PW, and radar charts, and hourly surface observations. Other data that were used, but that did not explicitly enter into the calculations included soundings (based on mandatory and significant level RAOB data) and hard-copy satellite pictures of the entire U.S. with county overlays (to get an overview of synoptic features).

There were several types of storms involved in this case study. The precipitation which fell in Missouri, southern Illinois, western Kentucky, and western Tennessee was mainly from a regenerative wedge type of convective thunderstorm cluster. Figure 12 shows this wedge after it had just formed late in the day on July 20, 1981 in Missouri. In Oklahoma, there was a combination of squall line and single-clustered thunderstorms. These moved into Arkansas by the early morning on July 21, 1981. Other shorter-lived cells occurred in the drier air in western Kansas.

Several of the factors in the Scofield-Oliver Technique were taken into account in computing the satellite estimates. In particular, explosive mergers occurred with the wedge system as it progressed through southeastern Missouri, where there was strong moisture flux convergence. Also, the clusters in northwestern Arkansas on July 21 were stationary for several hours. There were numerous instances where the overshooting top factor was used. No warm-top convection occurred on these days. The magnitudes of the estimates for this case study were subjectively adjusted up or down (by approximately 15%) to include the effects of moisture flux convergence into an area. These fields were derived by McIDAS using hourly surface observation data (Figure 13). Although the Technique prescribes a modification of old RH and PW charts to

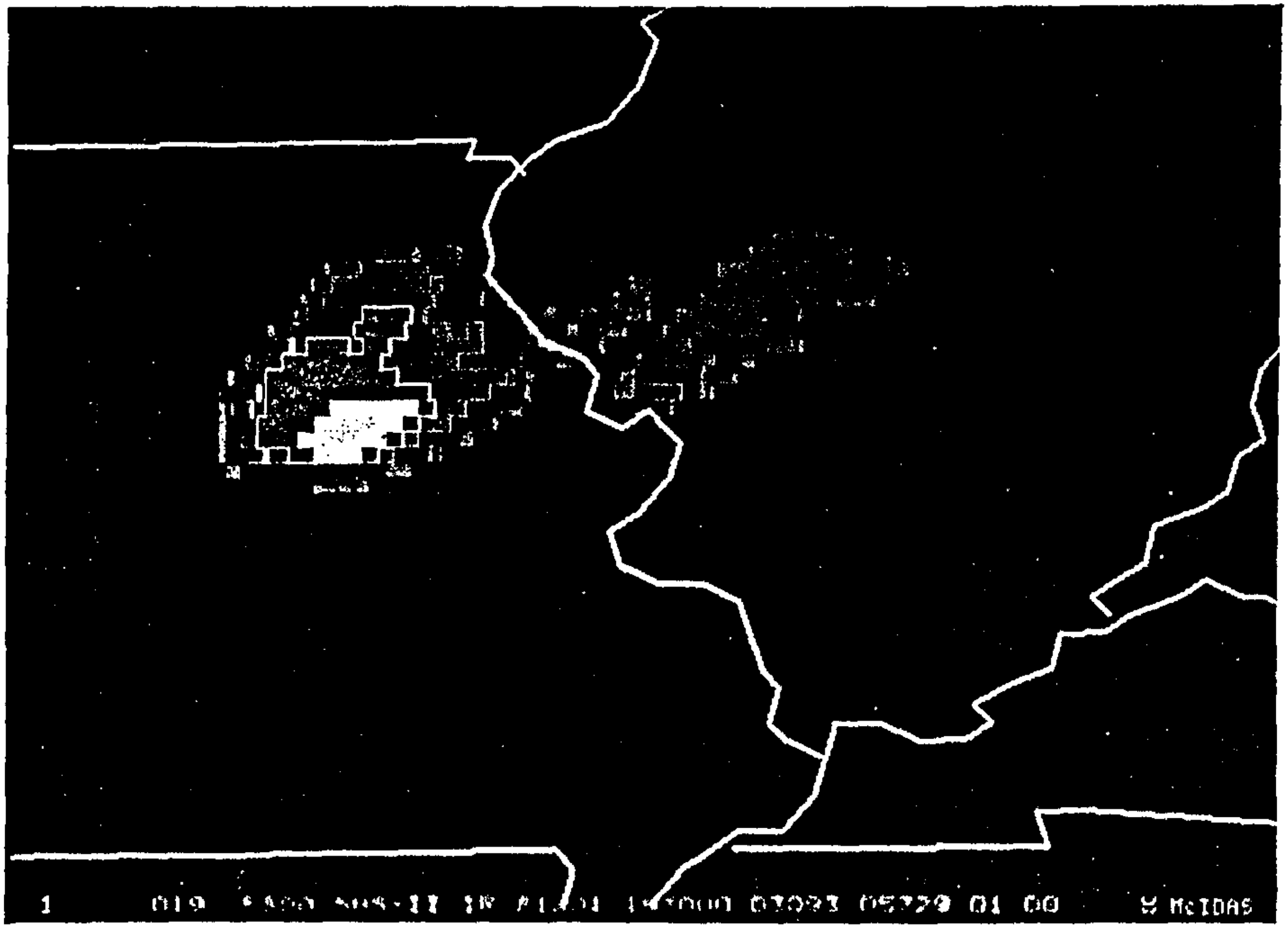

Figure 12. Infrared satellite photo of wedge-shaped thunderstorm cluster over Missouri at 1930Z on July 20, 1981, color enhanced with MB-curve temperature thresholds.

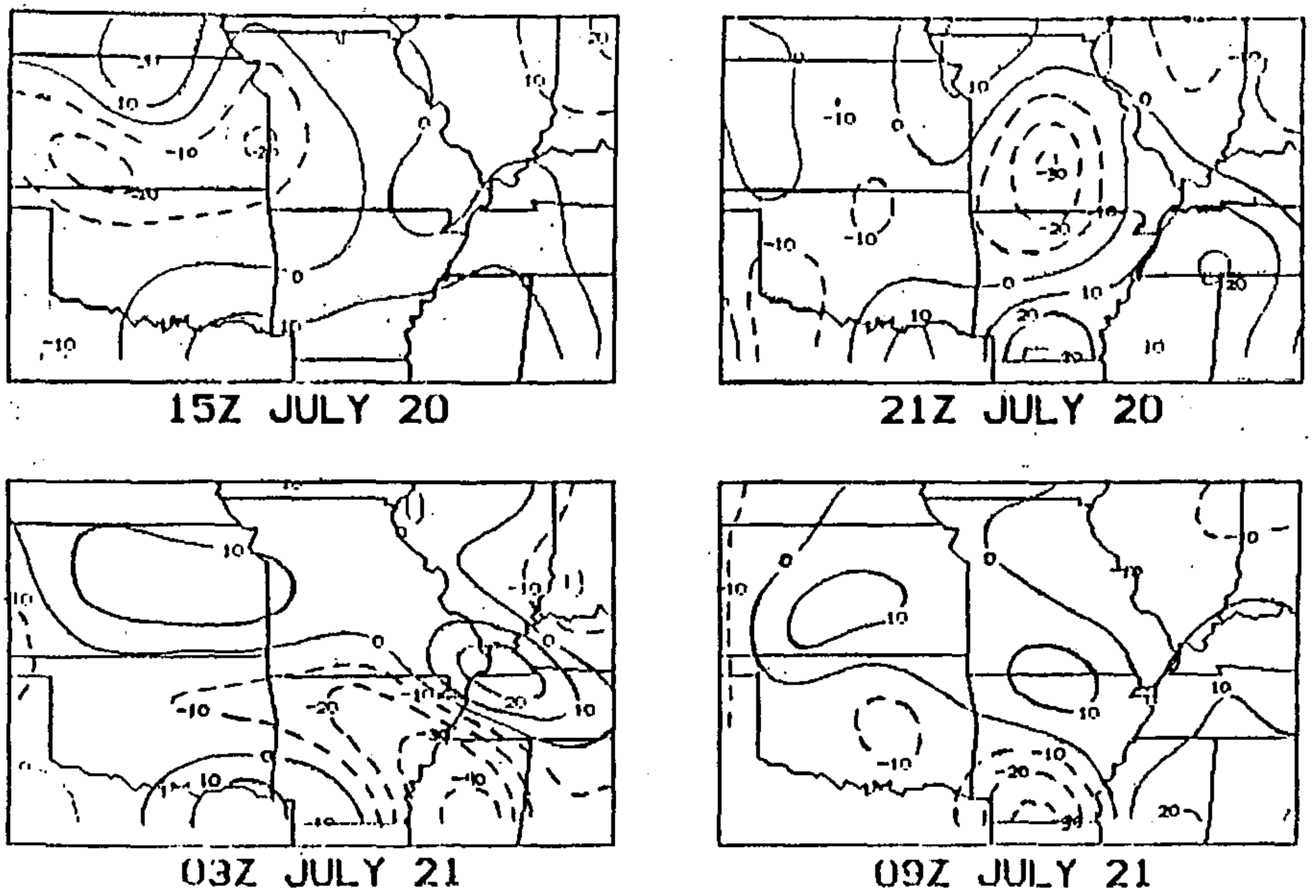

Figure 13. Surface moisture flux divergence at 6-hour intervals starting at 15Z July 20, 1981. Units are x $10^{-8}sec^{-1}$. Negative areas (dashed) represent convergence.

account for moisture advection, it was felt that moisture flux convergence would be an even better modification, since it includes both an advective term and a convergence term (see equation below):

$$\nabla \cdot q\vec{V} = q\nabla \cdot \vec{V}\ \vec{V} \cdot \nabla q$$

Note the convergence maximum over Missouri at 2100Z (Figure 13). Storm growth and decay was highly correlated with these fields.

It should be noted that the estimation procedure used in this research differed from that used by NESDIS' Synoptic Analysis Branch in two ways: (1) for this research, every convective event was estimated, not just those with flash flooding potential, and (2) the estimator was not concerned with which county the storms were in.

IV. OBSERVED RAINFALL

A dense network of rainfall observations was obtained from the National Weather Service Cooperative Observer reports listed in the July, 1981 Climatological Data (CD) for thirteen states in the Midwest. For the most part, these included reports from Class 1 and Class 2 Cooperative Observers. (Class 1 observers report at a specified time every day and Class 2 observers report only when the rainfall total surpasses a given threshold amount--usually taken to be 0.1".) A list was compiled of 24-hour reports, measured from 7AM-7AM on July 20-21, since these correspond to 12Z-12Z, July 20-21 (see Appendix C). This enabled the observed reports to be compared with the satellite estimates and model forecast for the same time period.

Another data source used was the Hourly Precipitation Data (HPD), which is available from the National Climatic Data Center in Asheville, North Carolina. It gives an hour-by-hour listing of precipitation for those stations which have recording rain gauges. Thus, stations which reported at a time other than at 7AM in the CD were now able to be considered, since it could be determined during which hours the precipitation fell. This was especially important because in the CD, observations from all National Weather Service Offices are reported from local midnight to local midnight, instead of 7AM to 7AM. These could now be included.

The stations from the original 7AM-7AM list from the CD were then compared with those in the HPD (if they had a recording rain gauge) to double-check that the 24-hour total rainfall reported in the CD did in fact fall between the hours of 7AM and 7AM. Several mistakes were found. For example, the CD listed David City, Nebraska as having had 0.53" from 7AM-7AM (12Z-12Z) ending on July 21. But the HPD showed that the 0.53" actually occurred later on July 21 (from 13Z-18Z). These erroneous reports were deleted from the data.

When one compares reports from the CD with those from the HPD, differences may be found, usually to only a small degree. According to Dr. Doug Clark, Wisconsin State Climatologist, this is because the data come from different weighing gauges, located at the same station. For example, at Centralia, Missouri, there are more than a dozen rain gauges. The CD reports rainfall from the Standard eight-inch gauges, except for National Weather Service stations, which use Universal eight-inch or 12-inch gauges. The HPD reports rainfall from both the Universal eight-inch or 12-inch gauges (which have strip charts) and the Fisher-Porter gauges (which have punched tape instead of a strip chart). Most reports from the HPD are rounded to the nearest tenth of an inch, whereas the CD reports to the nearest hundredth. The CD is generally considered to be more reliable and its values were used when both data sources were available for a given location.

The National Meteorological Center provides a 24-hour observed rainfall chart, which is available only over the NAFAX/DIFAX weather facsimile circuits. However, for the 24 hours ending at 12Z on July 21, 1981, this chart was lacking a significant amount of data and thus was unable to give an accurate representation of what actually occurred. The more than 300 observations acquired from the CD and HPD for 7AM-7AM (12Z-12Z) were invaluable. However, there still remained large sections of several states which had data voids. Because many Cooperative Observer reports are made from 8AM-8AM (13Z-13Z), the data set was expanded to include these. The additional reports gained in this manner helped fill large gaps in the precipitation data. (See Appendix B for an example of the effect of adding 8AM-8AM reports in Kentucky.) Treating these 13Z-13Z reports as being 12Z-12Z observations may have introduced some error in the data set. In regions where precipitation occurred from 12Z-13Z on July 20, the 8AM reports will be too low, since they do not include this. Similarly, in regions where rain fell from 12Z-13Z on July 21, the 8AM totals will be overstated. Nevertheless, some 8AM-8AM reports were included in the data set because it was felt that the improved spatial resolution from the inclusion of these additional reports probably far outweighed any magnitude error which may have been introduced.

Once the data were gathered, the observed amounts and locations were entered into the McIDAS system. The actual uncontoured observations for each state (from 7AM, July 20 to 8AM, July 21) can be found in Appendix D (plotted maps).

V. THE SUBSYNOPTIC SCALE MODEL

The Subsynoptic Scale Model (SSM) is a mesoscale numerical model that was developed and tested by the Australian Bureau of Meteorology (ABM) and the Australian Numerical Meteorology Research Center (ANMRC). Since its inception in 1972, it has undergone many revisions. The SSM has been and currently is being tested at the Space Science and Engineering Center and the NOAA/NESDIS Research Development Laboratory at the University of Wisconsin—Madison.

"The model originally was formulated by Maine (1972) and later substantially revised by Noar and Young (1972)" (McGregor, Leslie, and Gauntlett, 1978). It was implemented as a regional operational model by the ABM in September, 1977, after many revisions had taken place. One major revision included the use of primitive equations (McGregor, Leslie, and Gauntlett, 1978), after which the model became known as the Australian Region Primitive Equations (ARPE) model. Another revision included the introduction of a staggered horizontal grid (McGregor and Leslie, 1977). The exact formulations used for the staggered horizontal grid are given in Mills et al. (1981). Other improvements to the model are discussed in Leslie, Mills, and Gauntlett (1981) and in Mills and Hayden (1983).

For use in the United States, "the finite differencing scheme devised by Corby et al. (1972) to minimize truncation error in pressure gradient terms over regions of steep topography has been included in the ANMRC code" (Mills and Hayden, 1983). A Kuo-type convective parameterization scheme (see Kuo, 1965, 1974) has replaced the Arakawa-Schubert scheme described in McGregor, Leslie, and Gauntlett (1978). Also, a much more comprehensive planetary boundary layer (PBL) scheme has been included (Mills, Diak, and Hayden, 1983). The scheme includes stability-dependent eddy vertical diffusion in the PBL (Blackadar, 1974) for heat momentum and moisture, a similarity-theory surface layer (Businger et al., 1981), a description of the effects of atmosphere and clouds on the surface radiant flux (Katayama, 1972; Paltridge and Platt, 1976), and a surface energy balance equation.

The SSM's horizontal resolution, which was tested operationally at 250 km now has been upgraded to 67 km or 134 km. (The reason for the upgrade was to make it compatible with the resolution of satellite sounding information.) Thus, its grid spacings are smaller than those used in current operational numerical weather prediction models by the National Meteorological Center (NMC). For the July 20, 1981 case study, a resolution of 134 km was used. The main reason for this was that the model had already been run by NESDIS and no further costs would have to have been incurred. The model was initialized at 1200 GMT, July 20, 1981. A summary of the latest SSM characteristics -- those which were employed in this case study -- is shown in Table 4.

The precipitation forecasts produced by the SSM are broken down into large-scale precipitation and convective precipitation. For this case study, it so happened that all of the modeled rainfall was of convective origin. This is fortunate, since a comparison is being made between the SSM and satellite precipitation estimates derived from a purely convective technique.

Table 4
Prognosis Model Characteristics
(from Diak et al. (1985))

Primitive equations model in σ-coordinates

Ten vertical levels at $\sigma = .09, .19, .29, \ldots, .99$

Horizontal resolution: 67 km or 134 km

Staggered horizontal grid (Arakawa "C" grid)

Lambert Conformal horizontal grid projection

Semi-implicit time differencing (Δt = 10 min.)

Similarity theory surface layer

Stability dependent vertical diffusion of momentum, heat, moisture above surface layer through depth of PBL

Surface short wave and long wave flux modified by cloudiness

Surface energy balance equation

Large-scale precipitation

Kuo-type convective parameterization

Horizontal diffusion of momentum, heat, and moisture

Updated boundary conditions

VI. SMOOTHING REQUIREMENTS FOR DIFFERENT COMPARISONS

In order to be able to objectively evaluate and compare the model, estimates, and observations, it was desired to have grids with the same spacing and location. This would allow McIDAS to easily subtract the grid point values to obtain difference fields. However, this required interpolating observations to a uniformly spaced grid. The most noted examples of using weighted averages to interpolate to a uniform rectangular grid are the methods of Cressman (1959) and Barnes (1964). The interpolation scheme that McIDAS employs is called a "Fast Barnes Analysis" (Hibbard and Wylie, 1985).

The results from the "Fast Barnes Analysis" are nearly identical to those obtained using the standard Barnes technique, but are able to be calculated much more quickly. If x number of observed data points are to be interpolated to y number of grid points, the computing time used by the Barnes and Cressman methods is proportional to xy, whereas the "Fast Barnes" method's time is proportional to x+y. The only instance where deviations from the Barnes method can result are in large data void areas, where information has to be extrapolated over long distances (e.g., 850 mb radiosonde temperatures over the Rocky

Mountain states). However, for this case study, a dense network of cooperative observer reports and satellite estimates were available. For more information on the "Fast Barnes" method, refer to the Hibbard and Wylie paper.

The weighting factor used by McIDAS as a function of search radius away from the particular grid point in question is given by:

$$w = e^{-\frac{10}{\text{SMOOTH}}\left(\frac{r}{\text{INC}}\right)^2}$$

where r = distance from grid point to observation
INC = grid point spacing = Δx = 0.2° latitude = 22 km
SMOOTH = smoothing factor; an integer keyword on McIDAS.

Since the rainfall observations were at randomly oriented positions, they had to be interpolated to grid points and it was advantageous to use a minimum of smoothing. Using the above formula, in order for the "e-folding radius of influence" (i.e., that distance within which the weighting is higher than 1/e and observations significantly contribute to the final value at the grid point) to be equal to 1 Δx (22 km), the smoothing factor had to equal 10. This low smoothing factor was applied to the observed rainfall data. To be consistent, it also was applied to the satellite estimates, even though they were already at grid points. There was little noticeable change in magnitude or location when this minimal amount of smoothing was applied. In this way, the estimates and observations were compared.

While the aforementioned grids were "pseudo-latitude-longitude" projections with spacings of 22 km, the SSM model had a Lambert Conformal projection with a grid spacing of 134 km. A regridding and interpolation program developed by Geary Callan of the NESDIS Development Laboratory was employed to change the Lambert Conformal projection to the pseudo-latitude-longitude projections of the estimates and observations. (This was necessary in order to be able to objectively verify the SSM model on a common grid with the estimates and observations.) The program (named "REGD" on McIDAS) produced a model value every 22 km, even though in reality the true model resolution remained at 134 km. Since model precipitation values represent a large area average, it is not valid to directly compare them with the slightly smoothed estimates or observations. It is necessary to filter out small-scale features from the estimates and observations. Given the e-folding constraint that $w = e^{-1}$ and given INC = 22 km and r = 268 km (=2 Δx, the minimum needed to define a wave), it can be seen (by plugging these values into the above weighting factor formula and solving for "SMOOTH") that the smoothing factor had to be increased to 1,484. The exact degree to which different wave length features were filtered out can be determined by the Barnes Response Function (see Maddox, 1980). Thus, this large smoothing factor was applied to the estimates and observations for model verification. As a result of this large smoothing, maximum rainfall observations of 2.8" were reduced to nearly 1.0" (because the rainfall is spread out over the surrounding area) and there was some displacement of the maxima. The same reductions in magnitude and displacement of the maxima occurred when this high smoothing factor was applied to the satellite estimates.

Finally, a comparison was then made between the highly smoothed satellite estimates and observations.

VII. COMPARISONS

A. ESTIMATES VS. OBSERVATIONS -- LOW SMOOTHING

Figures 14-16 give an overview of the observations, satellite estimates, and a difference field (estimates minus observations), respectively, using the low smoothing factor. Detailed close-up maps will follow. Note that the contour intervals are not the same for each of these figures. The precipitation associated with the regenerative convective wedge can be seen over east central and southeast Missouri in both the estimates and the observations. Rainfall associated with the multiple clusters of thunderstorms in eastern Oklahoma and Arkansas also is depicted in both the estimates and observations. From Figure 16, it appears that there were large overestimates in these regions. No precipitation was observed at any of the reporting stations in central and western Oklahoma, where estimates from a squall line and subsequent single-clustered cells were derived. In the drier air over Kansas, rainfall from more isolated, single-clustered thunderstorms is depicted.

The observations, satellite estimates, and a difference field (estimates minus observations) for Arkansas are shown below in Figures 17-19, respectively. The estimates are in relatively good agreement with the observations with respect to location. The orientation of the entire estimate area as well as the location of the estimated maxima (Figure 18) corresponds closely to the precipitation area depicted by radar (Figure 4). However, there appear to be many overestimates. Figure 19 reveals two main overestimate areas of about 4". Much of this can be attributed to the sparsity of data in Arkansas. Figure 20 shows the distribution of the uncontoured observed data in Arkansas. The largest gaps were in the regions of the large errors in Figure 19. Thus, nearly 4" may actually have fallen, as suggested by radar, but was not officially observed. An examination of the digital printout of the gridded difference field (not shown here) showed that had the 4" estimate in northwest Arkansas been one grid point to the west, the 4" overestimate would only have been a 1.5" overestimate. This slight displacement probably resulted from the slight interpolation that was done. Another factor could also have contributed to overestimates. The McIDAS analysis procedure was such that even if the thunderstorm cell was very small, the isohyet had to be drawn large enough to ensure that it captured at least one grid point. For all of these reasons, looking only at difference fields can be misleading. The author's estimates compared favorably to those issued to the National Weather Service by the NESDIS Synoptic Analysis Branch (SAB) on the days of this study. SAB estimated a rainfall rate of 2.5"/hour for Pulaski County in central Arkansas from 0900-1000 GMT on July 21, with a two-hour accumulation of 3.9" from 0900-1100 GMT. The author estimated an hourly rate of 2.4" and a three-hour (0900-1200 GMT) total of 4.2".

Observations, satellite estimates, and difference fields for Missouri/Illinois/Kentucky/Tennessee and Kansas/Oklahoma are shown in Figures 21-23 and 24-26, respectively. The estimated areas and orientation of the maxima compare well with the observed data, with a few exceptions. The report of 1.76" at Van

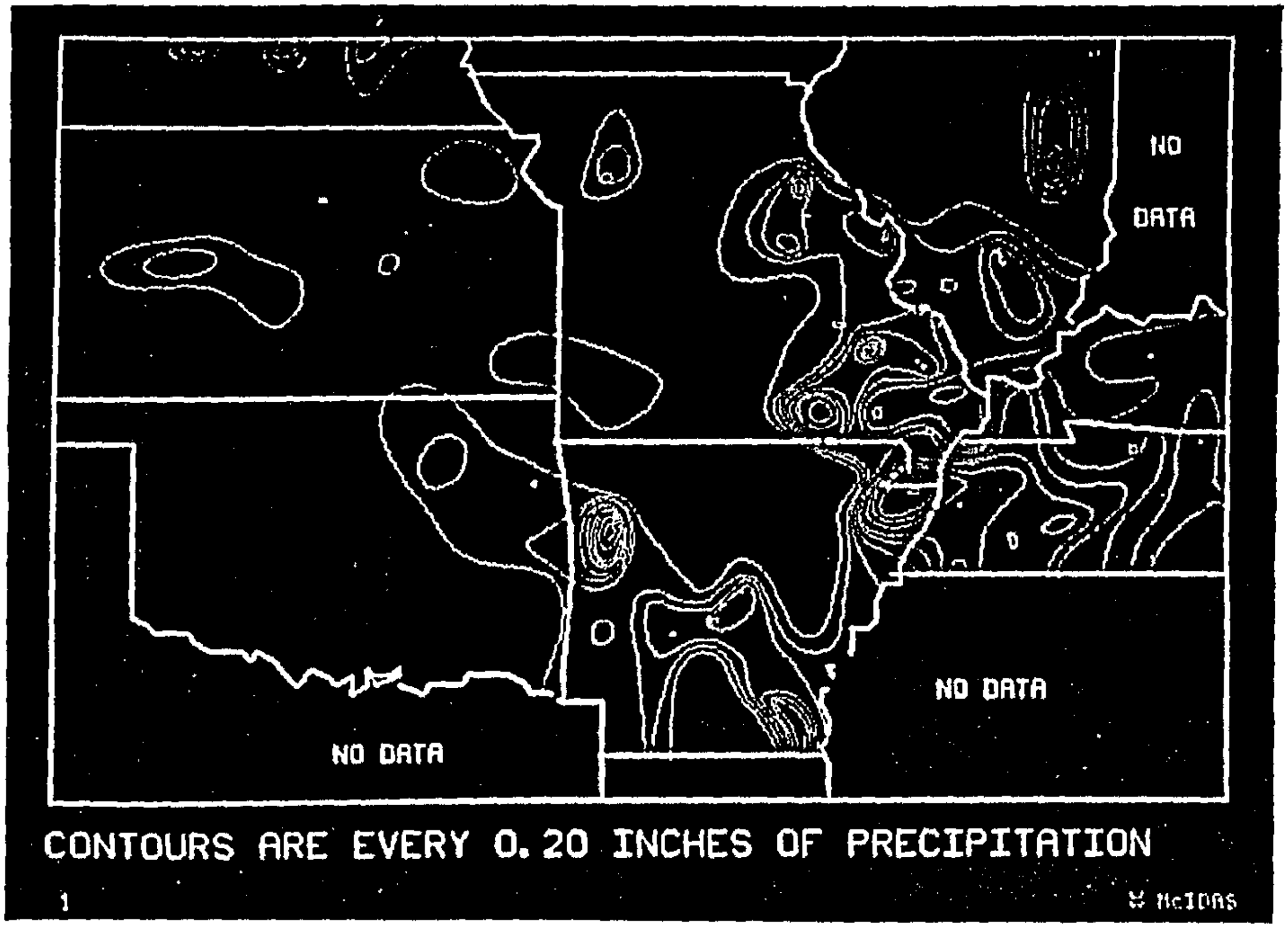

Figure 14. Overview of observed precipitation (for the 24-hour period starting at 12Z, July 20, 1981) with low smoothing factor. Contours every 0.2" starting at 0.2".

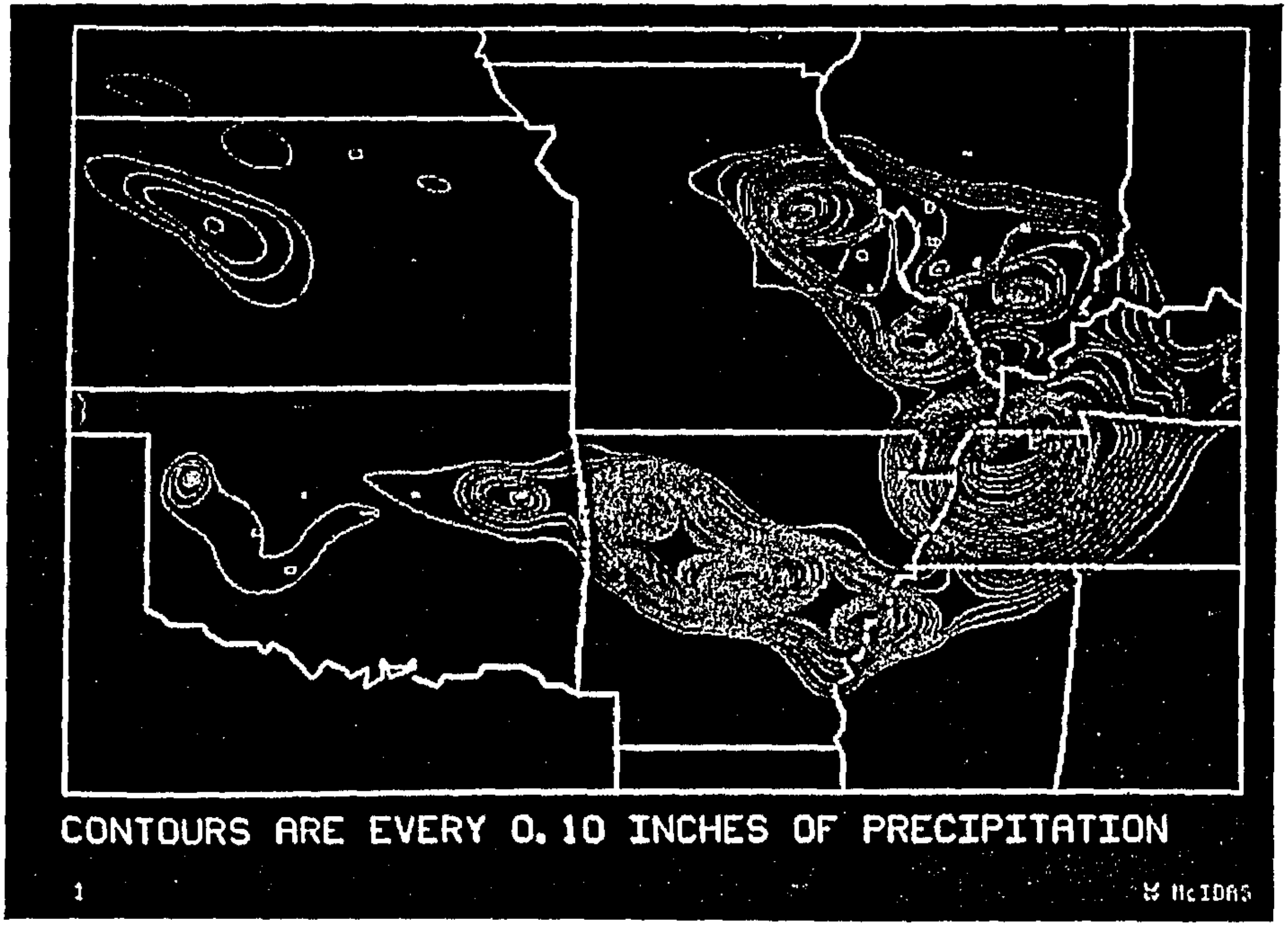

Figure 15. Overview of satellite rainfall estimates (for the 24-hour period starting at 12Z, July 20, 1981) with low smoothing factor. Contours every 0.1" starting at 0.1".

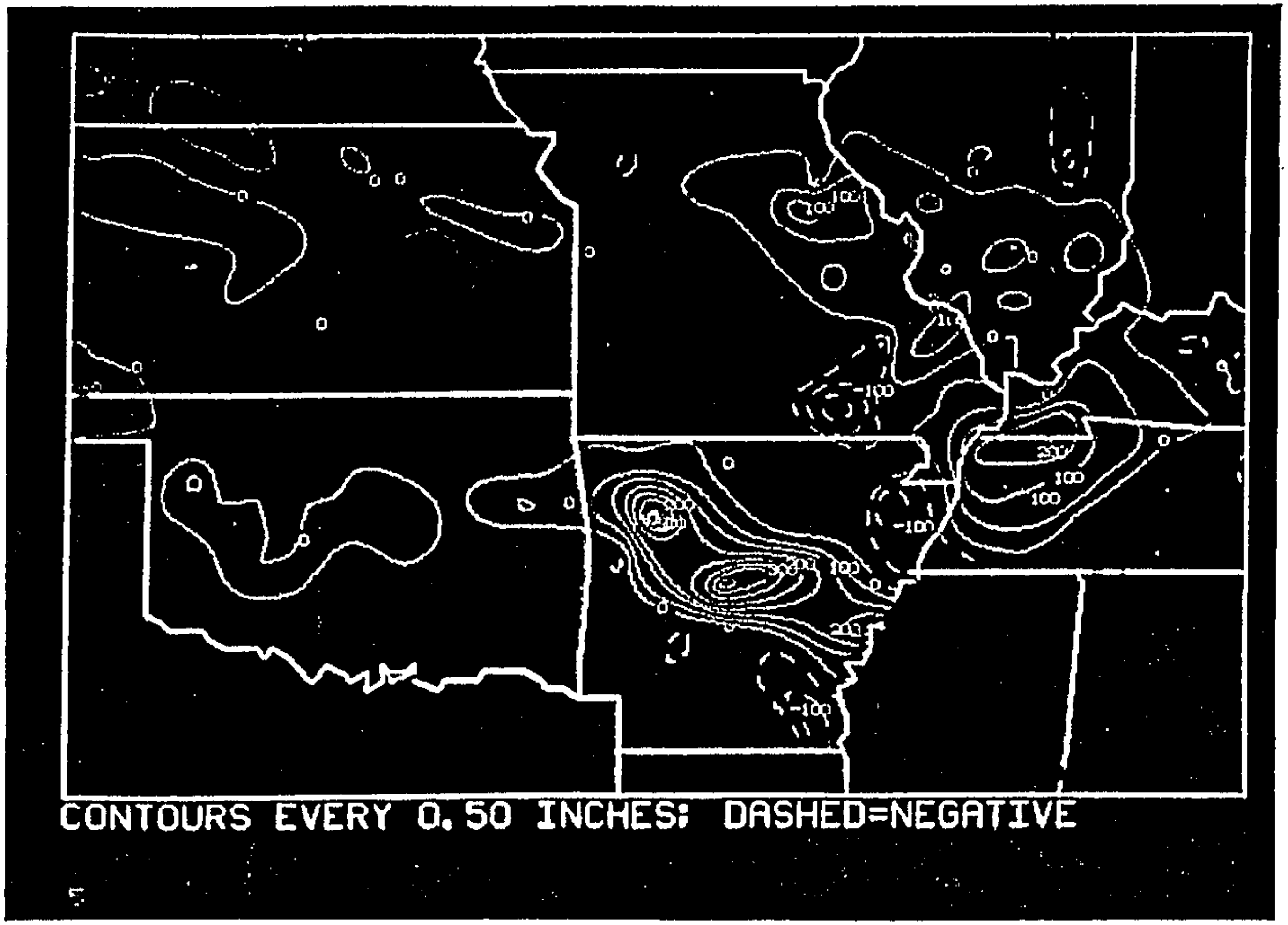

Figure 16. Overview of difference field (minimally smoothed estimates minus observations) for the 24-hour period starting at 12Z, July 20, 1981. Contours every 0.5" starting at 0.5"; dashed=negative.

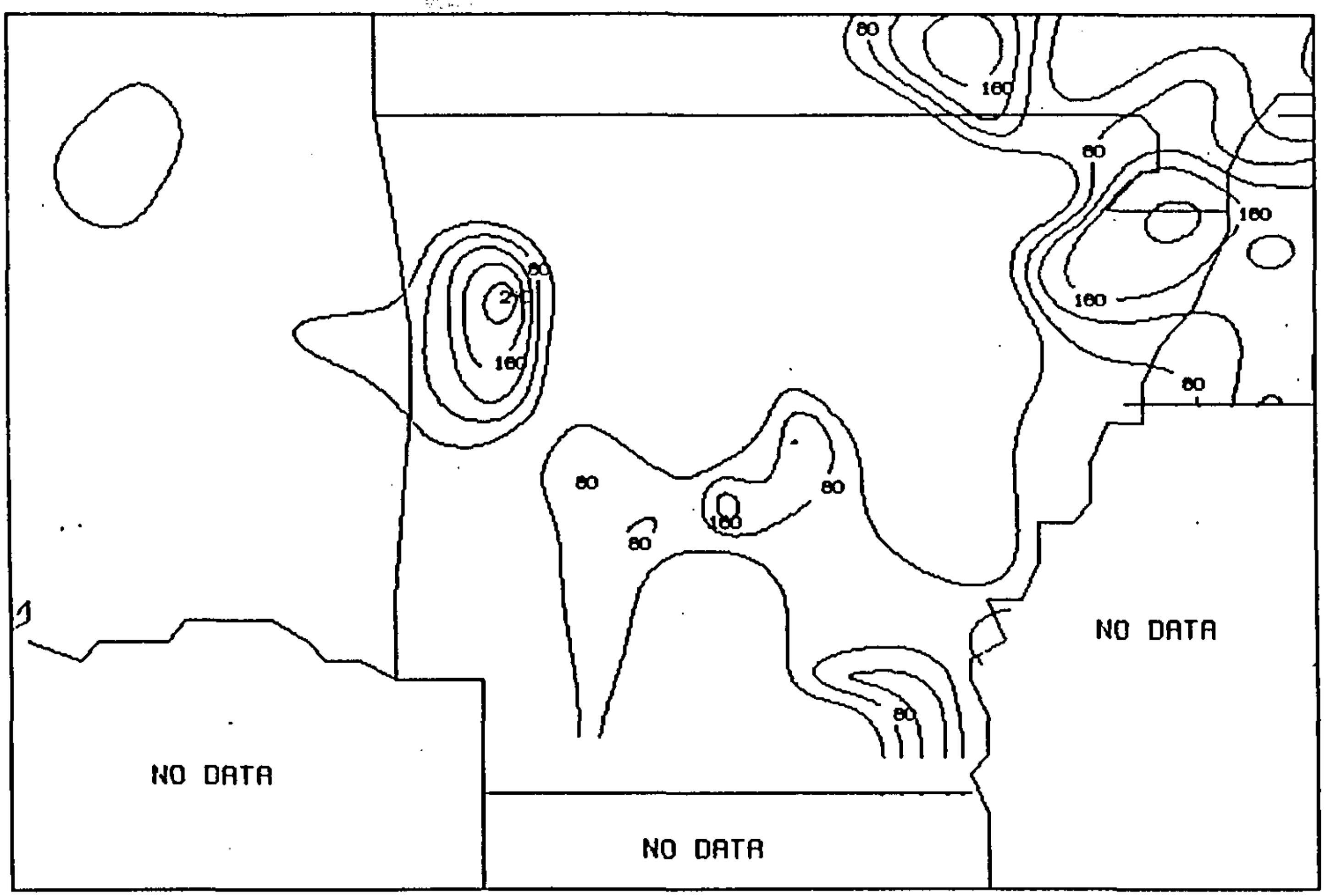

Figure 17. Observed precipitation for the 24-hour period starting at 12Z, July 20, 1981. Contours every 0.4" starting at 0.4"; labels every 0.8". Low smoothing.

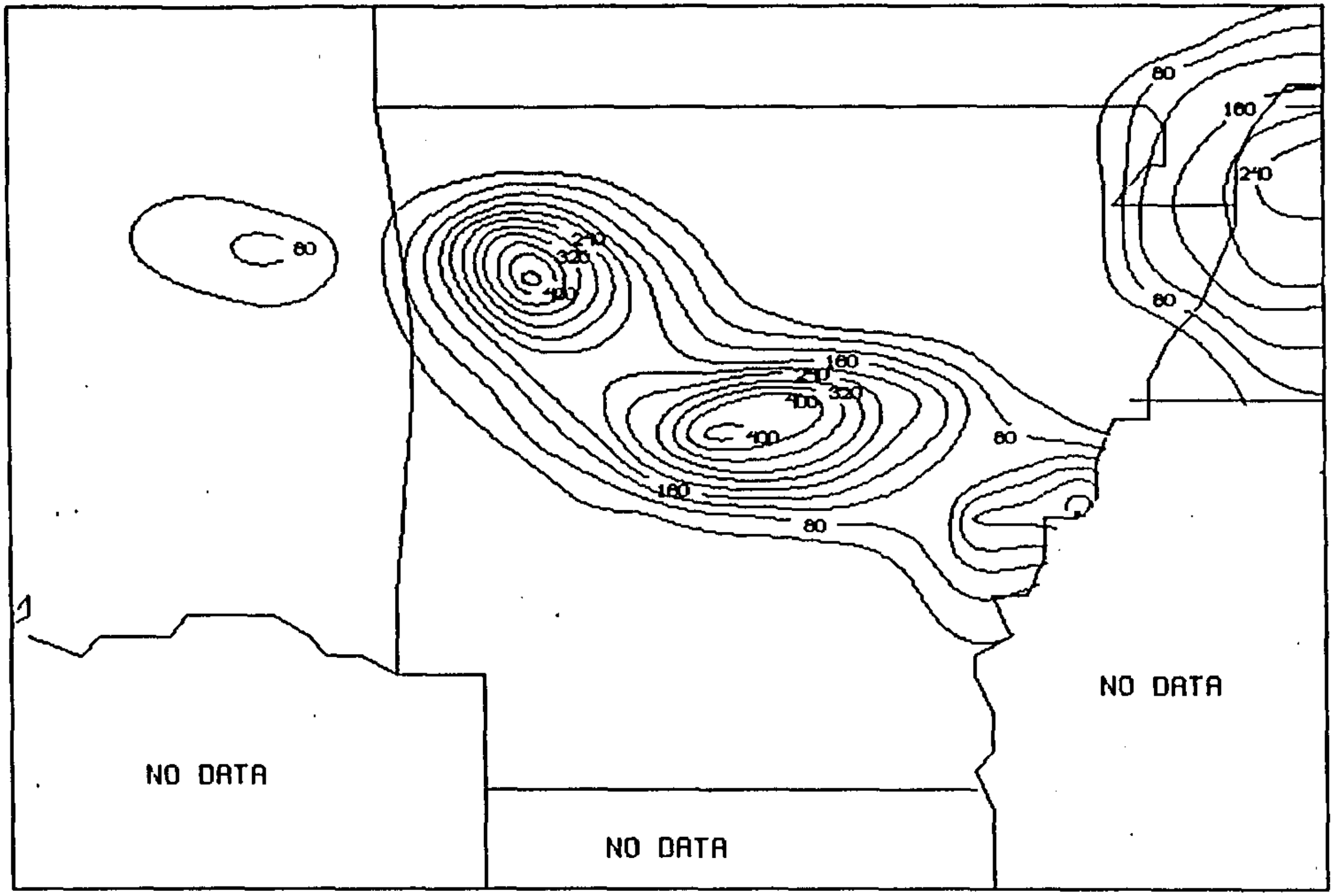

Figure 18. Satellite rainfall estimates for the 24-hour period starting at 12Z, July 20, 1981. Contours every 0.4" starting at 0.4"; labels every 0.8". Low smoothing.

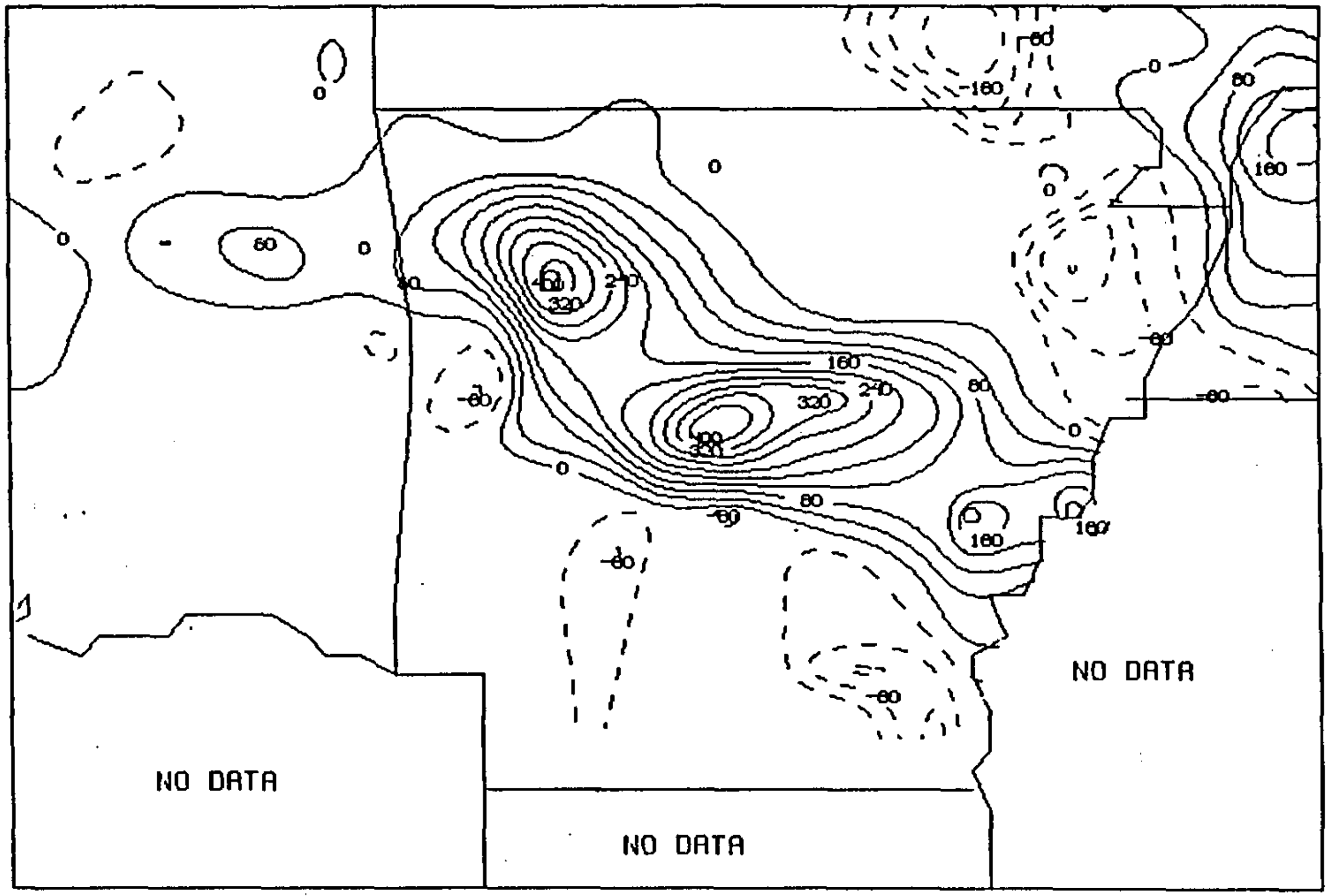

Figure 19. Estimates minus observations for the 24-hour period starting at 12Z, July 20, 1981. Contours every 0.4"; labels every 0.8"; dashed=negative. Low smoothing.

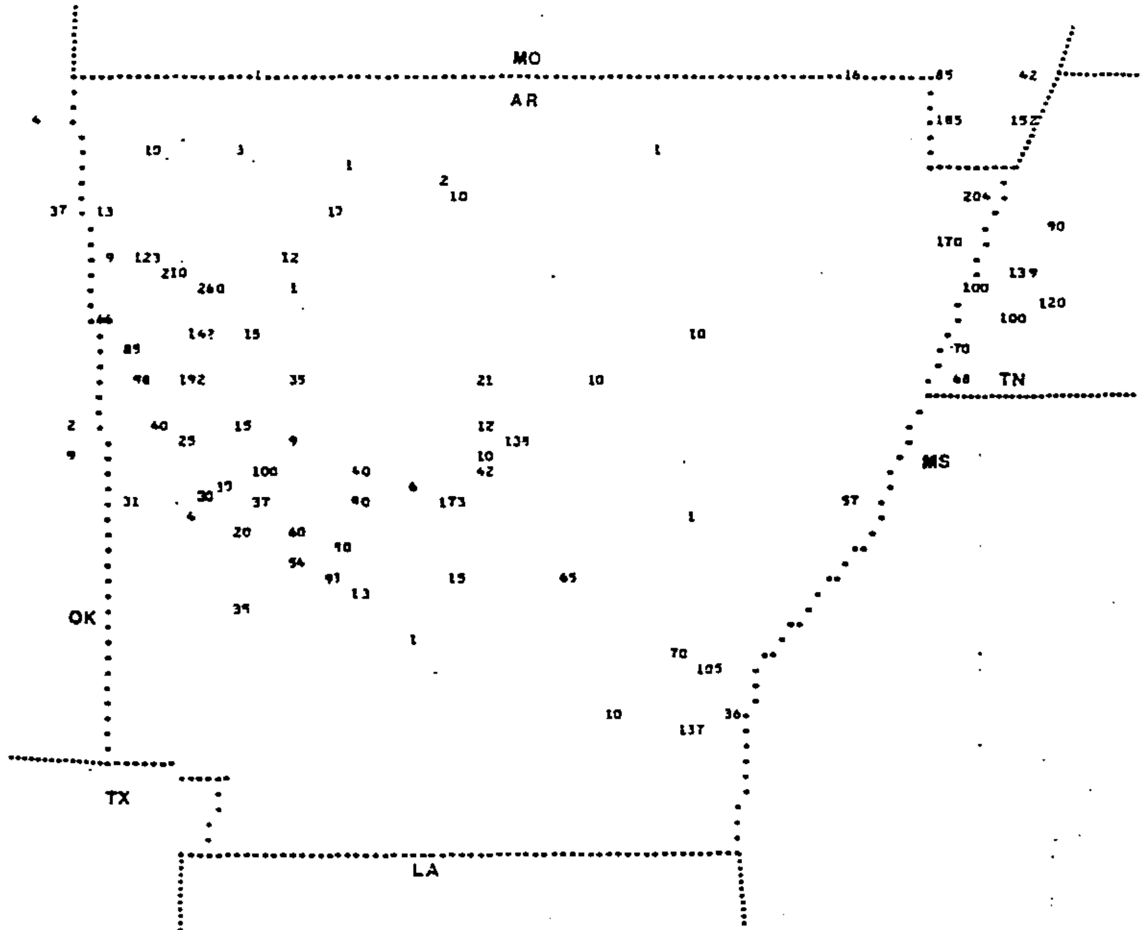

Figure 20. Distribution of rain gauge observations in Arkansas. Rainfall amounts (in hundredths of an inch) are from 12Z-12Z, July 20-21, 1981.

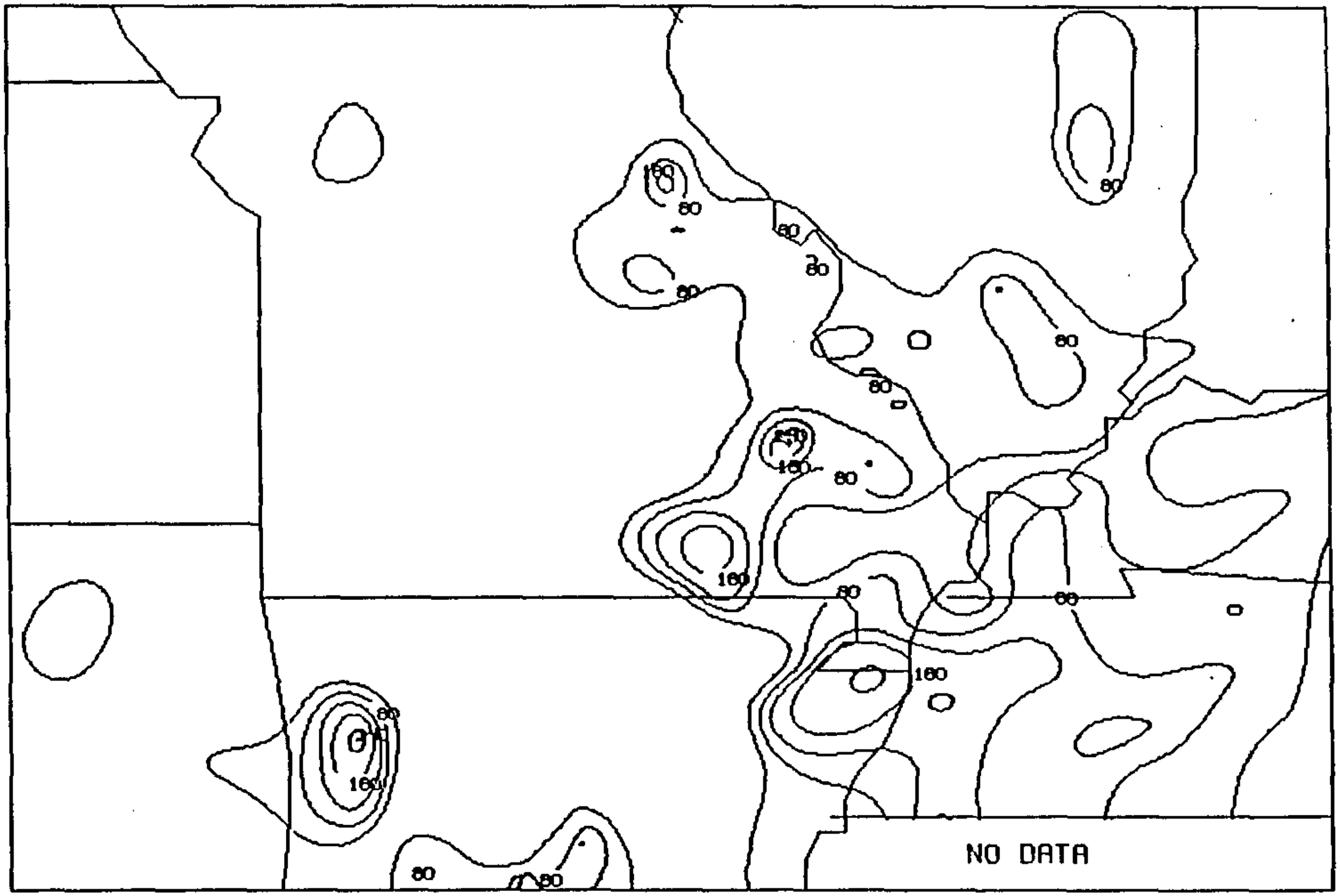

Figure 21. Observed precipitation for the 24-hour period starting at 12Z, July 20, 1981. Contours every 0.4" starting at 0.4"; labels every 0.8". Low smoothing.

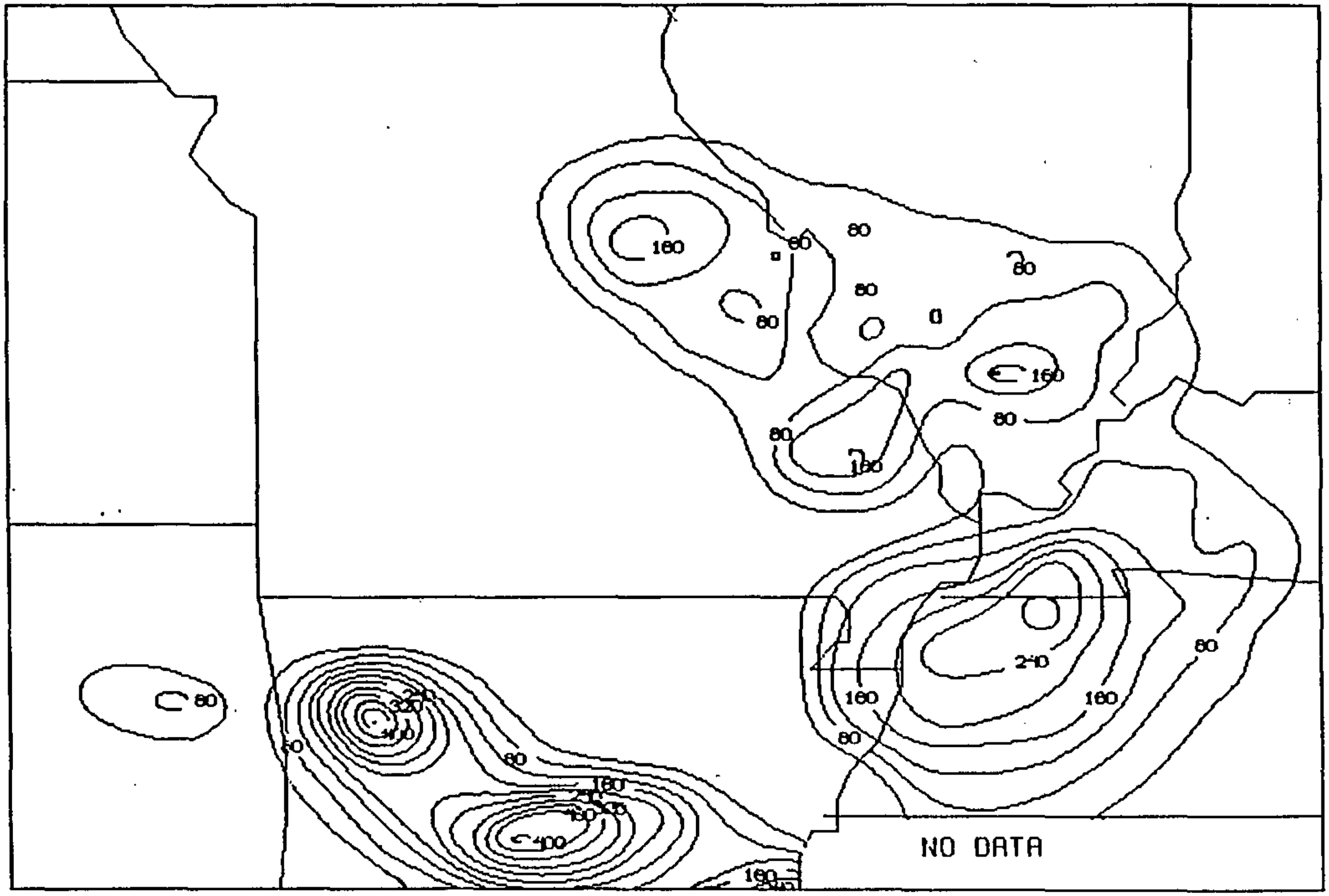

Figure 22. Satellite rainfall estimates for the 24-hour period starting at 12Z, July 20, 1981. Contours every 0.4" starting at 0.4"; labels every 0.8". Low smoothing.

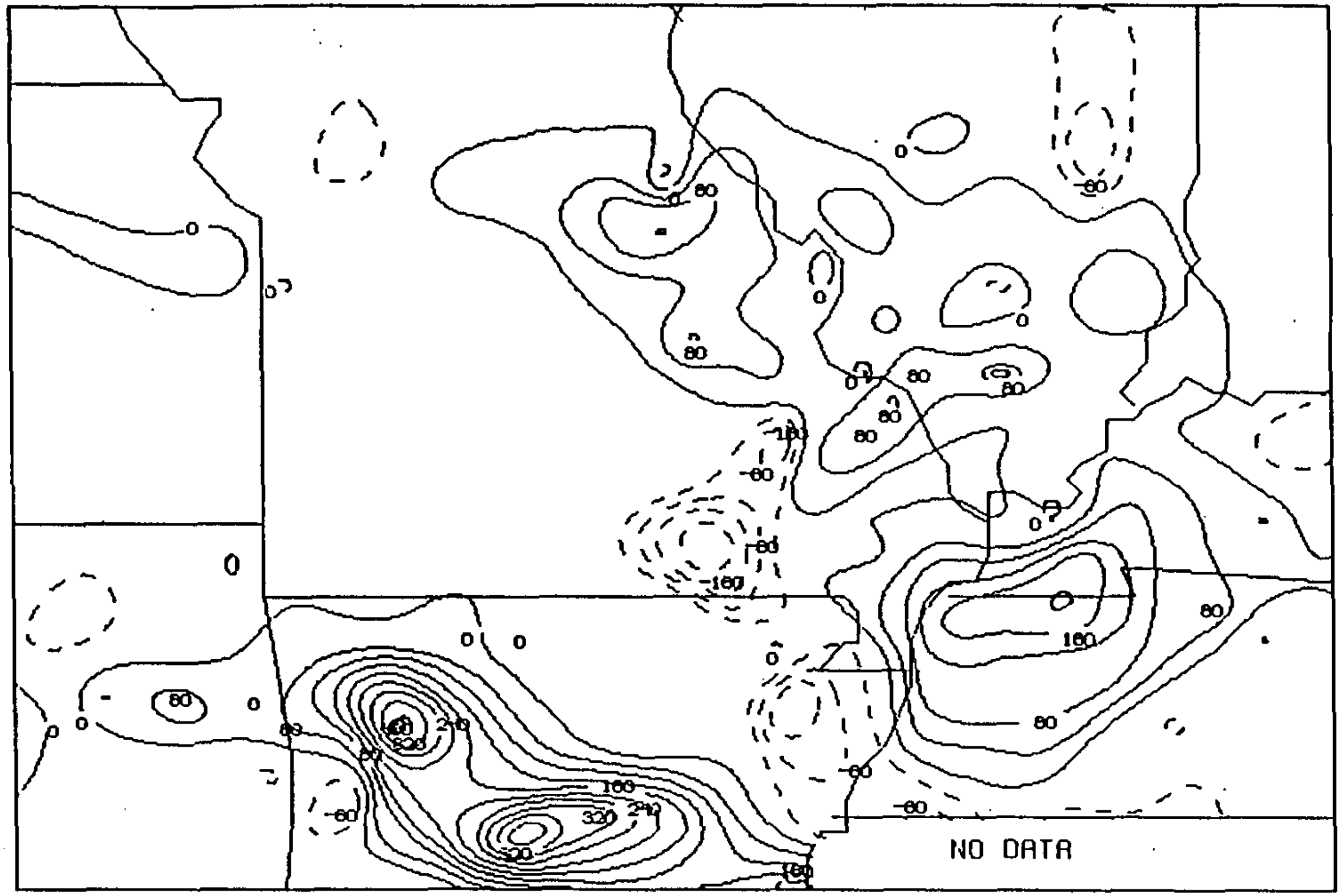

Figure 23. Estimates minus observations for the 24-hour period starting at 12Z, July 20, 1981. Contours every 0.4"; labels every 0.8"; dashed=negative. Low smoothing.

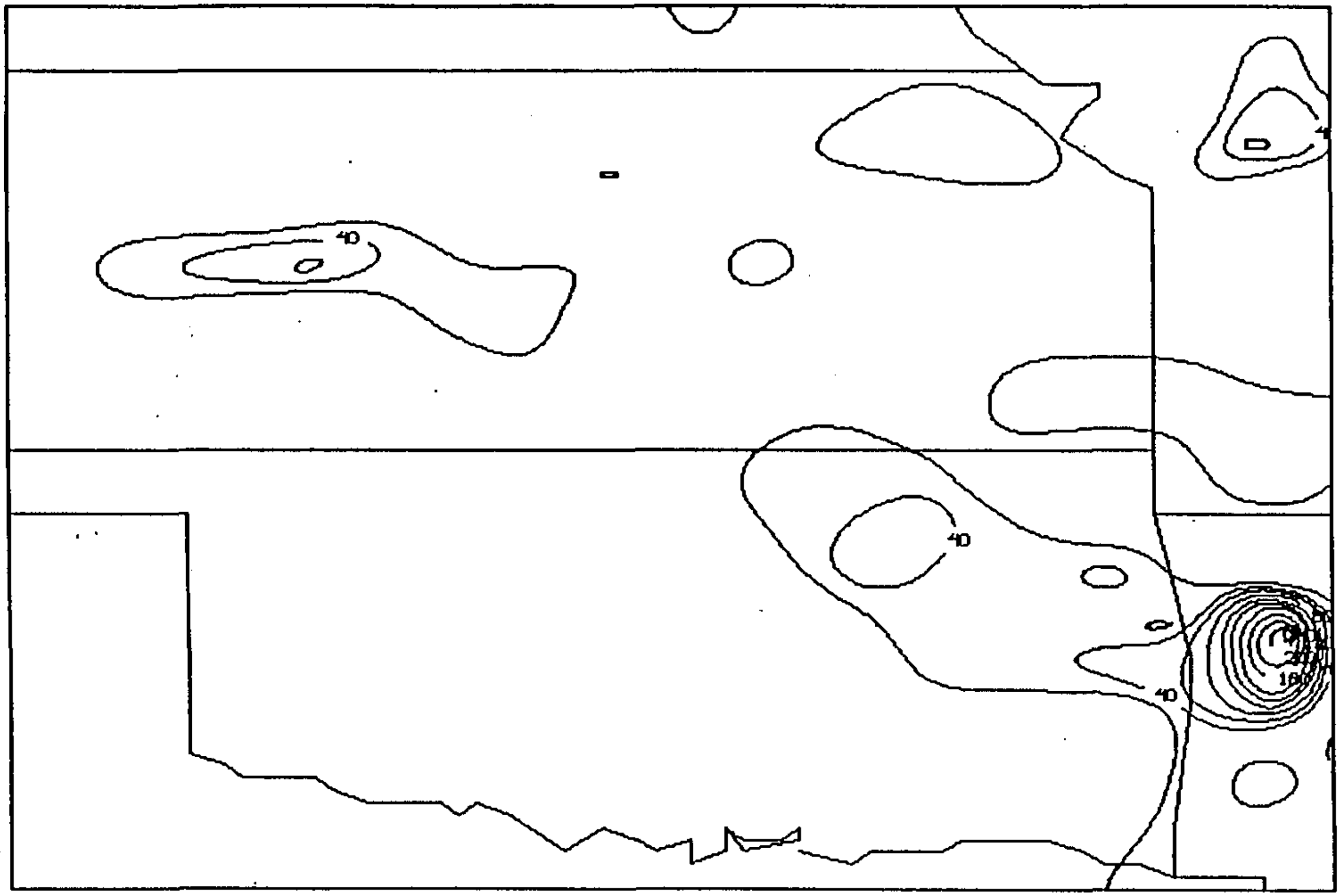

Figure 24. Observed precipitation for the 24-hour period starting at 12Z, July 20, 1981. Contours every 0.2" starting at 0.2"; labels every 0.4". Low smoothing.

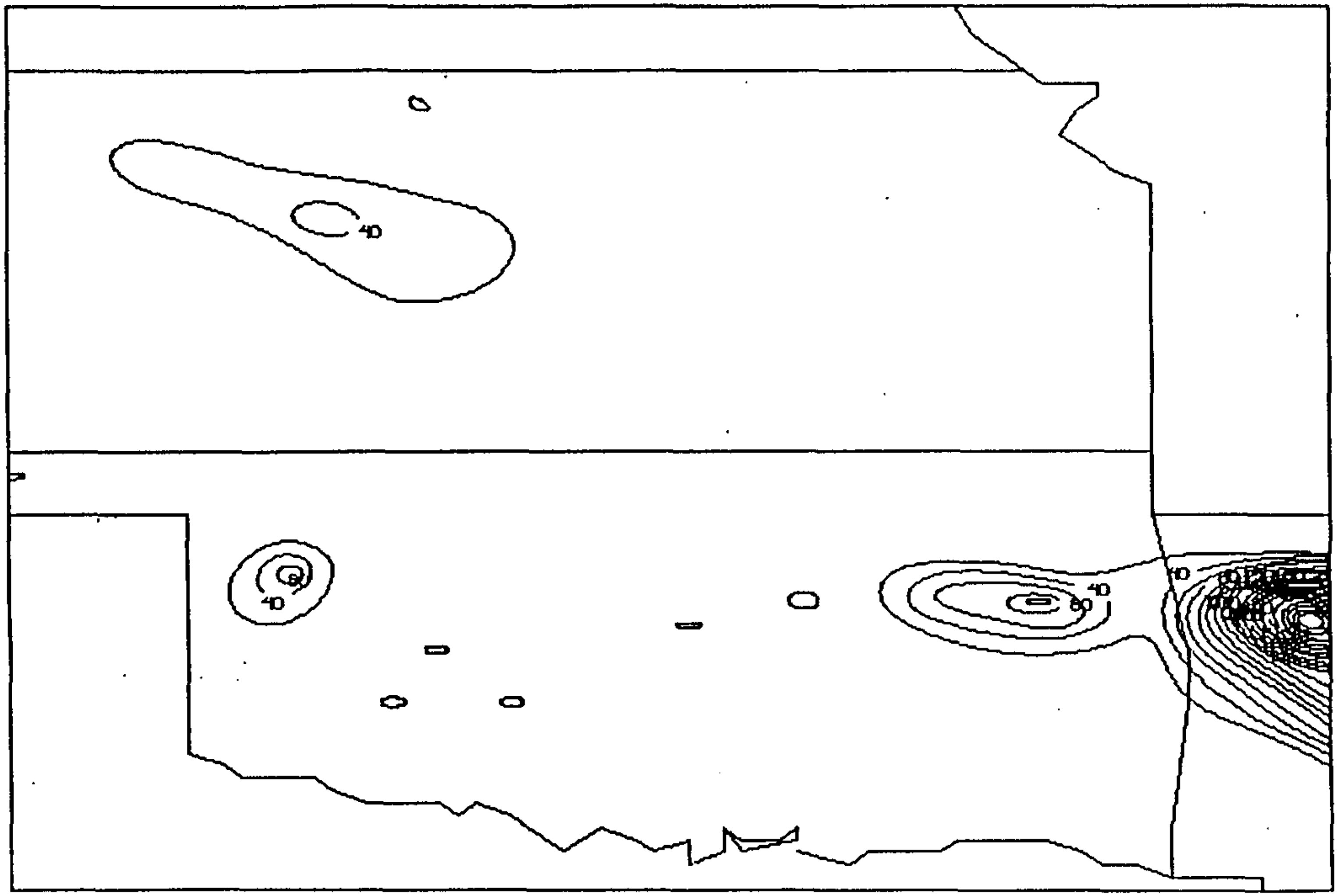

Figure 25. Satellite rainfall estimates for the 24-hour period starting at 12Z, July 20, 1981. Contours every 0.2" starting at 0.2"; labels every 0.4". Low smoothing.

Buren in southern Missouri was probably incorrect, since satellite imagery did not show any convection there, radar indicated little or no precipitation, and the National Meteorological Center's (NMC) in-house observations chart did not show any rainfall there. This accounts for the observed maximum which appears in Figure 21 and the underestimated area in southern Missouri in Figure 23. Although an estimate maximum appears in northwest Tennessee (Figure 22) instead of in northeast Arkansas (Figure 21), the estimates in the Missouri Bootheel generally are within 0.5" of the observations. Also, a wedge of estimates less than 0.4" in southeast Missouri corresponds to a wedge of observations less than 0.4" in the same area. Rainfall from the heavy, but short-lived thunderstorms in western Oklahoma (noted earlier in Figure 3) is depicted in the estimates (Figure 25) but not in the observations (Figure 24). Finally, the observations and estimates in western Kansas (Figures 24 and 25) are very similar. However, the two maxima are slightly displaced from one another. This, of course, is what led to the overestimate/underestimate couplet shown in the difference field (Figure 26).

B. SSM MODEL VS. HIGHLY SMOOTHED OBSERVATIONS AND SATELLITE ESTIMATES

The modeled precipitation is shown in Figure 27. The SSM did not come close to reflecting what actually transpired. It did predict a band of convective precipitation along the cold front, but it was too far north and the maximum rainfall predicted was less than 0.2"! (Unfortunately, the magnitude of the modeled precipitation was not known until most of this project was near completion.) On the positive side, the modeled precipitation was entirely of convective (not large-scale) origin and convective activity is what produced the rainfall on July 20-21, 1981.

The highly smoothed observations and satellite estimates (which are valid comparisons to the SSM data) are shown in Figures 28 and 29, respectively. Because the modeled precipitation did not coincide with either the observed or estimated rainfall, difference fields between the SSM and the observations (Figure 30) and between the SSM and the estimates (Figure 31) did not provide new information. Statistical calculations, such as the Threat Score*, might have been useful if applied to rainfall categories greater than 1/2" or 1". However, because the SSM predicted so little precipitation, Threat scores for all thresholds greater than 0.2" were meaningless (= 0).

* Threat Score is defined as:

$$\frac{\text{\# intersections}}{\text{\# pts. predicted} + \text{\# pts. observed} - \text{\# intersections}}$$

C. ESTIMATES VS. OBSERVATIONS -- HIGH SMOOTHING

A comparison of Figures 28 and 29 yielded an interesting result: when the estimates and observations were smoothed to a large degree, they were extremely similar. Almost all of the axes of the contours were identically aligned. McIDAS calculated that out of the 599 grid points that had estimates of between 0.5" and 1.0", 511 verified in this range, thus leading to a "Post-Agreement" skill score of 85 percent. The difference field (highly smoothed estimates

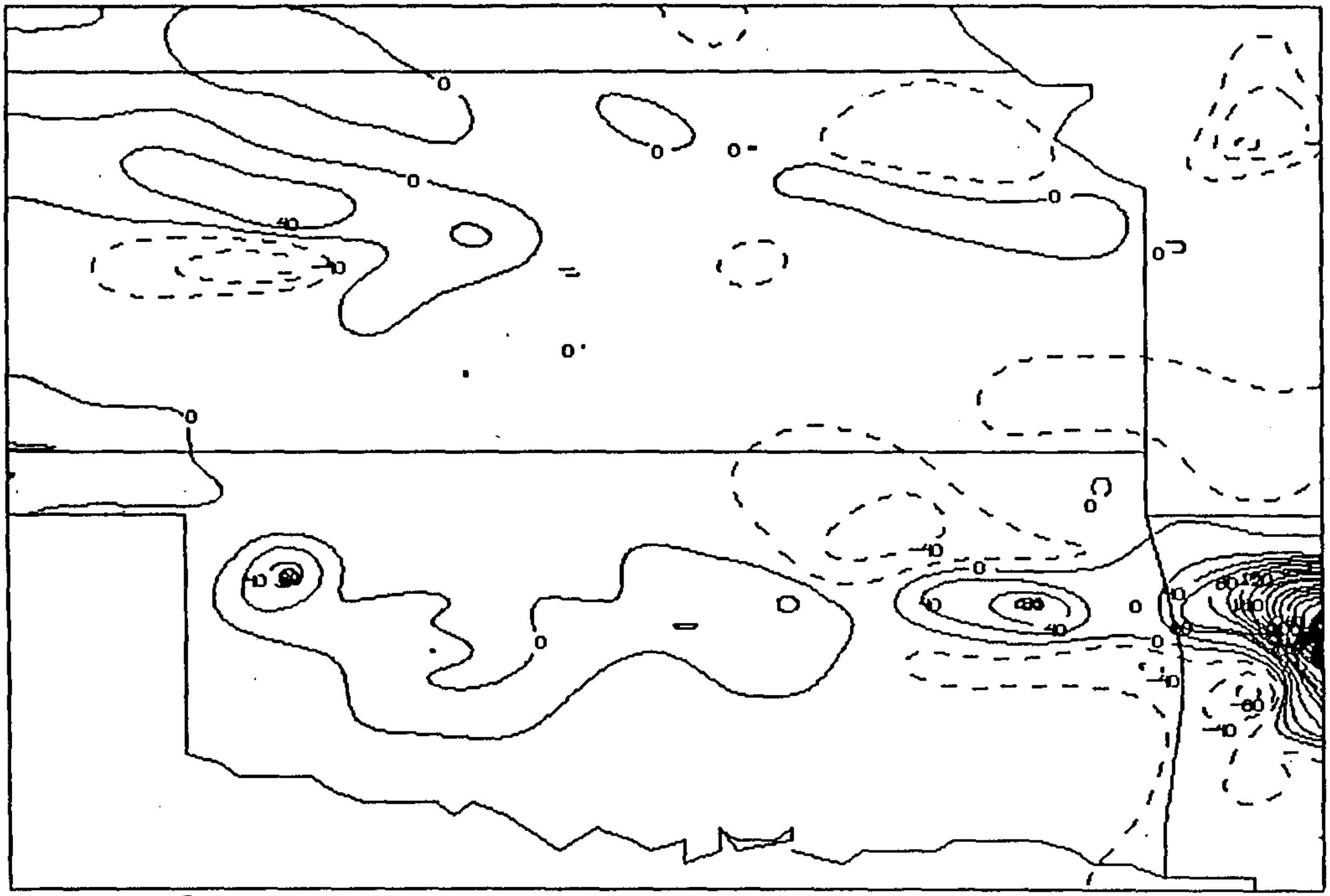

Figure 26. Estimates minus observations for the 24-hour period starting at 12Z, July 20, 1981. Contours every 0.2"; labels every 0.4"; dashed=negative. Low smoothing.

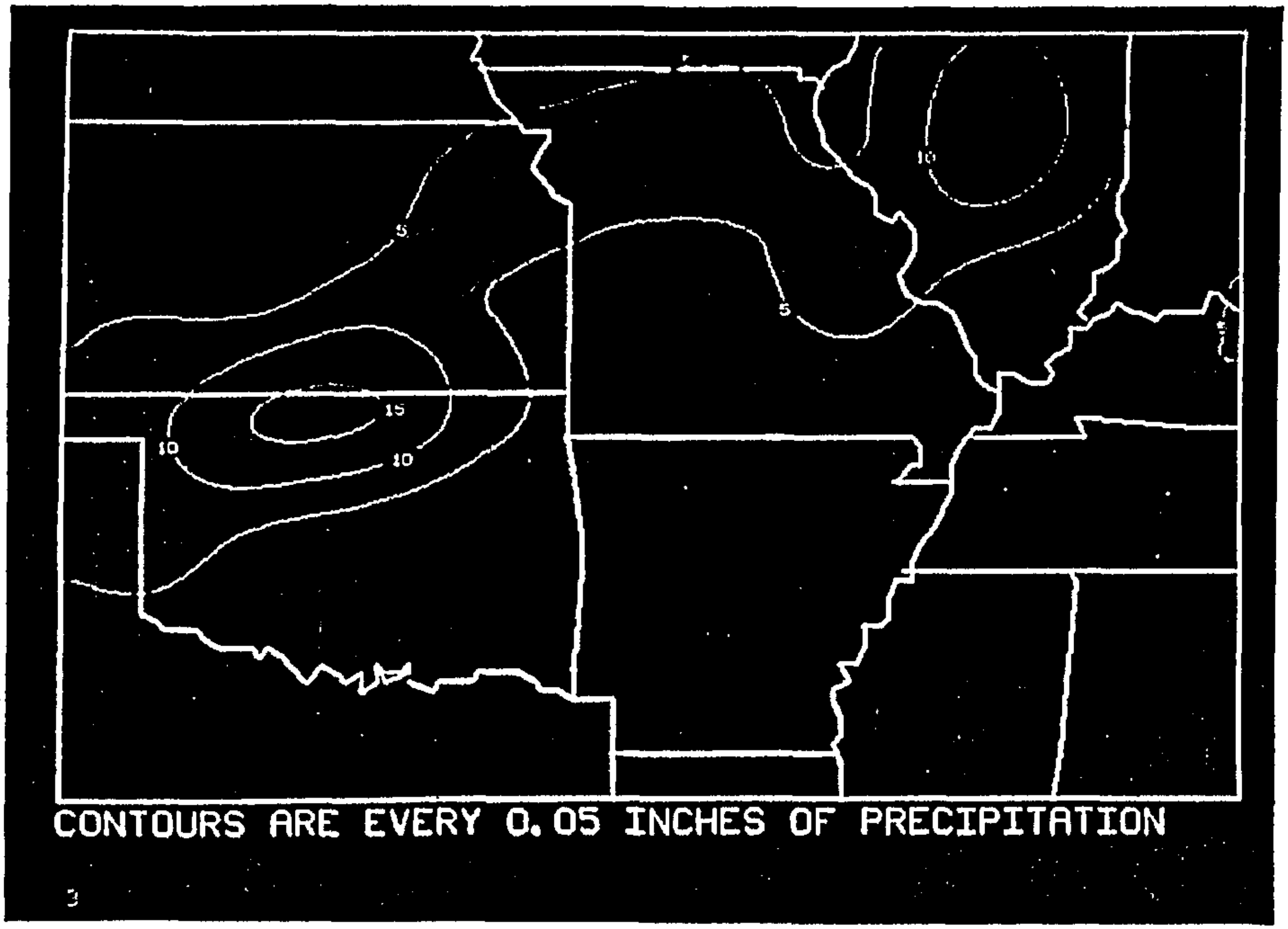

Figure 27. Modeled precipitation (from the SSM) for the 24-hour period starting at 12Z, July 20, 1981. Contours and labels every 0.05" starting at 0.05".

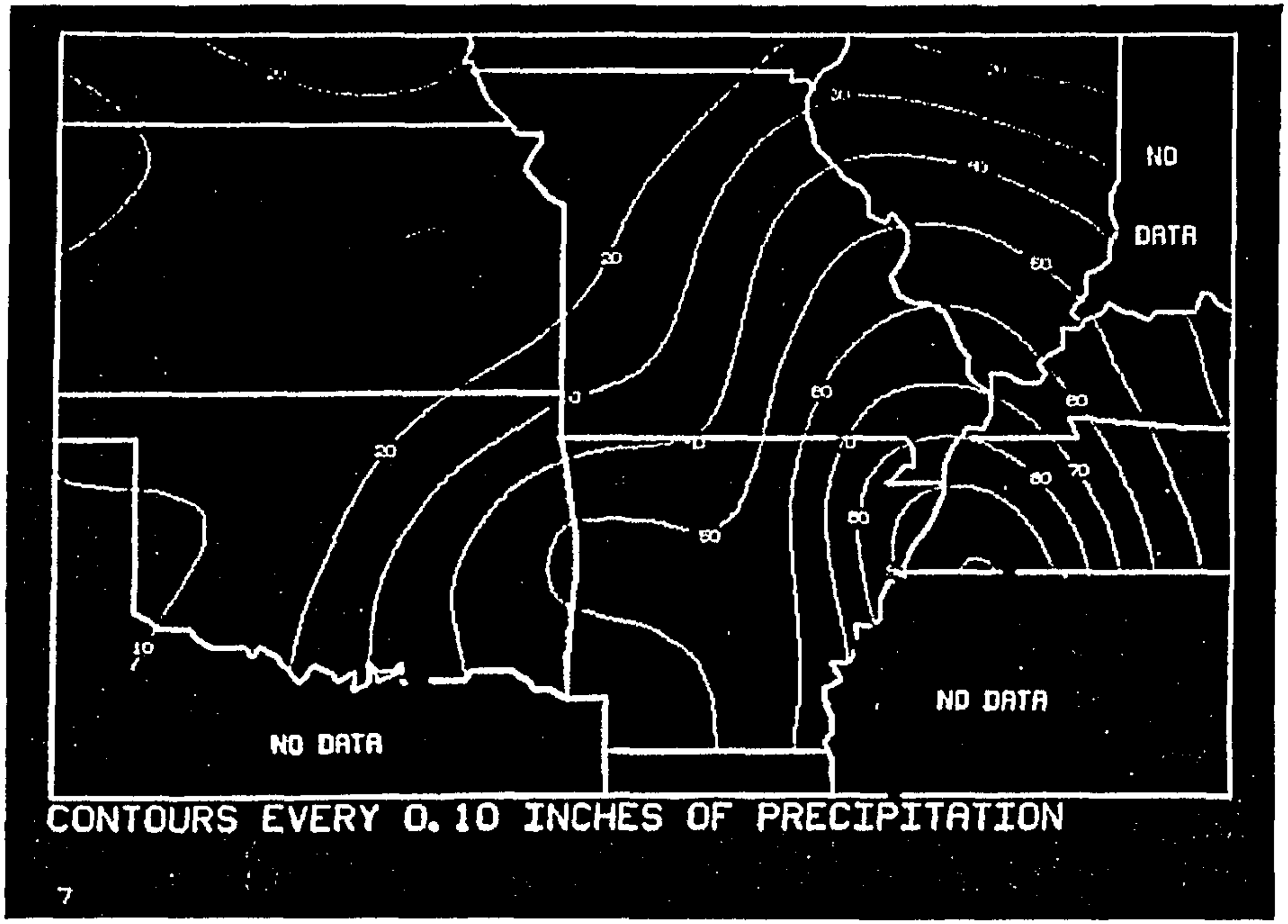

Figure 28. Observed precipitation for the 24-hour period starting at 12Z, July 20, 1981. Contours and labels every 0.1" starting at 0.1". High smoothing.

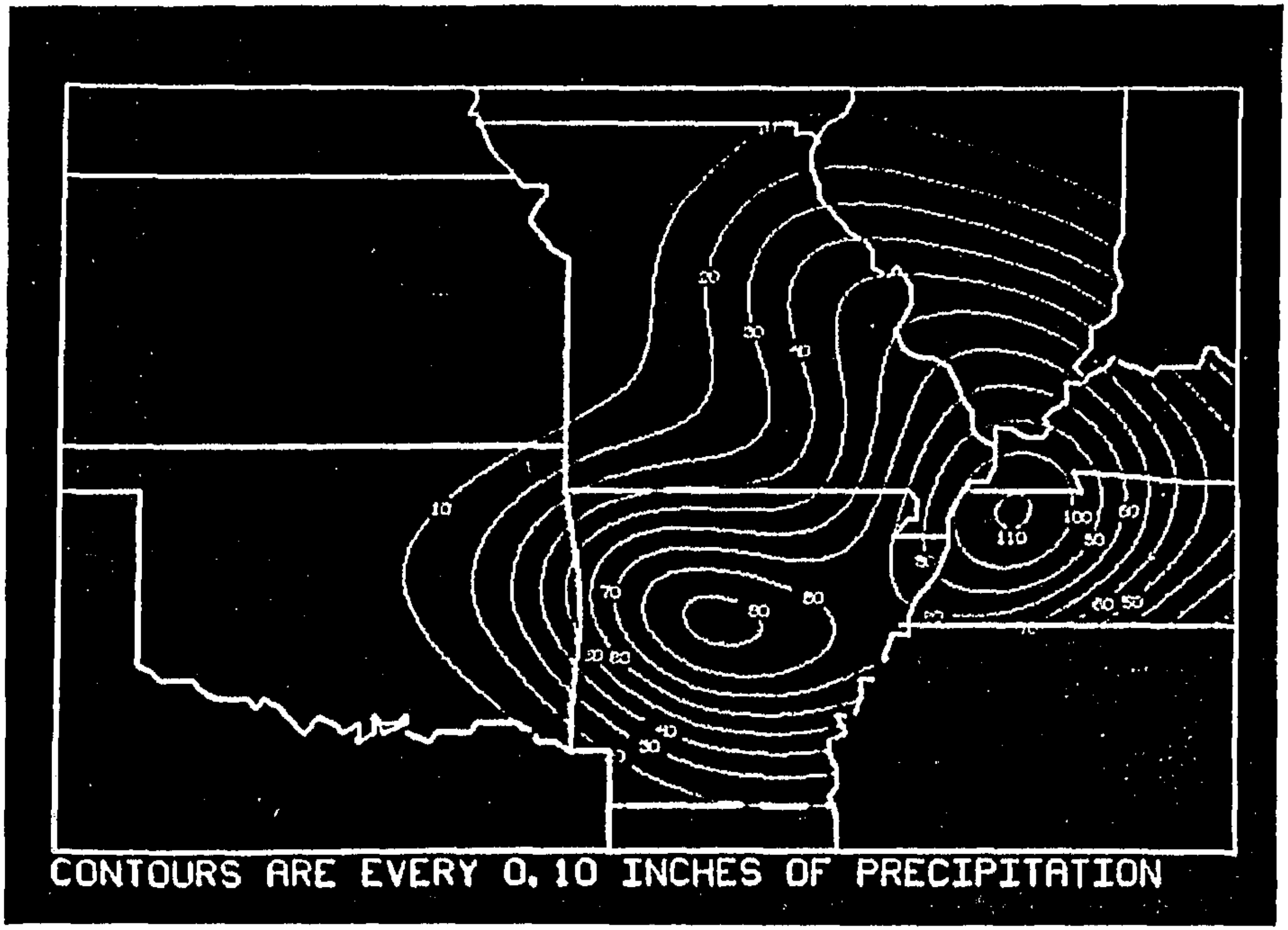

Figure 29. Satellite rainfall estimates for the 24-hour period starting at 12Z, July 20, 1981. Contours and labels every 0.1" starting at 0.1". High smoothing.

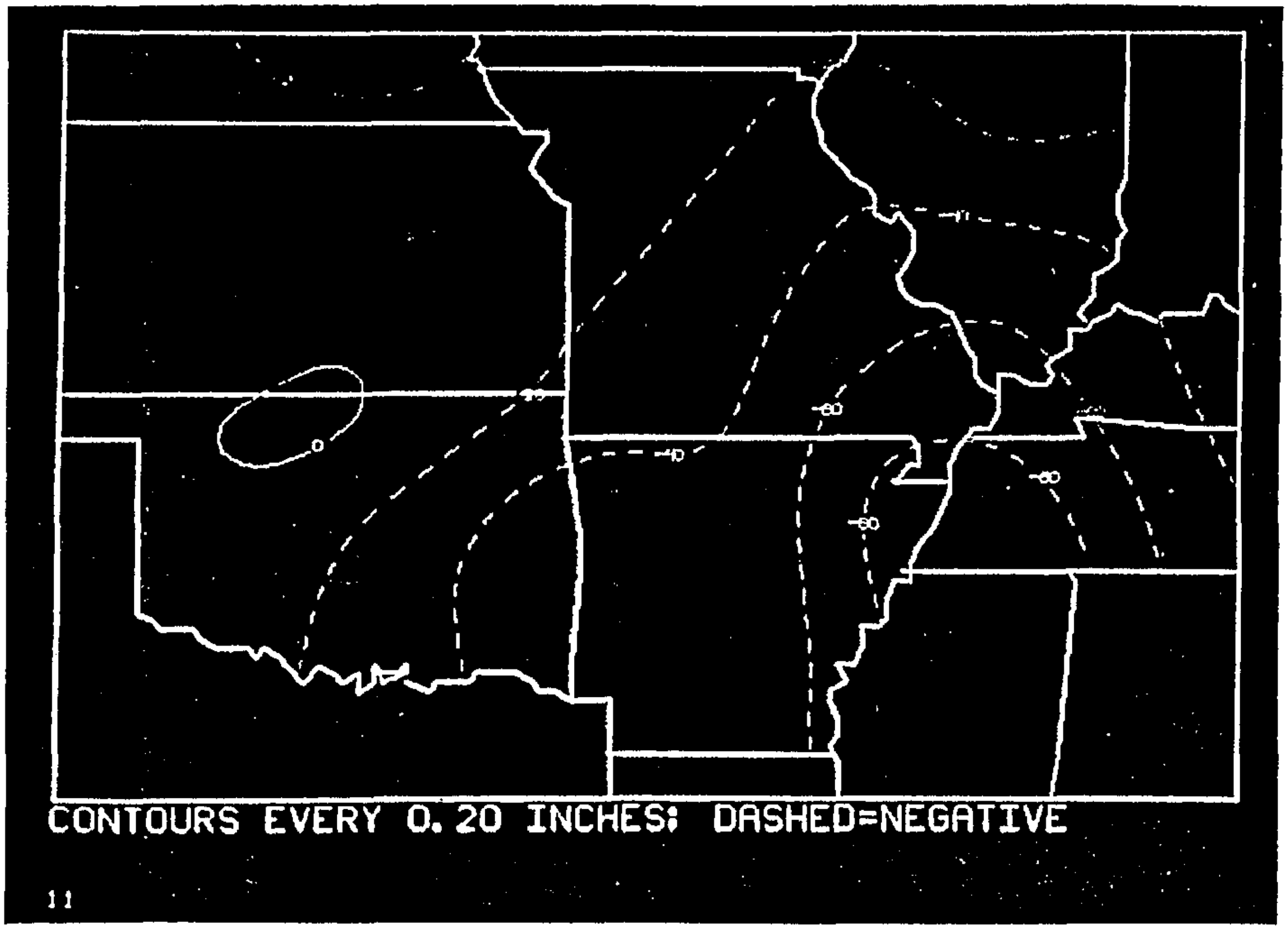

Figure 30. Modeled precipitation minus observed precipitation for the 24-hour period starting at 12Z, July 20, 1981. Contours and labels every 0.2" starting at 0; dashed=negative. High smoothing.

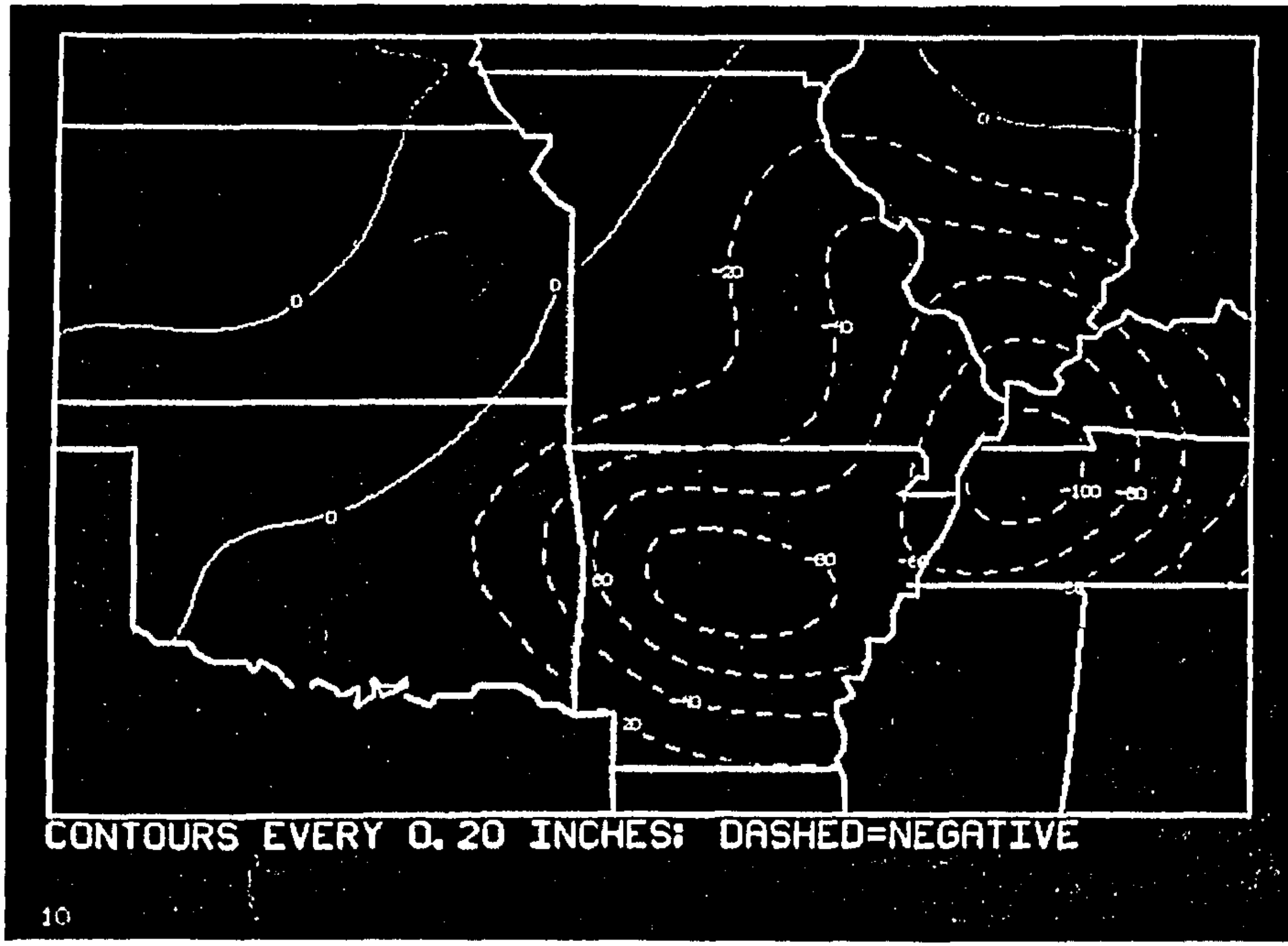

Figure 31. Modeled precipitation minus satellite rainfall estimates for the 24-hour period starting at 12Z, July 20, 1981. Contours and labels every 0.2" starting at 0; dashed=negative. High smoothing.

minus observations) is shown in Figure 32. The differences are much closer to zero than those in Figure 16. In fact, even some underestimates become apparent.

VIII. SUMMARY AND CONCLUSIONS

The goal of this project was to show that satellite-derived precipitation estimates can be a viable alternative to surface-based observations and that they can be used to verify a mesoscale numerical model. To accomplish this, an intercomparison between satellite rainfall estimates, ground-based observations, and modeled precipitation has been performed.

Because of the often short-lived and localized nature of convective storms, verification of satellite-derived rainfall estimates is a difficult task. Observations from exactly the same time period and location as the estimate are very rare. This case study eliminated the temporal problem by computing estimates for the same time period as the observations. Yet many factors still complicated the verification procedure. It was shown how the density of observations is very important, especially when attempting to verify on a grid point for grid point basis. Small location errors can lead to large local errors in a difference field. But, overall, the results showed that the satellite estimates compared favorably with the observations.

The SSM model failed to accurately predict convective precipitation in this case study. Its forecast precipitation area was too far to the north and the amounts were much too small. As a result, comparisons of estimates and observations with the model did not provide much new information. Nevertheless, by using satellite estimates to verify the SSM model, this study has suggested a new application for the use of the Scofield-Oliver Technique. The procedures and methodology for computing the estimates and then verifying the model have been demonstrated. Thus, the potential exists for operational numerical (mesoscale) modeling to benefit by having such satellite verification information for precipitation, which can be produced in near real-time.

Because satellite estimates generally provide useful rainfall information every half-hour, this study treated satellite estimates as being a viable substitute for observations. However, since both satellite and radar precipitation estimates can be used to fill gaps in the observed data, perhaps some combination of these three types of information would provide the best verification data set for precipitation forecasts. In fact, the Heavy Precipitation Unit of NMC currently tries to incorporate satellite estimates from the Synoptic Analysis Branch of NESDIS and radar report when verifying their operational hand-drawn forecasts. The state-of-the-art in mesoscale numerical modeling, as reviewed by Anthes (1983), is improving. More is becoming known about the physical and dynamical processes associated with mesoscale phenomena. Hopefully, in the not-so-distant future, when mesoscale models are better able to forecast convective rainfall events, such a complete data set could be used to verify the model forecasts.

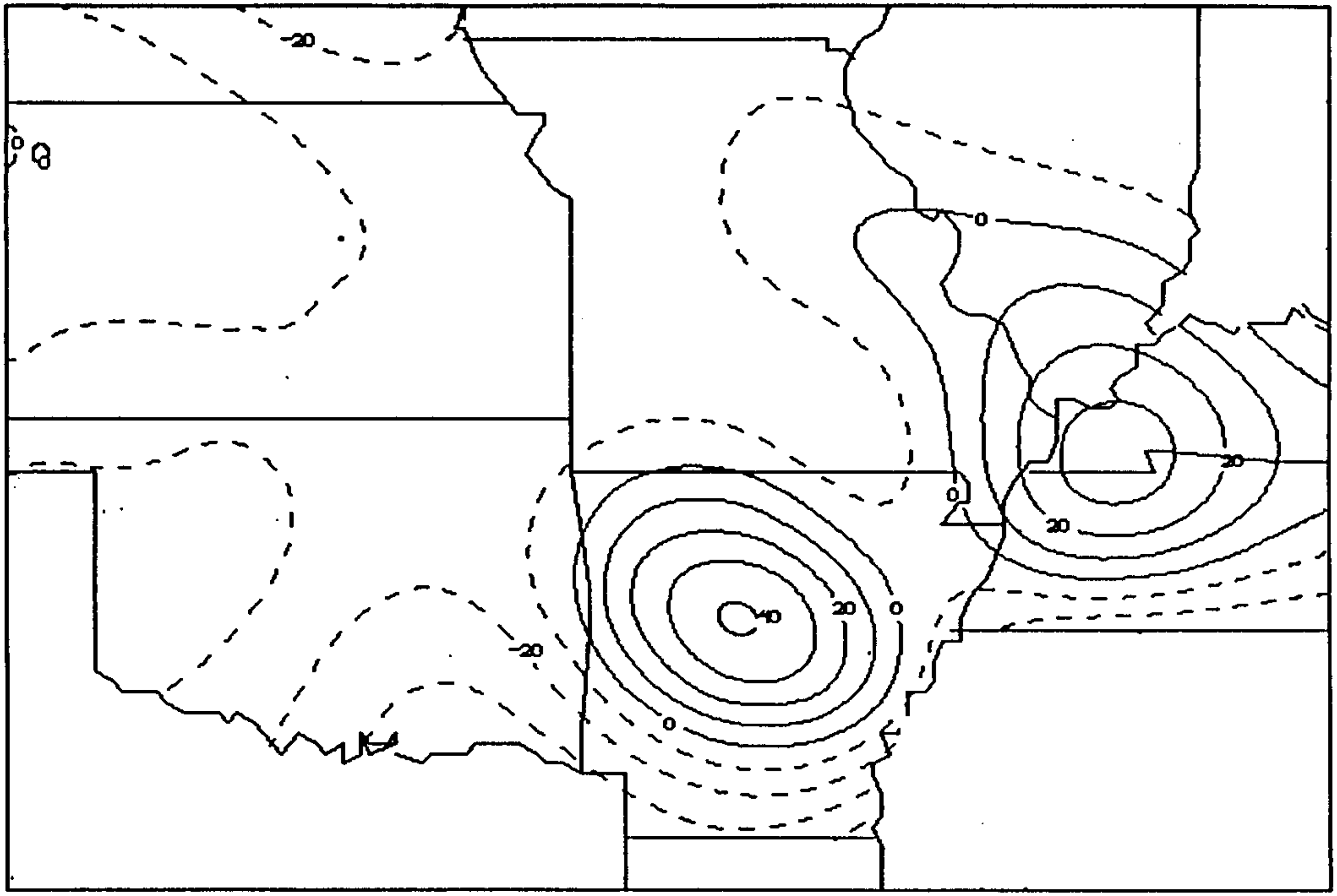

Figure 32. Estimates minus observations for the 24-hour period starting at 12Z, July 20, 1981. Contours every 0.1" starting at 0; labels every 0.2"; dashed=negative. High smoothing.

IX. ACKNOWLEDGEMENTS

This research was supported by the National Science Foundation: Grant ATM-8005369 provided the Research Assistantship and Grant ATM-8514730 provided for Dr. Houghton's time during the final reading process. In addition, the McIDAS computer time used for running the SSM model and other help given by George Diak and Geary Callan was supported by the NASA Marshall Space Flight Center Contract NA58-34732.

X. REFERENCES

Anthes, R. A., 1983: Regional Models of the Atmosphere in Middle Latitudes. Mon. Wea. Rev., 111, 1306-1335.

Barnes, S. L., 1964: A Technique for Maximizing Details in Numerical Weather Map Analysis. J. Appl. Meteor., 3, 396-409.

Blackadar, A. K., 1974: Experiments with Simplified Second-Moment Approximations for Use in Regional Scale Models. Select Research Group in Air Pollution Meteorology, Second Annual Progress Report, EPA-650/4-74-045, 676 pp.

Businger, J. A., J. C. Wyngaard, Y. Izumi, and E. F. Bradley, 1971: Flux Profile Relationships in the Atmospheric Surface Layer. J. Atmos. Sci., 28, 181-189.

Chesters, D., L. W. Uccellini, and W. Robinson, 1983: Low-Level Moisture Images from the VISSR Atmospheric Sounder (VAS) "Split-Windows" Channels. Accepted by the J. Climate and Appl. Meteor.

Clark, J. D., 1983: The GOES User's Guide, Chapter 7, U.S. Dept. of Commerce/NOAA/NESDIS, Washington, D.C., 38-39.

Clark, D., Wisconsin State Climatologist, located at the University of Wisconsin-Madison. Provided information about rain gauges and types of cooperative observers.

Climatological Data, for individual Midwest states, U.S. Dept. of Commerce/NOAA/Environmental Data and Information Service/National Climatic Data Center, Asheville, N.C., Vol. 31, No. 7, July, 1981.

Corby, G. A., A. Gilchrist, and R. L. Mewson, 1972: A General Circulation Model of the Atmosphere Suitable for Long Period Integrations. Quart. J. Roy. Meteor. Soc., 98, 809-832.

Cressman, G. P., 1959: An Operational Objective Analysis System. Mon. Wea. Rev., 87, 367-374.

Diak, G., S. Heikkinen, and J. Bates, 1986: The Influence of Variations in Surface Treatment on 24-hour Forecasts With a Limited Area Model, Including a Comparison of Modeled and Satellite-Measured Surface Temperatures. Mon. Wea. Rev., 114, 215-232.

Ferraro, R. R., J. V. Fiore, Jr., and J. C. Alishouse, 1988: Comparison of Weather Radar and Satellite-Based Passive Microwave Observations of Rainfall Over Land and Oceans. Preprint, Third Conf. on Satellite Meteorology and Oceanography (Anaheim, CA), Amer. Meteor. Soc., 309-314.

Field, G. A., 1985a: A Case Study Evaluation of Satellite-Derived Rainfall Estimates. Preprint, Sixth Conf. on Hydrometeorology (Indianapolis, IN), Amer. Meteor. Soc., 298-304.

__________, 1985b: Verification of SAB's Satellite Precipitation Estimates for the 1984 Convective Season. Nat. Wea. Dig., 39-44.

Hibbard, W. L. and D. P. Wylie, 1985: An Efficient Method of Interpolating Observations to Uniformly Spaced Grids. Preprint, Conf. on Interactive Information and Processing Systems for Meteorology, Oceanography, and Hydrology (Los Angeles, CA), Amer. Meteor. Soc., 144-147.

Hood, R. E. and R. W. Spencer, 1988: Thunderstorm Ice Induced Brightness Temperature Depressions at 18, 37, and 92 GHz During COHMEX and Their Implications for Satellite Precipitation Retrievals. Preprint, Third Conf. on Satellite Meteorology and Oceanography (Anaheim, CA), Amer. Meteor. Soc., 303-308.

Houghton, D. D., 1984: Proposal to the National Science Foundation for Funding for Continued Mesoscale Research.

Hourly Precipitation Data, U.S. Dept. of Commerce/NOAA/Environmental Data and Information Service/National Climatic Data Center, Asheville, N.C., Vol. 31, No. 7, July, 1981.

Katayama, A., 1972: A Simplified Scheme for Computing Radiative Transfer in the Troposphere. University of California at Los Angeles Technical Report No. 6, 77 pp.

Kuo, H. L., 1965: On Formation and Intensification of Tropical Cyclones Through Latent Heat Release By Cumulus Convection. J. Atmos. Sci., 22, 40-63.

__________, 1974: Further Studies of the Parameterization of the Influence of Cumulus Convection on Large Scale Flow. J. Atmos. Sci., 31, 1232-1240.

Leslie, L. M., G. A. Mills, and D. J. Gauntlett, 1981: The Impact of FGGE Data Coverage and Improved Numerical Techniques in Numerical Weather Prediction in the Australian Region. Quart. J. Roy. Meteor. Soc., 107, 629-642.

Lindstrom, S. S., 1984: Analysis of Mesoscale Model Results Using a Bandpass Filter. M.S. Thesis, University of Wisconsin-Madison, pp. 1-5.

Maddox, R. A., 1980: An Objective Technique for Separating Macroscale and Mesoscale Features in Meteorological Data. Mon. Wea. Rev., 108, 1108-1121.

Maine, R., 1972: A Filtered Education Model for Operations and Research. J. Appl. Meteor., 11, 7-15.

McGregor, J. L., and L. M. Leslie, 1977: On the Selection of Grids for Semi-implicit Schemes. Mon. Wea. Rev., 105, 236-238.

__________, __________, and D. J. Gauntlett, 1978: The ANMRC Limited-area Model: Consolidated Formulation and Operational Results. Mon. Wea. Rev., 106, 427-438.

Mills, G. A., L. M. Leslie, J. L. McGregor, and G. A. M. Kelly, 1981: A High Resolution Numerical Analysis/Forecast System for Short Term Prediction Over the North American Region. Unpublished ANMRC Report, Australian Meteorology Research Center, Melbourne, Australia, 76 pp.

__________, G. R. Diak, and C. M. Hayden, 1983: The Subsynoptic Scale Model and Investigations of the Value of Satellite Sounding Data in Numerical Weather Prediction. In-house publication of the Space Science and Engineering Center, University of Wisconsin-Madison, p. 6.

__________, and C. M. Hayden, 1983: The Use of High Horizontal Resolution Satellite Temperature and Moisture Profiles to Initialize a Mesoscale Numerical Weather Prediction Model -- a Severe Weather Event Case Study. J. Climate and Appl. Meteor., 22, 649-663.

Noar, P. and J. Young, 1972: The C.M.R.C. Optimized Filtered Baroclinic Model --Evaluation of the Australian Region Version Under Parallel Real Time Conditions. C.M.R.C. Int. Sci. Rep. No. 16, Melbourne, Australia, 3001.

Paltridge, G. W. and C. M. R. Platt, 1976: Radiative Processes In Meteorology and Climatology. New York, Elsevier Scientific Publishing Company, 318 pp.

Petersen, R. A., D. A. Keyser, A. Mostek, and L. W. Uccellini, 1983a: Severe Storms Analysis and Forecasting Techniques Using VAS Satellite Data. Preprint, Thirteenth Conf. on Severe Local Storms (Tulsa, OK), Amer. Meteor. Soc., J29-J32.

__________, L. W. Uccellini, A. Mostek, and D. A. Keyser, 1983b: The Use of VAS Moisture Channels in Delineating Regions With a Potential for Convective Instability. Submitted to Mon. Wea. Rev.

__________, D. A. Keyser, A. Mostek, and L. W. Uccellini, 1983c: Techniques for Diagnosing Mesoscale Phenomena Affecting Aviation Using VAS Satellite Data. Preprint, Ninth Conf. on Aerospace and Aeronautical Meteorology, Amer. Meteor. Soc., Boston, MA, 12-17.

Ray, P. S., 1986: Mesoscale Meteorology and Forecasting. Boston, MA, Amer. Meteor. Soc., 151-153.

Scofield, R. A., 1981: Satellite-Derived Rainfall Estimates for the Brady's Bend, Pennsylvania Flash Flood. Preprint, Fourth Conf. on Hydrometeorology (Reno, NV), Amer. Meteor. Soc., 188-193.

__________, 1984: The NESDIS Operational Convective Precipitation Estimation Technique. Preprint, Tenth Conf. on Weather Forecasting and Analysis (Clearwater Beach, FL), Amer. Meteor. Soc., 171-180.

__________, and V. J. Oliver, 1977: A scheme for Estimating Convective Rainfall from Satellite Imagery. NOAA Technical Memorandum NESS-86, Washington, D.C., 47 pp.

__________, and L. E. Spayd, Jr., 1984: A Technique That Uses Satellite, Radar, and Conventional Data for Analyzing and Short-Range Forecasting of Precipitation from Extratropical Cyclones. NOAA Technical Memorandum NESDIS 8, Washington, D.C., 51 pp.

Spayd, L. E., Jr., 1982: Estimating Rainfall Using Satellite Imagery for Warm-Top Thunderstorms Embedded in a Synoptic-Scale Cyclonic Circulation. Preprint, International Symposium on Hydrometeorology, American Water Resources Association, Denver, CO, 139-146.

__________, 1985: In-House Flash Flood Training Seminar, World Weather Building, Camp Springs, MD, October, 1985.

__________, and R. A. Scofield, 1984a: An Experimental Satellite-Derived Heavy Convective Rainfall Short-Range Forecasting Technique. Preprint, Tenth Conf. on Weather Forecasting and Analysis (Clearwater Beach, FL), Amer. Meteor. Soc., 400-408.

__________, and __________, 1984b: A Tropical Cyclone Precipitation Estimation Technique Using Geostationary Satellite Data. NOAA Technical Memorandum NESDIS 5, Washington, D.C., 36 pp.

Spencer, R. W., 1984: Satellite Passive Microwave Rain Rate Measurement over Croplands During Spring, Summer, and Fall. J. Climate and Appl. Meteor., 23, 1553-1562.

__________, W. S. Olson, W. Rongzhanz, D. W. Martin, J. A. Weinman and D. A. Santek, 1983a: Heavy Thunderstorms Observed Over Land by the Nimbus 7 Scanning Multichannel Microwave Radiometer. J. Climate and Appl. Meteor., 22, 1041-1046.

__________, D. W. Martin, B. B. Hinton, and J. A. Weinman, 1983b: Satellite Microwave Radiances Correlated With Rain Rates Over Land. Nature, 304, 141-143.

"Storm Data," U.S. Dept. of Commerce/NOAA/Environmental Data and Information Service/National Climatic Data Center, Asheville, N.C., Vol. 23, No. 7, July, 1981, Suomi, V. E., R. Fox, S. S. Limaye, and W. L. Smith, 1983: McIDAS III: A Modern Interactive Data Access and Analysis System. J. Climate and Appl. Meteor., 22, 766-778.

Weinman, J. A. and P. J. Guetter, 1977: Determination of Rainfall Distributions from Microwave Radiation Measured by the Nimbus 6 ESMR. J. Appl. Meteor., 16, 437-442.

APPENDIX A
MORE INFORMATION ABOUT VAS DATA USED IN JULY 20, 1981 CASE STUDY

A method developed by Chesters et al. (1983), known as the "split-window" technique, was used by Petersen et al. (1983) to derive fields of low-level moisture every hour. The technique uses the difference in radiation between two of the 12 VAS channels, both of which have their largest sensitivity at the earth's surface. In a completely dry atmosphere, they should be recording the earth's surface temperature. However, one of the channels (12.7 microns, known as the "dirty window") is significantly more attenuated by water vapor than the other channel (11.2 microns, known as the "clean window"), which is completely transparent to water vapor. Thus, the difference between the channels gives a measure of low-level moisture. Petersen also used 6.7 micron water vapor imagery, which has a peak weighting from 300-600 MB, to derive fields of mid-level moisture every hour.

By using the "split-window" technique to identify areas of low-level moisture and then overlaying them by regions of mid-level dryness, Petersen was able to identify areas of strong convective potential, since severe storms often have a mid-level dry air intrusion, and thus a large vertical moisture difference. The following examples show the type of data that were available on that day (Figure A-1). Images on the left show mid-level moisture (top) and low-level moisture (bottom). In these panels, red and yellow signals indicated dryness, while aqua and blue signals indicate increasing moisture content. Images on the right show a visible satellite photograph (top) and the vertical moisture difference (bottom). Here, red and yellow shades depict areas of large vertical moisture difference, while aqua and blue represent small vertical moisture differences. The clock on each image shows that the sequence is from 2:00 p.m. CDT to 6:00 p.m. CDT.

At both middle and lower levels, the patterns are observed to move across Kansas, Missouri, and Oklahoma towards the east, but the mid-level dryness moves slightly faster than the low-level moisture, producing conditions favorable for thunderstorm development. Note that at 2:00 p.m., deep clouds can be seen by the dark blue in the mid-level moisture over Missouri, along the leading edge of the mid-level dryness. Later in the afternoon and early evening, thunderstorms are observed also along the edge of the mid-level dryness over central Oklahoma.

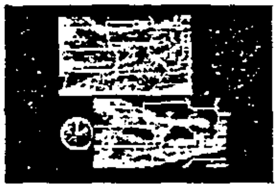

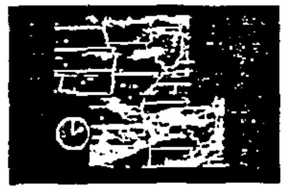

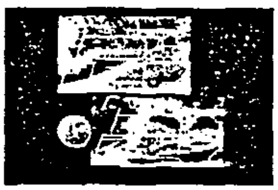

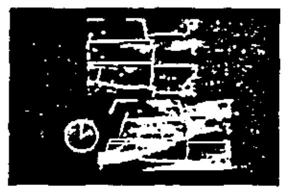

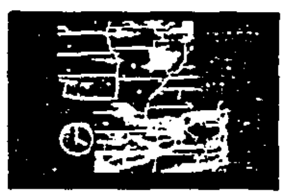

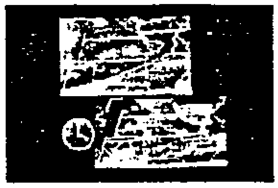

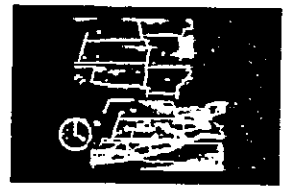

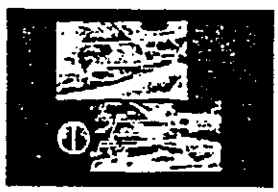

APPENDIX B
AN EXAMPLE OF THE EFFECT OF ADDING 8 AM-8 AM REPORTS KENTUCKY

Ten additional rainfall reports were gained when 8AM-8AM observations were added to the data collection in western Kentucky. These helped fill the gaps significantly.

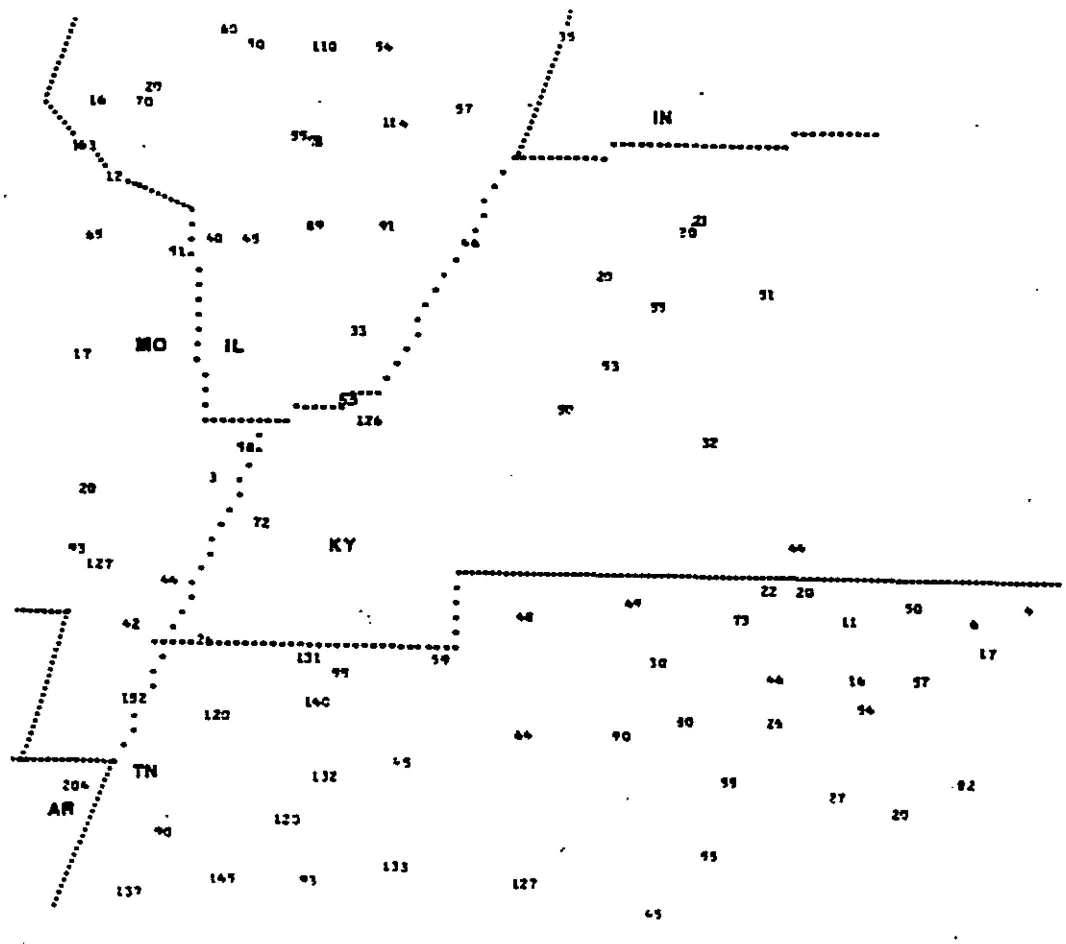

Rainfall observations in Kentucky using 7AM-7AM cooperative observer reports.

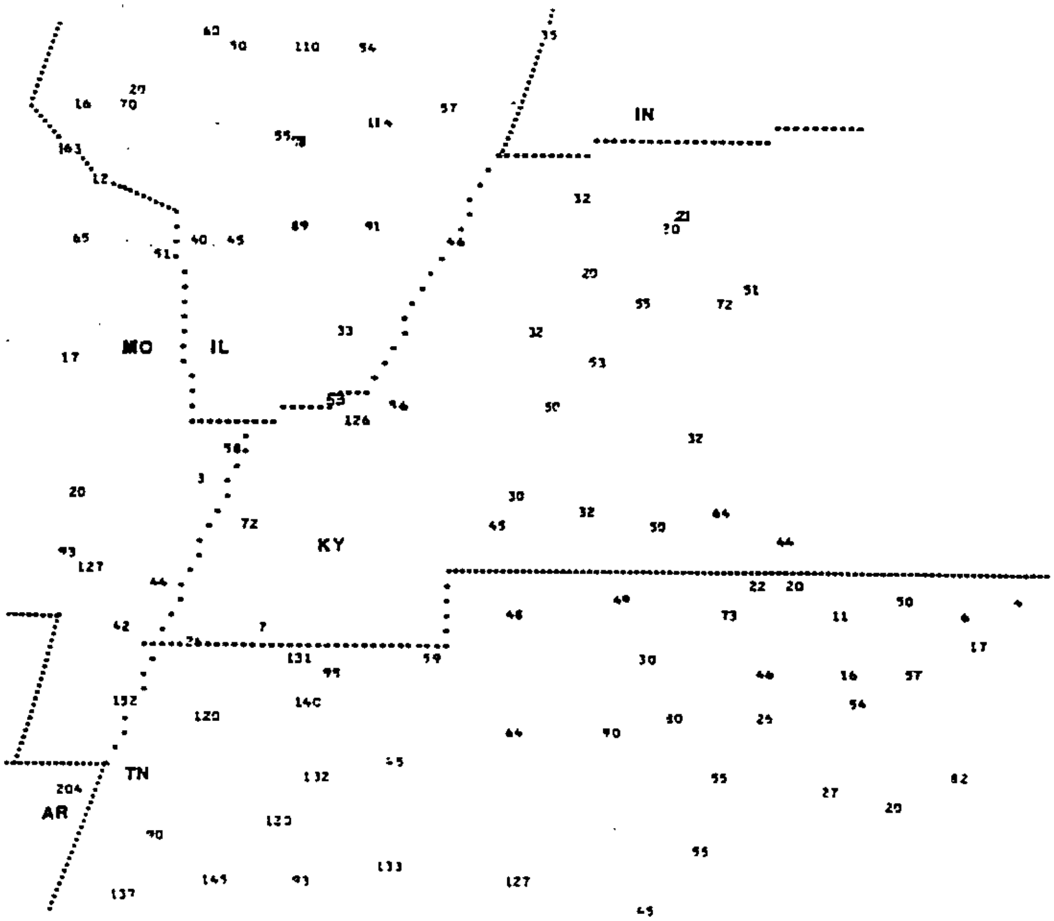

Rainfall observations in Kentucky after 8AM-8AM reports were added.

APPENDIX C
TABLES OF OBSERVED PRECIPITATION
(7 AM - 7 AM REPORTS)

ARKANSAS

STATION NAME	LATITUDE DEG.	LATITUDE MIN.	LONGITUDE DEG.	LONGITUDE MIN.	24-HR. TOTAL	SPECIFIC TIMES(if known)
Abbott	35	04	94	12	.98	
Aly	34	48	93	28	.09	
Amity 3 NE	34	17	93	25	.54	
Arkadelphia 2 N	34	09	93	03	.13	11-12Z
Arkansas City	33	37	91	12	.36	
Augusta 2 NW	35	18	91	23	.1	14-15Z
Beebe	35	04	91	54	.1	07-08Z
Benton	34	33	92	37	1.73	
Berryville 4 NW	36	24	93	37	Tr	
Big Fork	34	29	93	58	.04	
Bismarck 2 SE	34	18	93	09	.80	
Blytheville	35	55	89	54	2.04	
Bonnerdale	34	23	93	23	.60	
Booneville 3 SSE	35	06	93	55	1.92	09-12Z
Clarksville	35	29	93	27	Tr	
Conway	35	06	92	29	.21	
Corning	36	24	90	35	.16	
Crystal Valley	34	42	92	27	.42	
Danville	35	03	93	24	.35	07-09Z
Deer	35	50	93	12	.10	
Dumas	33	53	91	29	.7	10-12Z
Evening Shade 1 NNE	36	05	91	37	Tr	
Fayetteville Exp. Sta.	36	06	94	10	.1	06-07Z
Ferndale 6 E	34	46	92	27	.1	10-11Z
Fort Smith Water Plant	35	39	94	09	1.23	
Fort Smith WSO AP	35	20	94	22	.66	10-12Z
Gilbert	35	59	92	43	.02	
Gravelly 1 ESE	34	52	93	41	.15	
Greenwood	35	13	94	15	.85	
Hopper 1 E	34	22	93	40	.20	
Hot Springs 1 NNE	34	31	93	03	.90	
Huntsville	36	05	93	44	.03	
Jasper	36	01	93	11	Tr	
Jessieville	34	42	93	04	.40	
Keiser	35	41	90	05	1.70	
Leola	34	10	92	35	.15	
Marshall	35	55	92	37	.10	
Mena	34	34	94	16	.31	11-12Z
Monticello 3 SW	33	36	91	48	.10	10-11Z
Mount Ida 3 SE	34	32	93	36	.37	09-12Z
Mulberry 6 NNE	35	34	94	01	2.10	
Murfreesboro 2 NNW	34	05	93	42	.35	
Natural Dam	35	38	94	23	.09	
North Little Rock WSFO AP	34	50	92	16	1.38	07-12Z; .48"/10-11Z
Odell 3 N	35	48	94	24	.13	
Oden 1 E	34	37	93	46	.30	
Ozark	35	29	93	50	2.60	
Ozone	35	38	93	27	.12	
Parks	34	48	93	58	.25	
Pine Bluff	34	13	92	01	.65	9-10Z, 11-12Z
Pine Ridge	34	35	93	54	.30	
Piney Grove	34	11	93	12	.93	
Ratcliff	35	18	93	53	1.42	
Saint Francis	36	27	90	08	.85	
Subiaco	35	18	93	39	.15	
Waldron	34	54	94	06	.4	11-12Z
Wasnita	34	39	93	32	1.00	

ILLINOIS

STATION NAME	LATITUDE DEG.	LATITUDE MIN.	LONGITUDE DEG.	LONGITUDE MIN.	24-HR. TOTAL	SPECIFIC TIMES (if known)
Alton Dam 26	38	53	90	11	.31	
Antioch 2 NW	42	30	88	08	.05	
Argonne National Lab	41	42	87	59	.06	19-21Z
Ashley	38	20	89	12	.5	20-21Z
Aurora	41	45	88	21	Tr	
Belleville So. Ill. Univ.	38	30	89	51	.6	20-21Z
Cairo WSO CI	37	00	89	10	.58	22-00Z
Carbondale Sewage Plant	37	44	89	10	.45	
Carlyle Reservoir	38	38	89	20	.25	20-22Z
Carmi 6 NW	38	10	88	12	.57	
Casey	39	18	87	59	Tr	
Centralia 2 SW	38	31	89	10	1.19	
Channahon Dresden Isl.	41	24	88	17	.18	
Chester	37	54	89	50	.12	
Chicago O'Hare WSO AP	41	59	87	54	.04	20-21Z, 07-08Z
Chicago Midway AP 3 SW	41	44	87	46	.3	07-09Z, 10-11Z
Clay City 6 SSE	38	36	88	19	.16	
Clinton 1 SSW	40	08	88	58	.08	
Coulterville 3 NW	38	13	89	39	.2	20-21Z
Crete	41	27	87	38	.1	11-12Z
Danville Sewage Plant	40	06	87	36	.01	
Diona 3 SW	39	21	88	10	1.20	02-06Z; .52"/02-03Z
Dixon Springs Agric. Center	37	26	88	40	.33	21-00Z
Edwardsville 1 NE	38	50	89	57	.18	
Effingham 3 W	39	08	88	37	.06	21-23Z
Grafton	38	58	90	27	.86	
Grand Tower 2 N	37	40	89	31	.51	
Greenville 1 E	38	53	89	24	.38	
Harrisburg Disposal Plant	37	45	88	32	.91	mainly 21-00Z; .7"/21-22Z
Hoopeston 1 NE	40	28	87	40	.06	
Jacksonville 2 E	39	44	90	12	Tr	
Joliet Brandon Rd. Dam	41	30	88	06	.09	
Kankakee Water Pollution Ctr.	41	08	87	53	.16	21-22Z
Kaskaskia R. Nav. Lock	37	59	89	57	1.63	
Lawrenceville	38	44	87	41	.10	
Marengo	42	15	88	36	.03	
Marion 4 NNE	37	46	88	54	.89	
Mc Leansboro 2 ENE	38	06	88	30	1.14	
Morris	41	21	88	26	.01	
Morrison	41	49	89	58	.01	
Mt. Carmel	38	24	87	45	.35	22-00Z; .3"/22-23Z
Mt. Vernon 3 NE	38	21	88	52	1.10	
Murphysboro 2 SW	37	44	89	22	.4	21-22Z
Nashville 4 NE	38	23	89	20	.60	
Newton 6 SSE	38	55	88	07	.15	21-22Z
Oregon	42	00	89	20	.17	17-00Z
Pana	39	23	89	05	Tr	
Paw Paw	41	41	88	59	.13	
Peotone	41	20	87	48	.50	
Piper City 3 SE	40	48	88	08	Tr	
Pontiac	40	53	88	38	.03	
Prairie Du Rocher 1 WSW	38	05	90	07	.26	20-21Z
Rantoul	40	19	88	10	.73	
Red Bud 5 SE	38	10	89	56	.16	
Rend Lake Dam	38	02	88	59	.55	
Rochelle	41	54	89	04	Tr	
Shawneetown New Town	37	43	88	11	.46	
Sparta	38	08	89	43	.7	19-20Z
Utica Starved Rock Dam	41	19	88	59	.12	
Waterloo	38	20	90	09	.41	
Waterman 1 ESE	41	46	88	45	.26	18-20Z
Watseka 2 NW	40	47	87	46	.22	
Wayne City 1 N	38	21	88	35	.54	
West Salem	38	31	88	00	.1	21-22Z

IOWA

STATION NAME	LATITUDE DEG.	LATITUDE MIN.	LONGITUDE DEG.	LONGITUDE MIN.	24-HR. TOTAL	SPECIFIC TIMES (if known)
Algona 3 W	43	04	94	18	.21	
Ames 2 SE	42	00	93	36	.09	
Atlantic 1 NE	41	25	95	00	.1	
Bellevue Lock and Dam #12	42	16	90	25	.5	16-17Z
Cascade	42	18	91	01	.19	23-00Z
Clarion	42	44	93	45	.12	21-22Z, 23-00Z
Colo	42	01	93	20	.13	
Conrad	42	14	92	52	Tr	
Coon Rapids	41	52	94	40	.1	21-22Z
Derby	40	56	93	27	.1	20-21Z
Dubuque WSO AP	42	24	90	42	.02	01-03Z
Elkader 5 SSW	42	49	91	25	.27	
Emmetsburg	43	06	94	41	.01	
Fayette	42	50	91	48	.34	
Grundy Center	42	22	92	47	.01	
Guttenberg Lock and Dam #10	42	47	91	06	.06	
Hubbard	42	18	93	18	.93	
Iowa Falls	42	32	93	16	.1	16-17Z
Jewell	42	18	93	39	.14	
Kanawha	42	56	93	48	.07	
Killduff	41	37	92	54	.21	
Lansing	43	22	91	13	.05	
Marble Rock	42	58	92	52	.07	
Mason City	43	09	93	12	.12	
Mc Gregor	43	01	91	11	.16	21-22Z
New Hampton	43	03	92	19	.16	
Newton	41	42	93	03	.11	
Northwood	43	27	93	13	Tr	
Ocheyedan	43	25	95	32	.64	
Parkersburg	42	35	92	47	.12	
Popejoy 1 NE	42	37	93	25	.02	
Sheffield	42	54	93	13	.1	15-16Z
Spencer	43	08	95	08	.1	15-16Z
Story City	42	11	93	35	.3	21-23Z
Strawberry Point	42	41	91	32	.11	23-01Z
Traer	42	11	92	28	.35	23-07Z; .3"/23-00Z
Waterloo WSO AP	42	33	92	24	.25	22-00Z; .22"/22-23Z
Waukon	43	16	91	29	Tr	
Webster City	42	28	93	48	.21	
Williams	42	29	93	33	.05	
Zearing	42	09	93	18	Tr	

KANSAS

STATION NAME	LATITUDE DEG.	LATITUDE MIN.	LONGITUDE DEG.	LONGITUDE MIN.	24-HR. TOTAL	SPECIFIC TIMES (if known)
Alton	39	28	98	56	.21	
Atwood 12 SSE	39	38	100	57	.08	07-08Z
Auburn 1 N	38	56	95	49	Tr	
Brookville	38	46	97	52	.10	
Cawker City	39	31	98	26	.06	
Circleville 7 SW	39	26	95	56	.38	
Clifton	39	34	97	17	.06	
Covert	39	15	98	52	.01	
Ellsworth	38	43	98	14	.03	
Elmdale 10 WNW	38	25	96	50	.35	
Elmo 1 NW	38	42	97	14	.02	
Esbon 7 N	39	56	98	26	.11	
Fredonia 1 E	37	32	95	48	Tr	
Galesburg	37	28	95	21	.29	
Goessel	38	15	97	21	Tr	
Great Bend	38	21	98	46	.32	
Harlan	39	36	98	46	.13	
Hays 1 S	38	52	99	20	.04	10-11Z
Hillsboro	38	21	97	12	.07	
Hoxie	39	21	100	27	.03	
Hoyt	39	15	95	42	.30	
Iola 1 W	37	55	95	26	.13	
Kanopolis Dam	38	36	97	57	.22	11-12Z
Larned	38	11	99	06	Tr	
Lebo	38	25	95	51	Tr	
Lillis	39	36	96	20	.62	
Lincoln 1 ESE	39	02	98	07	Tr	
Loretta	38	39	99	11	.52	
Luray	39	07	98	41	.1	10-11Z
Manhattan	39	12	96	35	Tr	
Matfield Green 2 N	38	11	96	34	.05	
Mc Farland	39	03	96	14	Tr	
Mingo 5 E	39	16	100	52	Tr	
Minneapolis	39	08	97	43	.20	
Natoma	39	11	99	02	.04	
Norton Dam	39	49	99	56	Tr	
Oxford	37	16	97	09	.18	
Phillipsburg 1 SSE	39	44	99	19	.1	11-12Z
Quinter	30	04	100	14	.02	
Reading 2 N	38	33	95	57	Tr	
Saint Peter 4 ENE	39	12	100	02	.12	
Smith Center	39	47	98	47	.04	
Stillwell	38	46	94	40	Tr	
Tuttle Creek Lake	39	15	96	36	.10	18-20Z
Wakeeney 9 N	39	10	99	50	.03	
Wamego	39	13	96	18	.12	
Winkler	39	28	96	50	.09	
Worden	38	48	95	22	.03	

KENTUCKY (West)

STATION NAME	LATITUDE DEG.	LATITUDE MIN.	LONGITUDE DEG.	LONGITUDE MIN.	24-HR. TOTAL	SPECIFIC TIMES(if known)
Calhoun Lock 2	37	32	87	16	.55	
Columbus	36	46	89	07	.72	
Dundee	37	33	86	46	.51	
Dunmor	37	05	87	00	.32	
Franklin 1 E	36	43	86	34	.44	
Hartford 6 NW	37	32	86	54	.72	
Madisonville 1 SE	37	19	87	29	.53	
Owensboro 3 W	37	46	87	09	.20	
Owensboro English Pk.	37	47	87	08	.21	
Paducah Sewage Plant	37	06	88	36	1.26	
Sebree	37	36	87	32	.20	

MINNESOTA

STATION NAME	LATITUDE DEG.	LATITUDE MIN.	LONGITUDE DEG.	LONGITUDE MIN.	24-HR. TOTAL	SPECIFIC TIMES(if known)
Aitkin	46	32	93	43	.03	
Blanchard Power Station	45	52	94	21	Tr	
Brimson 1 E	47	16	91	51	.34	
Caledonia 5 SE	43	34	91	27	.25	
Cambridge St. Hospital	45	34	93	14	.1	21-22Z
Campbell	46	06	96	25	.29	
Canby	44	43	96	17	.3	01-02Z, 06-07Z
Cokato	45	05	94	12	.05	
Dodge Center	44	02	92	50	.04	12-14Z
Duluth WSO AP	46	50	92	11	1.13	16-01Z; 1.00"/18-19Z
Elgin	44	08	92	15	.34	
Elk River	45	18	93	35	Tr	
Fairmont	43	38	94	28	Tr	
Fort Ripley	46	11	94	22	Tr	
Frazee	46	44	95	43	.1	22-23Z
Hastings Dam 2	44	46	92	52	.08	
Hinckley	46	01	92	56	.84	mainly 14-20Z
Hokah 1 SW	43	45	91	23	.04	
Island Lake Reservoir	46	59	92	14	.77	
Karlstad	48	35	96	31	.09	
Lake City	44	27	92	16	Tr	
Lanesboro	43	43	91	59	.24	
Litchfield	45	07	94	32	.02	
Luverne	43	40	96	12	.62	
Meadowlands 9 S	46	59	92	44	.63	mainly 17-23Z; .42"/21-22Z
Minneapolis-St. Paul WSO AP	44	53	93	13	.32	mainly 20-22Z
Minneota	44	34	95	59	.49	
Minnesota City Dam #5	44	10	91	49	Tr	
Montevideo 1 SW	44	56	95	45	.10	
New Ulm 2 SE	44	17	94	25	.06	
Northfield 2 NNE	44	28	93	09	.1	13-14Z
North Mankato	44	10	94	02	.16	
Pokegama Dam	47	15	93	35	.37	mainly 18-19Z
Red Lake Indian Agency	47	52	95	02	.14	mainly 18-19Z
Rushford 1 SSW	43	47	91	45	.07	21-22Z
Sandy Lake Dam Libby	46	48	93	19	.2	12-13Z, 14-15Z
Springfield 1 NW	44	15	94	59	Tr	
St. Paul	44	58	93	05	.12	
Theilman	44	18	92	12	.15	
Wabasha	44	23	92	03	.17	
Wadena 3 S	46	24	95	09	Tr	
Walker Ranger Station	47	06	94	34	.1	19-20Z
Wells 1 NW	43	45	93	44	.05	
Whiteface Reservoir	47	17	92	11	.04	
Willmar State Hospital	45	08	95	01	.01	
Winona Dam 5 A	44	05	91	41	.03	
Winton Power Plant	47	56	91	46	.02	15-17Z
Worthington 2 NNE	43	39	95	35	.02	
Young America	44	47	93	55	.01	
Zumbro Falls	44	17	92	26	.65	
Zumbrota	44	18	92	40	.33	

MISSOURI

STATION NAME	LATITUDE DEG.	LATITUDE MIN.	LONGITUDE DEG.	LONGITUDE MIN.	24-HR. TOTAL	SPECIFIC TIMES (if known)
Arcadia	37	35	90	37	2.80	
Bernie	36	40	89	58	.93	
Belleview	37	41	90	44	.7	off & on; .4"/22-04Z
Bloomfield	36	53	89	56	.20	
Boonville	38	58	92	45	.07	
Brunswick	39	25	93	07	.03	
Bunker	37	27	91	13	.26	
Burlington Junction	40	27	95	04	.06	
Cap Au Gris Lock & Dam 25	39	00	90	42	.4	18-20Z
Caruthersville	36	12	89	40	1.52	
Cassville Ranger Station	36	41	93	52	.22	06-09Z
Centralia	39	13	92	08	.41	1352-1406Z
Charleston	36	55	89	21	.03	
Clarksville Lock & Dam 24	39	22	90	54	.1	13-14Z
Clinton	38	22	93	46	.1	12-13Z
Columbia WSO AP	38	49	92	13	.39	18-19Z; main storm just south of airport
De Soto	38	09	90	33	.40	
Farmington	37	47	90	23	.60	21-22Z
Fredericktown	37	34	92	37	.20	
Greenville 6 N	37	12	90	27	.87	
Hermann	38	42	91	26	1.10	
Higbee 4 S	39	15	92	30	.07	17-19Z
Jefferson Barracks 2 SW	38	29	90	20	.5	18-20Z
Jerome	37	55	91	59	.13	
Jewett 7 E	37	22	90	21	.8	21-00Z
Kennett Radio KBOA	36	13	90	04	1.85	
Marble Hill	37	18	89	58	1.17	
McCredie Exp. Station	38	57	91	54	.83	19-20Z
Mexico	39	11	91	54	.16	
Milan	40	12	93	07	.03	
Monroe City	39	39	91	44	.08	
New Florence 2	38	55	91	27	.3	18-19Z
New Madrid	36	35	89	32	.44	
Ozark	37	00	93	14	.10	
Pacific	38	30	90	44	.36	
Parma	36	37	89	49	1.27	
Perryville Water Plant	37	44	89	55	.65	
Plattsburg Waterworks	39	34	94	27	.05	
Poplar Bluff Ranger Station	36	46	90	25	.11	
Portageville	36	25	89	42	.42	
Quilin	36	36	90	15	1.01	
Reynolds	37	24	91	05	.16	
Richmond	39	20	93	58	.69	03-04Z
Richwoods	38	09	90	50	.50	19-21Z
Rosebud	38	23	91	20	.21	
Saint Charles	38	47	90	30	.71	
Saint Louis WSCMO AP	38	45	90	22	1.10	19-21Z; 1.05"/19-20Z
Saint Louis WSFO	38	48	90	34	.65	
Salem	37	38	91	32	.4	23-00Z
Steelville 2 N	38	00	91	22	.62	
Steffenville	39	58	91	53	.04	
Sullivan 10 NW	38	20	91	20	.09	19-20Z
Tarkio 1 SW	40	25	95	24	.06	
Troy	38	57	90	58	.81	
Union	38	27	91	00	.43	
Valley Park	38	33	90	29	.78	
Van Buren	36	59	91	01	1.76	
Vandalia	39	19	91	29	1.58	
Vienna 2 WNW	38	12	91	59	.07	19-00Z
Wappapello Dam	36	56	90	17	.30	00-01Z, 03-04Z
Warrenton 1 N	38	49	91	08	.48	
Washington 2	38	33	91	00	.2	19-20Z
Waverly	39	12	93	31	.10	
Wentzville	38	49	90	52	.5	19-20Z
Williamsville	36	58	90	33	.10	

NEBRASKA

STATION NAME	LATITUDE DEG.	MIN.	LONGITUDE DEG.	MIN.	24-HR. TOTAL	SPECIFIC TIMES(if known)
Amelia 2 W	42	14	98	55	.26	09-11Z
Anselmo 2 SE	41	36	99	50	.1	13-14Z
Arcadia	41	25	99	08	Tr	
Ashton	41	15	98	48	.04	11-12Z
Bartlett	41	52	98	33	.63	
Bassett	42	35	99	32	.5	08-11Z
Beatrice	40	16	96	45	.2	11-12Z
Bennington 2 NW	41	24	96	12	.20	
Bennington 3 E	41	21	96	06	.1	11-12Z
Broken Bow 2	41	24	99	38	.1	11-12Z
Broken Bow 2 W	41	25	99	41	Tr	
Chambers	42	12	98	45	.43	
Comstock	41	33	99	15	.38	
Creston	41	43	97	22	.1	11-12Z
Elgin 10 W	41	59	98	17	.11	
Ericson 6 WNW	41	48	98	47	.21	
Gavins Point Dam	42	51	97	29	.01	
Gresham 3 SSW	40	59	97	26	.02	
Hartington	42	37	97	16	Tr	
Howells	41	43	97	00	Tr	
Lynch	42	50	98	28	.25	10-12Z
Malcolm	40	55	96	52	.43	
Meadow Grove	42	02	97	44	Tr	
Neligh	42	08	98	02	.14	
Norfolk WSO AP	41	59	97	26	.10	10-12Z
North Loup	41	30	98	46	Tr	
O'Neill	42	28	98	39	.20	
Orleans 2 W	40	08	99	30	Tr	
Pawnee City	40	06	96	09	.14	
Petersburg 11 E	41	53	97	52	.15	11-12Z
Pierce	42	12	97	32	.1	11-12Z
Rose 7 WNW	42	10	99	40	.20	
Spalding	41	41	98	22	.3	11-12Z
Staplehurst 3 WNW	41	00	97	15	.50	
Surprise 1 S	41	05	97	19	.47	
Ulysses	41	04	97	12	.48	
Valentine WSO AP	42	52	100	33	.32	08-10Z
Wahoo	41	12	96	38	.50	
Wilsonville	40	06	100	06	.12	
Winside	42	10	97	10	.18	

NORTH DAKOTA

STATION NAME	LATITUDE DEG.	MIN.	LONGITUDE DEG.	MIN.	24-HR. TOTAL	SPECIFIC TIMES(if known)
Alexander 7 SE	47	49	103	32	.13	
Ashley	46	02	99	22	.2	13-14Z, 09-10Z
Beulah	47	16	101	47	.01	
Bismarck WSFO AP	46	46	100	46	.07	07-08Z
Bowbells	48	48	102	15	.63	
Columbus	48	55	102	50	.03	
Dawson	46	52	99	45	.2	08-09Z
Dickinson Exp. Station	46	53	102	48	.01	
Dunn Center 2 SW	47	21	102	39	.08	
Garrison	47	39	101	25	.35	
Glen Ullin	46	49	101	49	.1	05-06Z
Hannaford	47	19	98	11	.1	11-12Z
Hillsboro 3 N	47	27	97	04	.06	
Hurdsfield 8 SW	47	21	100	01	.44	
Lake Metigoshe St. Park	48	59	100	21	Tr	
Mandan Exp. Station	46	48	100	54	.11	07-08Z
Mc Gregor	48	36	102	56	.1	22-23Z
Minot Exp. Station	48	11	101	18	.15	07-08Z
Montpelier	46	42	98	35	.1	06-07Z
Napoleon	46	30	99	46	.44	
Oakes 2 S	46	08	98	05	.16	15-16Z, 11-12Z
Reeder 13 N	46	17	102	57	Tr	
Richardton Abbey	46	53	102	19	Tr	
Sheyenne	47	50	99	07	.1	18-19Z
Stanley 3 NNW	48	21	102	25	.45	
Towner 2 NE	48	21	100	24	.35	23-00Z
Watford City 12 E	47	48	102	59	.1	23-00Z
Wilton	47	09	100	47	.17	

OKLAHOMA

STATION NAME	LATITUDE DEG.	LATITUDE MIN.	LONGITUDE DEG.	LONGITUDE MIN.	24-HR. TOTAL	SPECIFIC TIMES(if known)
El Reno 1 N	35	33	97	58	.06	
Heavener 1 SE	34	53	94	35	.02	
Hobart 1 WSW	35	01	99	06	.1	
Inola 6 SSW	36	04	95	33	.33	mainly 00-01Z
Kansas 1 ESE	36	12	94	47	.04	
Keystone Dam	36	09	96	15	.49	mainly 23-01Z
Pawhuska	36	40	96	21	.3	07-09Z
Pawnee 5 N	36	24	96	49	.1	23-00Z
Perry	36	17	97	18	Tr	
Skiatook	36	22	96	00	.49	
Stillwell 1 NE	35	50	94	37	.37	
Stroud 1 N	35	45	96	39	Tr	
Vinita 3 NNE	36	41	95	08	.02	
Wagoner	35	58	95	22	.31	
Zoe 1 E	34	46	94	36	.09	

SOUTH DAKOTA

STATION NAME	LATITUDE DEG.	LATITUDE MIN.	LONGITUDE DEG.	LONGITUDE MIN.	24-HR. TOTAL	SPECIFIC TIMES(if known)
Aberdeen WSO AP	45	27	98	26	.02	11-12Z
Chamberlain 5 S	43	44	99	19	.24	
Cottonwood 2 E	43	58	101	52	.60	
Gettysburg 16 WSW	44	59	100	17	.1	06-07Z
Hopewell 1 SE	44	30	100	52	.12	05-08Z
Interior 3 NE	43	45	101	57	.1	05-06Z
Lake Sharpe Project	44	04	99	28	.11	07-08Z
Maurine 10 SW	44	54	102	43	.25	
Milesville 8 NE	44	32	101	34	.1	23-00Z
Mission	43	18	100	40	.30	07-10Z
Oahe Dam	44	27	100	25	.16	07-08Z
Pickstown	43	04	98	32	.2	08-10Z
Plainview 4 SSW	44	33	102	11	.3	03-04Z
Rapid City WSO AP	44	03	103	04	.06	18-19Z, 05-06Z, 08-09Z
Sioux Falls WSFO AP	43	34	96	44	.07	17-18Z
Spearfish	44	29	103	52	.03	
Wessington 5 S	44	23	98	42	.23	
Zeona 10 SSW	45	04	103	00	.2	02-03Z

TENNESSEE (West & Middle)

STATION NAME	LATITUDE DEG.	LATITUDE MIN.	LONGITUDE DEG.	LONGITUDE MIN.	24-HR. TOTAL	SPECIFIC TIMES(if known)
Ames Plantation	35	06	89	13	1.14	
Bethpage	36	29	86	19	.11	
Bolivar Water Works	35	16	88	59	1.03	02-05Z; .6"/02-03Z
Brownsville	35	35	89	15	1.45	
Brownsville Sewage Plant	35	35	89	16	1.3	01-04Z; .7"/01-02Z
Carthage	36	16	85	58	.57	00-02Z
Covington 1 W	35	34	89	40	1.39	
Dickson	36	04	87	23	.9	00-05Z; .6"/00-01Z
Drummonds	35	27	89	55	1.0	02-05Z; .5"/03-04Z
Franklin Sewage Plant	35	56	86	52	.55	
Gainesboro 3 N	36	24	85	40	.17	
Greenfield	36	10	88	47	1.4	00-02Z; 1.2"/00-01Z
Humboldt	35	49	88	56	1.2	01-03Z; .6" each hour
Jackson Exp. Sta.	35	37	88	50	.93	01-03Z; .63"/01-02Z
Kingston Springs 2 NNE	36	07	87	06	.80	
Lafayette	36	31	86	02	.50	
Lebanon 2 SE	36	11	86	15	.54	16-17Z, 00-02Z
Lebanon 7 N-Hunters Point	36	18	86	16	.16	
Lexington	35	40	88	25	1.33	
Martin U of T Branch	36	20	88	52	1.31	
Mason	35	24	89	32	1.2	02-04Z; .6" each hour
Memphis	35	12	90	02	.7	04-06Z; .6"/05-06Z
Memphis WSFO	35	03	90	00	.68	03-06Z; .32"/03-04Z; .25"/05-06Z
Milan	35	56	88	46	1.32	
Murfreesboro 5 N	35	55	86	22	.27	18-19Z, 00-01Z
Nashville WSO AP	36	07	86	41	.26	00-06Z
Neapolis Exp. Station	35	43	86	58	.55	
North Springs	36	28	85	46	.06	
Paris 5 E	36	19	88	14	.59	
Portland Sewage Plant	36	35	86	32	.2	00-03Z
Ripley	35	45	89	32	.90	
Samburg Wildlife Refuge	36	23	89	21	.26	00-02Z
Smithville 2 SE	35	57	85	47	.82	
Springfield Exp. Station	36	28	86	50	.73	23-00Z, 01-02Z; .6"/23-00Z
Union City	36	25	89	04	.07	
Waynesboro	35	18	87	46	.63	
Woodbury 1 NNW	35	50	86	05	.20	

WISCONSIN

STATION NAME	LATITUDE DEG.	LATITUDE MIN.	LONGITUDE DEG.	LONGITUDE MIN.	24-HR. TOTAL	SPECIFIC TIMES(if known)
Alma Dam 4	44	20	91	56	.42	18-19Z
Antigo 1 SSW	45	08	89	09	1.63	
Arlington Univ. Farm	43	18	89	21	.04	23-01Z
Ashland Exp. Farm	46	34	90	58	1.4	12-02Z; .8"/19-20Z
Babcock 1 WNW	44	18	90	07	.15	17-20Z
Baldwin 1 SW	44	58	92	23	.08	
Blanchardville 2	42	48	89	52	.03	
Breed 6 SSE	45	03	88	25	.14	
Buckatabon	46	01	89	19	.27	
Chippewa Falls	44	56	91	23	.1	13-14Z
Clintonville	44	37	88	45	.44	12-18Z
Coddington 1 E	44	22	89	32	.36	14-16Z
Cumberland	45	32	92	01	.13	
Danbury	46	01	92	22	.20	
Darlington	42	41	90	07	.05	
Eagle 5 N	42	57	88	27	.58	16-17Z, 20-22Z
Eagle River	45	55	89	15	.64	
Eau Pleine Reservoir	44	44	89	45	.42	13-18Z
Genoa Dam 8	43	34	91	14	.09	20-21Z
Green Bay WSO AP	44	29	88	08	.29	14-02Z
Hartford 2 W	43	19	88	24	.38	17-04Z; .27"/18-19Z
Hatfield Hydro Plant	44	24	90	44	.32	
Horicon	43	27	88	38	.23	
Lac Vieux Desert	46	08	89	08	.39	
Ladysmith Ranger Station	45	28	91	08	.1	15-16Z
La Farge	43	34	90	38	.09	19-20Z
Lancaster 4 WSW	42	50	90	47	.07	21-23Z
Lone Rock FAA AP	43	12	90	11	Tr	
Long Lake Dam	45	54	89	08	.63	
Luck	45	34	92	28	.1	16-17Z
Lynxville Dam 9	43	13	91	06	.15	
Madison WSO AP	43	08	89	20	.10	19-21Z
Mather 3 NW	44	11	90	22	.55	
Medford	45	08	90	21	.55	12-20Z; .3"/12-13Z
Mercer Ranger Station	46	10	90	04	.7	12-14Z; .6"/12-13Z
Merrill	45	11	89	41	.40	14-16Z
Milwaukee WSO AP	42	57	87	54	1.13	13-21Z; 1.07"/19-20Z
Minocqua Dam	45	53	89	44	.35	
Minong Ranger Station	46	06	91	49	.1	18-19Z
Monroe 1 W	42	36	89	40	Tr	
Kuscoda	43	12	90	26	.15	
New London	44	23	88	44	1.02	
North Pelican	45	38	89	15	.35	
Oconto 4 W	44	54	87	57	.20	
Peshtigo	45	04	87	44	.2	13-14Z, 18-19Z
Phelps Deerskin Dam	46	03	89	02	.52	13-18Z
Portage	43	32	89	26	.19	mainly 23-00Z
Prairie Du Chien	43	02	91	09	Tr	
Prentice 2	45	31	90	17	.29	mainly 12-14Z
Rainbow Reservoir	45	50	89	33	.08	
Rib Falls	44	58	89	54	.32	
Rice Lake	45	30	91	45	.2	16-18Z
Rice Reservoir	45	32	89	45	.22	13-16Z, 21-23Z
Soldiers Grove	43	24	90	47	.24	
Spirit Falls	45	27	89	58	.27	
Spooner Exp. Farm	45	49	91	53	.2	22-23Z
Stratford 2 NNW	44	50	90	05	.23	
Sturgeon Bay Exp. Farm	44	52	87	20	.44	21-00Z
Sugar Camp	45	52	89	24	.22	
Three Lakes 10 SE	45	43	89	00	.1	17-18Z
Tomah Ranger Station	44	00	90	30	.1	15-16Z
Trempealeau Dam 6	44	00	91	26	.03	
Watertown	43	11	88	44	.21	
Westby 2 NE	43	40	90	48	Tr	
White Lake 3 WNW	45	10	88	49	.2	15-17Z
Willow Reservoir	45	43	89	51	.32	
Winter 6 NNW	45	53	91	04	.80	15-17Z, 20-21Z
Wisconsin Rapids Grand Av. Br.	44	24	89	49	.02	

APPENDIX D
PLOTTED MAPS OF OBSERVED PRECIPITATION

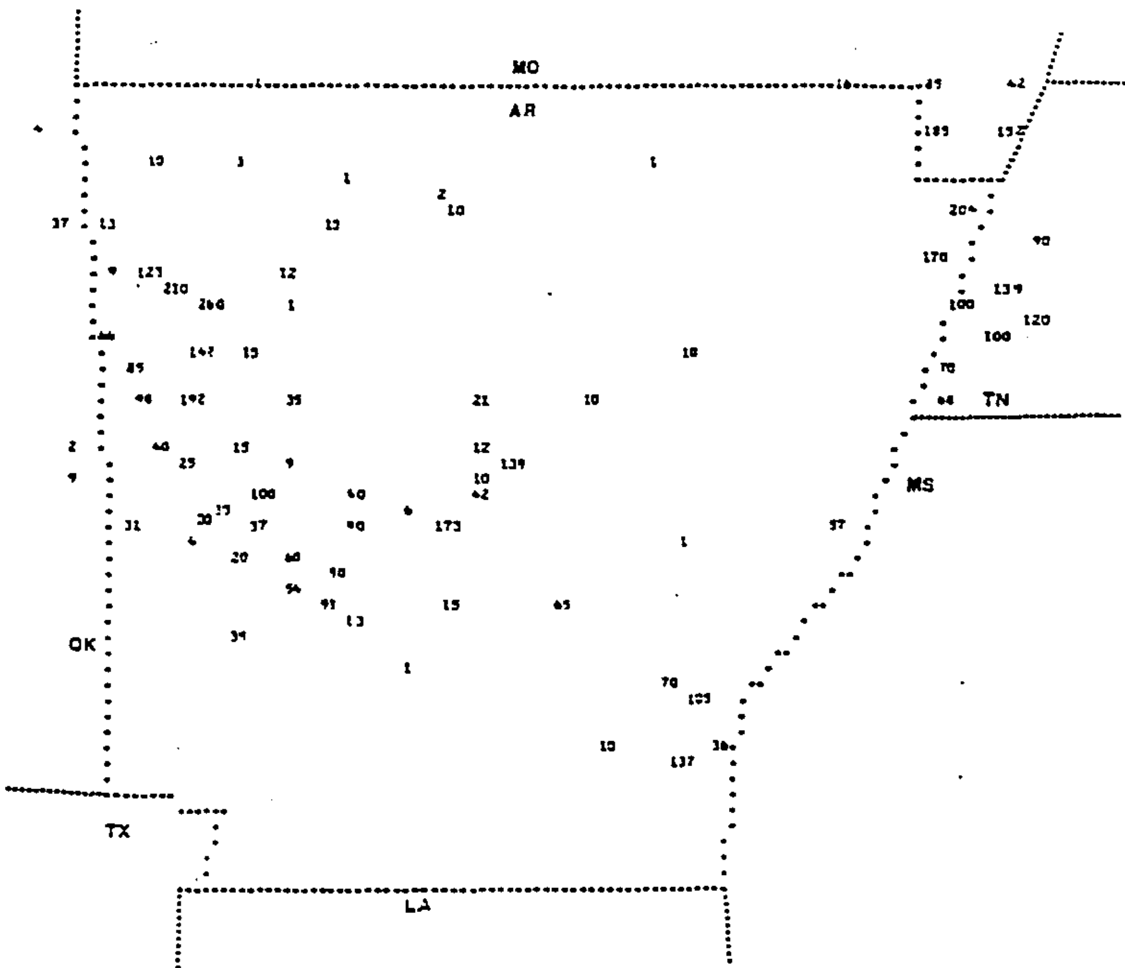

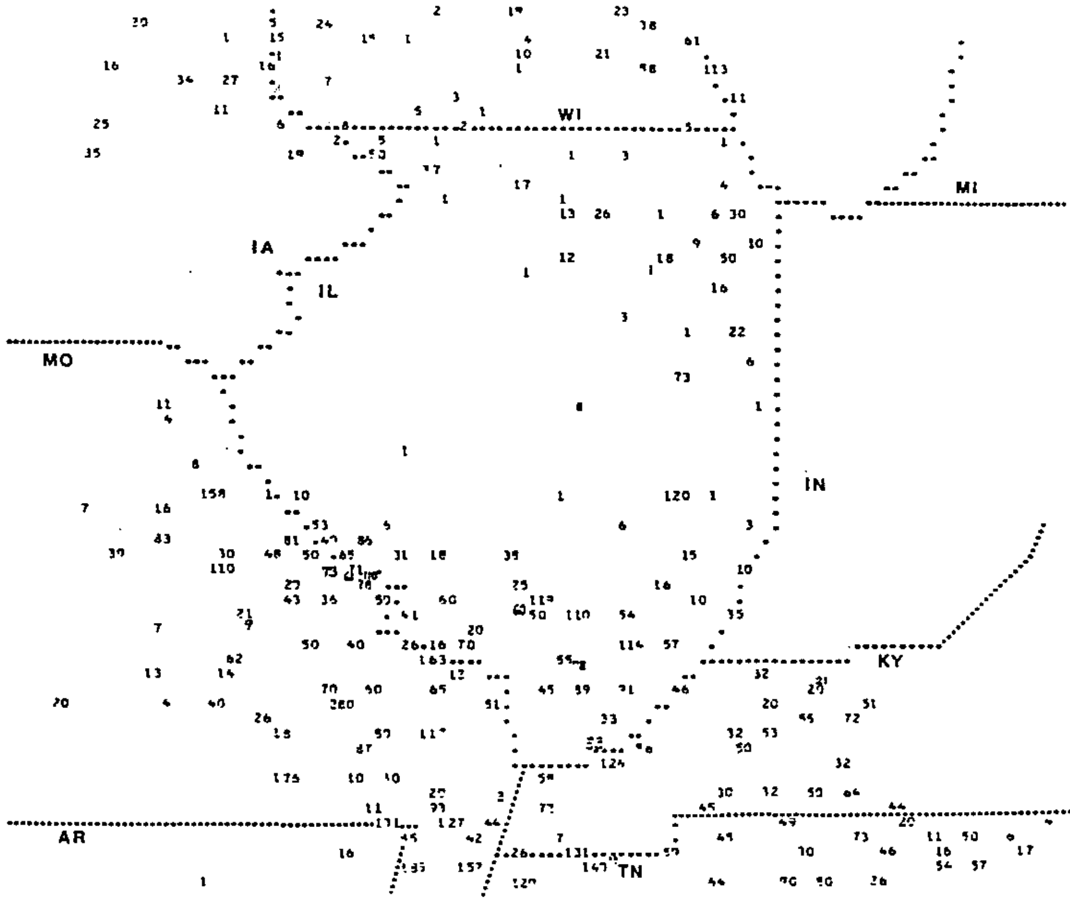
WI
MI
IA
IL
MO
IN
KY
AR
TN

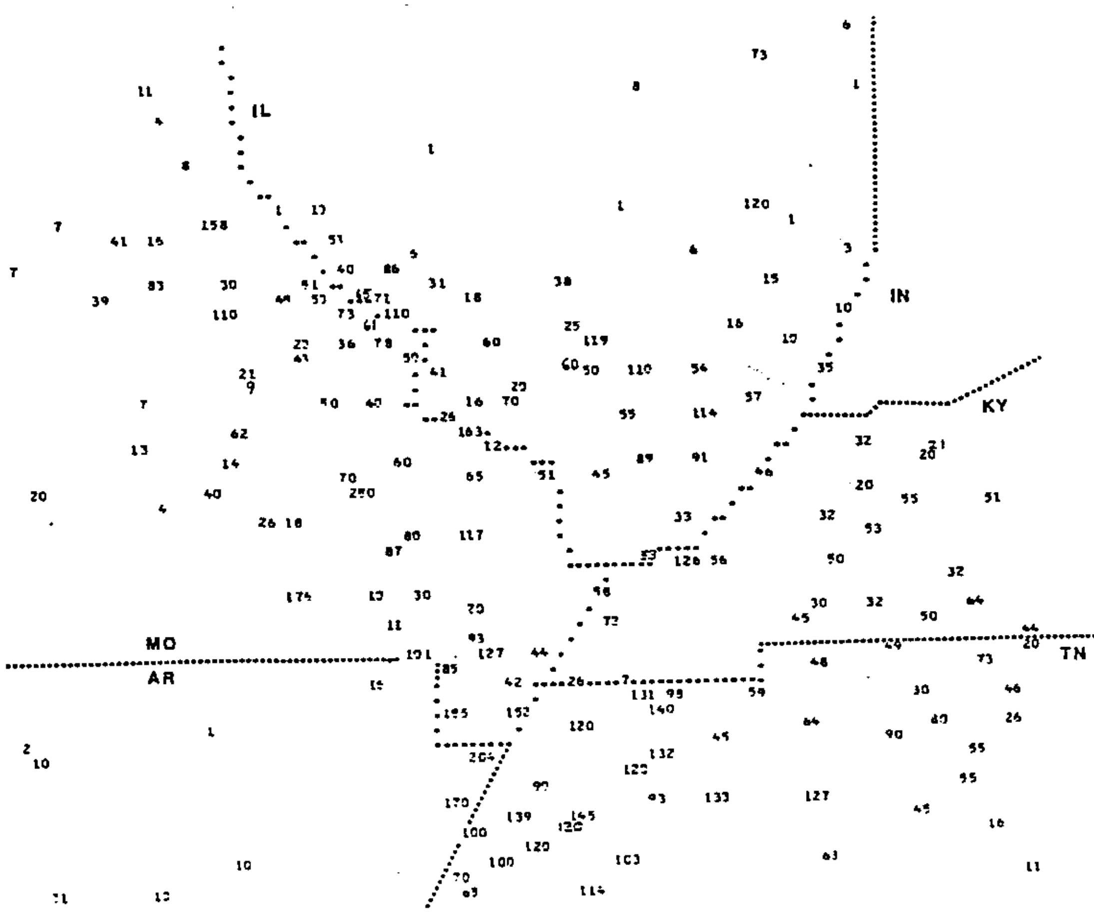
IL
IN
KY
MO
AR
TN

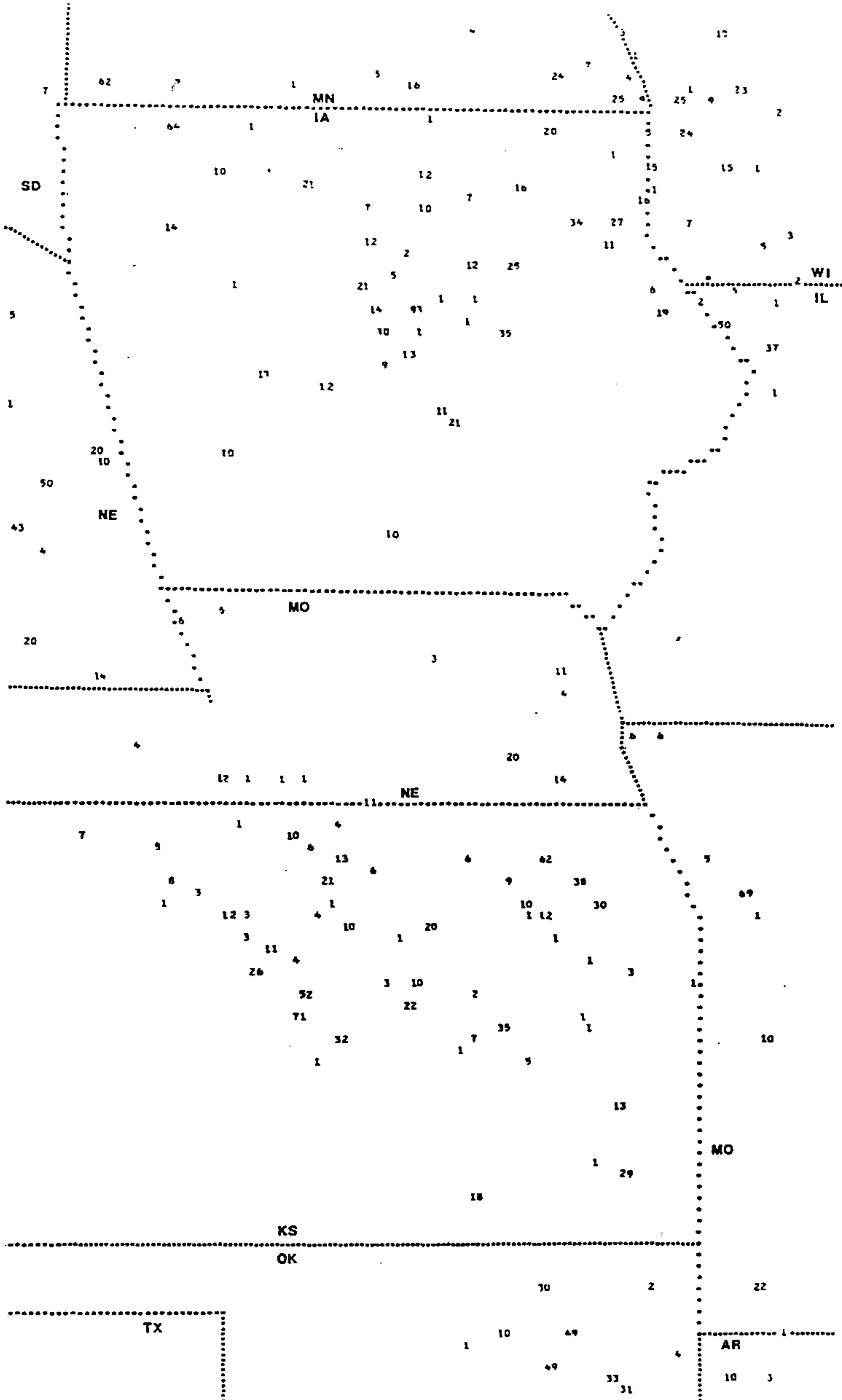
MN
IA
SD
WI
IL
NE
MO
NE
KS
OK
TX
MO
AR

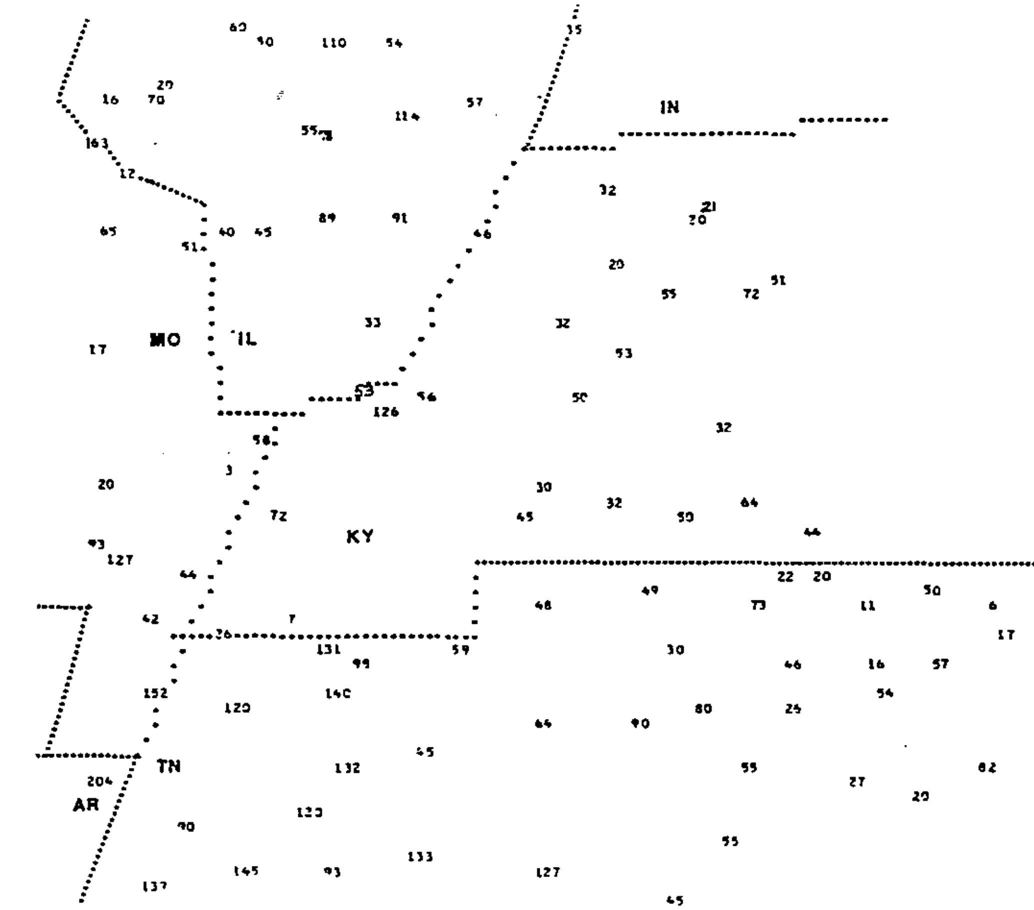
IN
MO
IL
KY
TN
AR

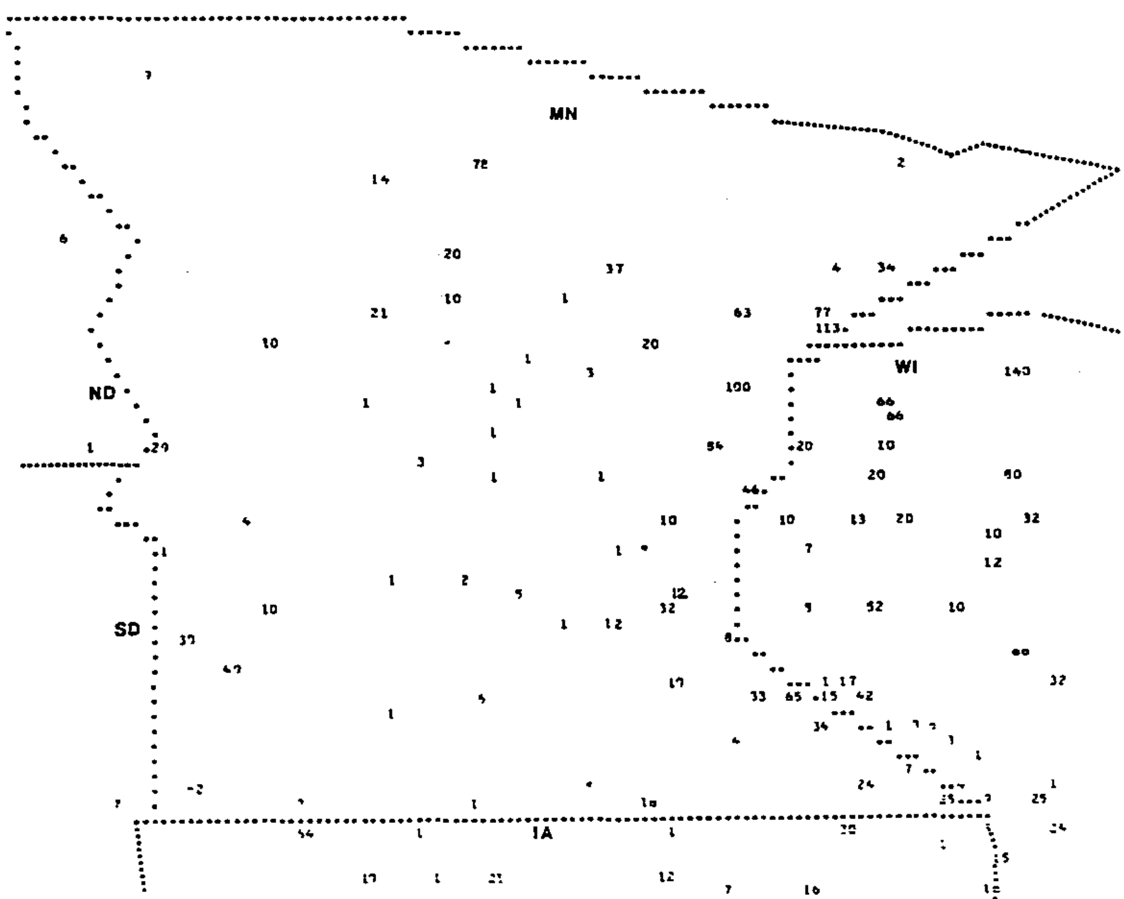
MN
WI
ND
SD
IA

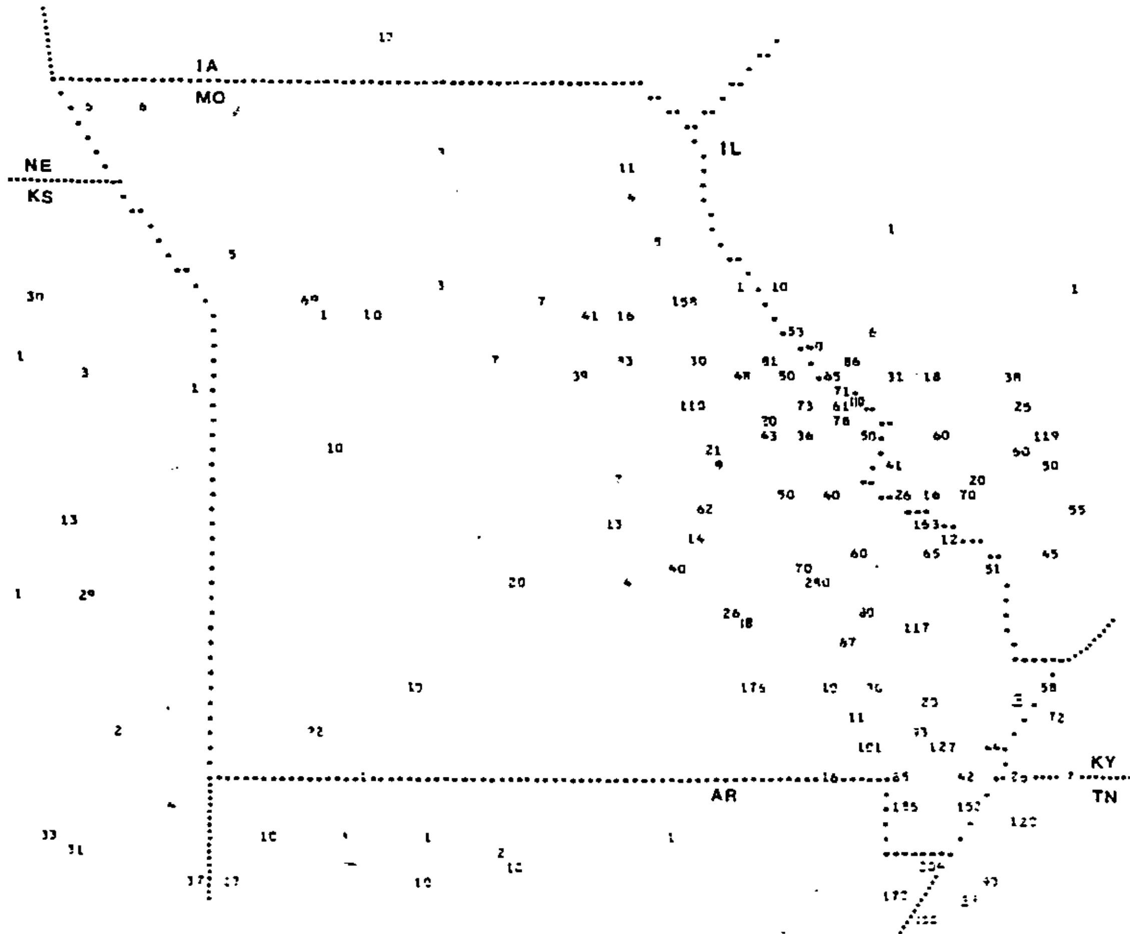
IA
MO
IL
NE
KS
AR
KY
TN

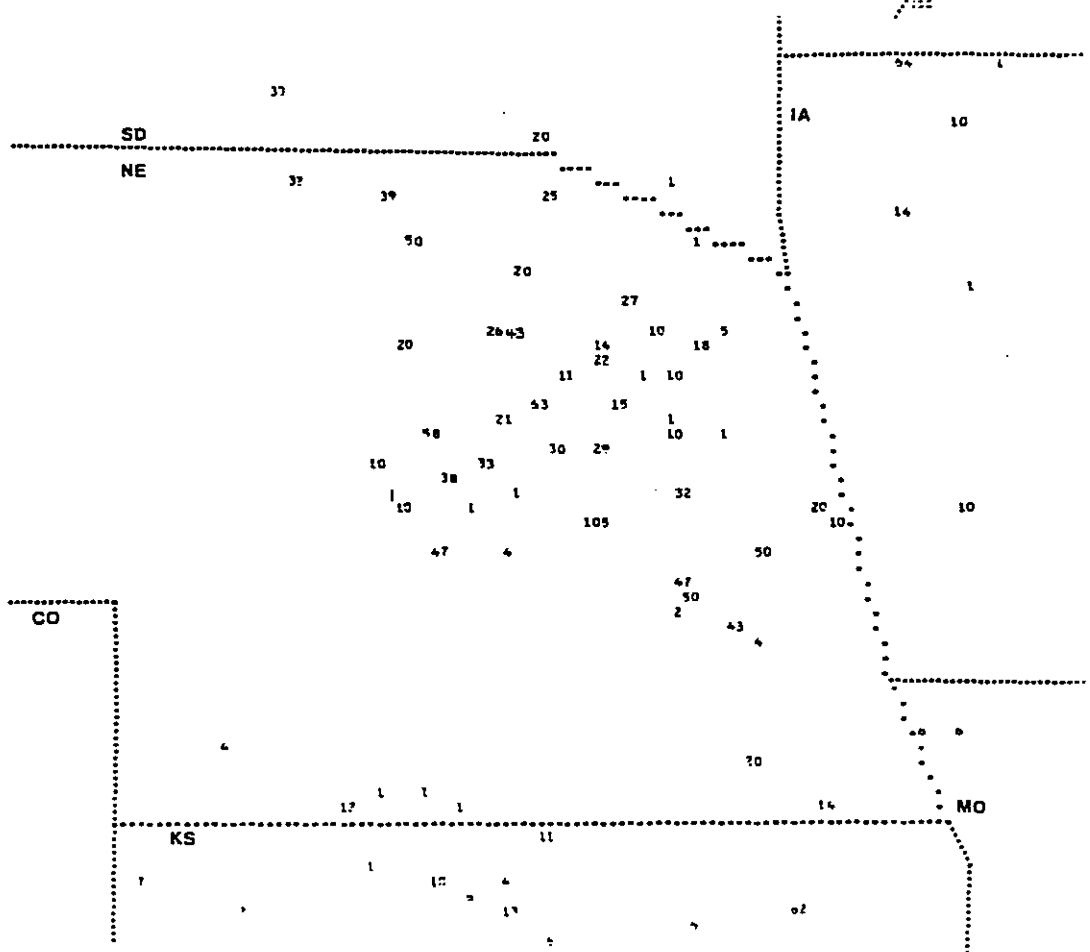
SD
NE
IA
CO
KS
MO

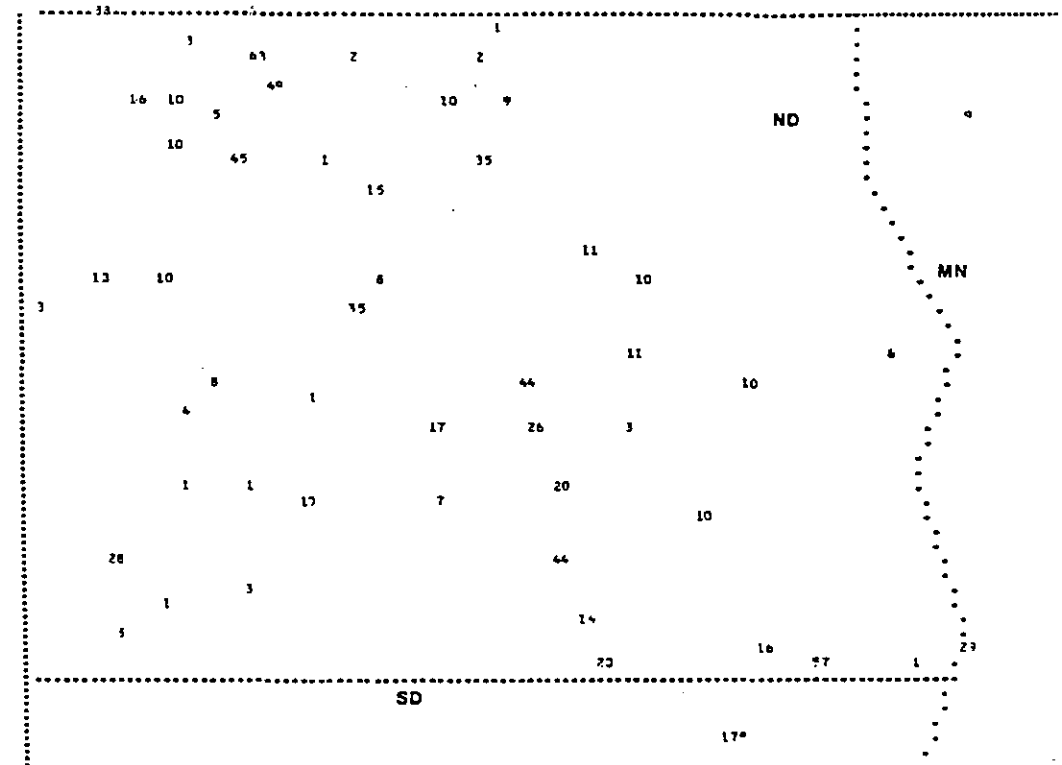
ND
MN
SD

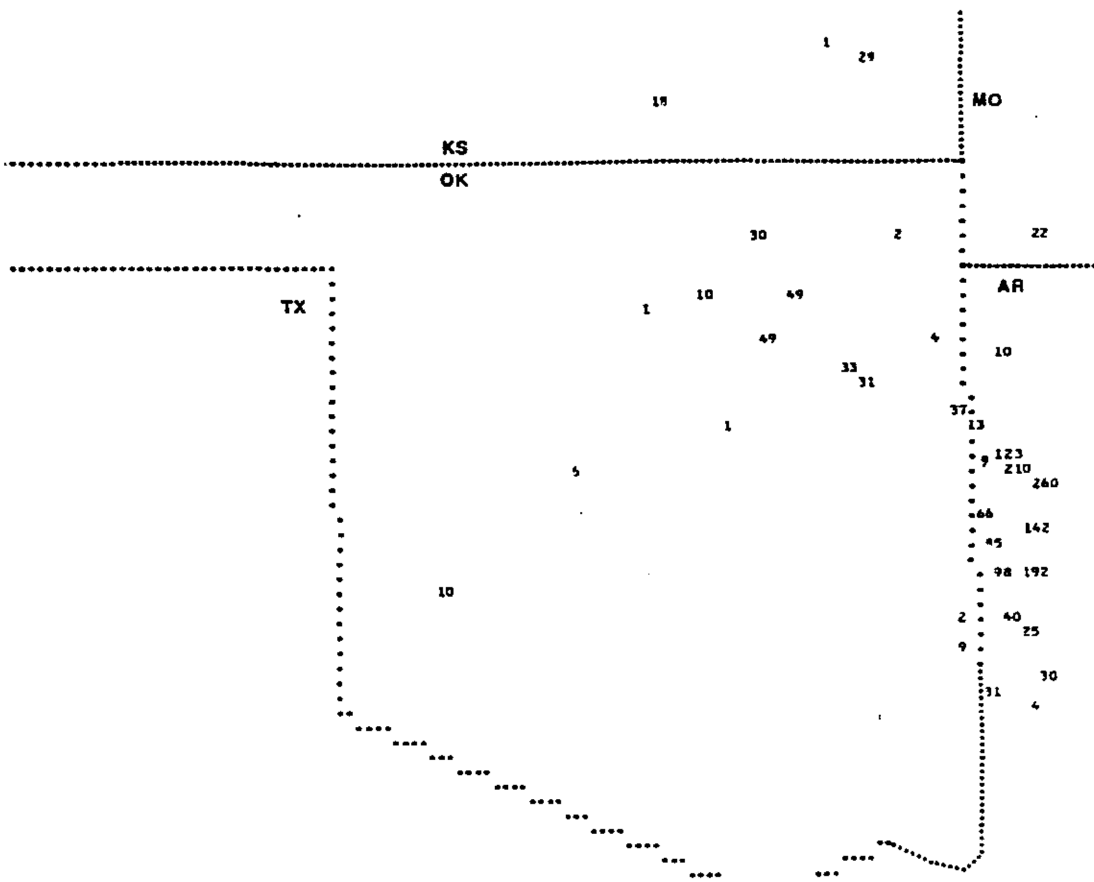
MO
KS
OK
TX
AR

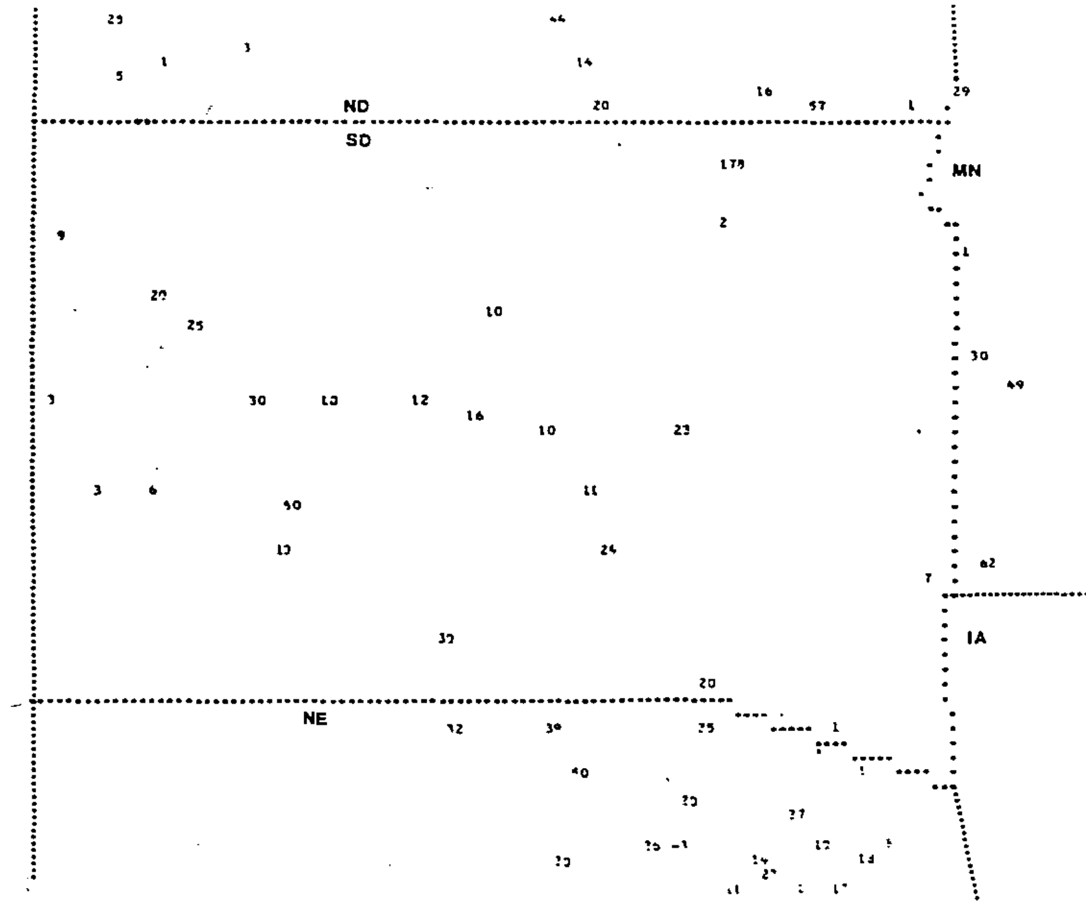
ND
SD
MN
IA
NE

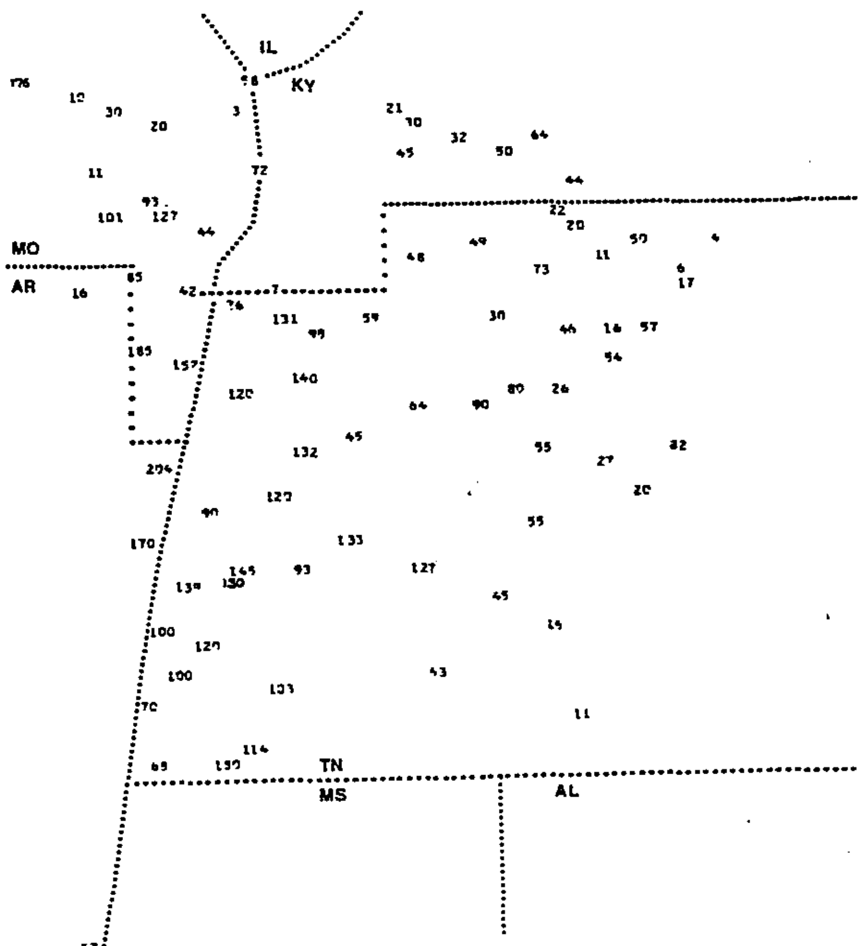
IL
KY
MO
AR
TN
MS
AL

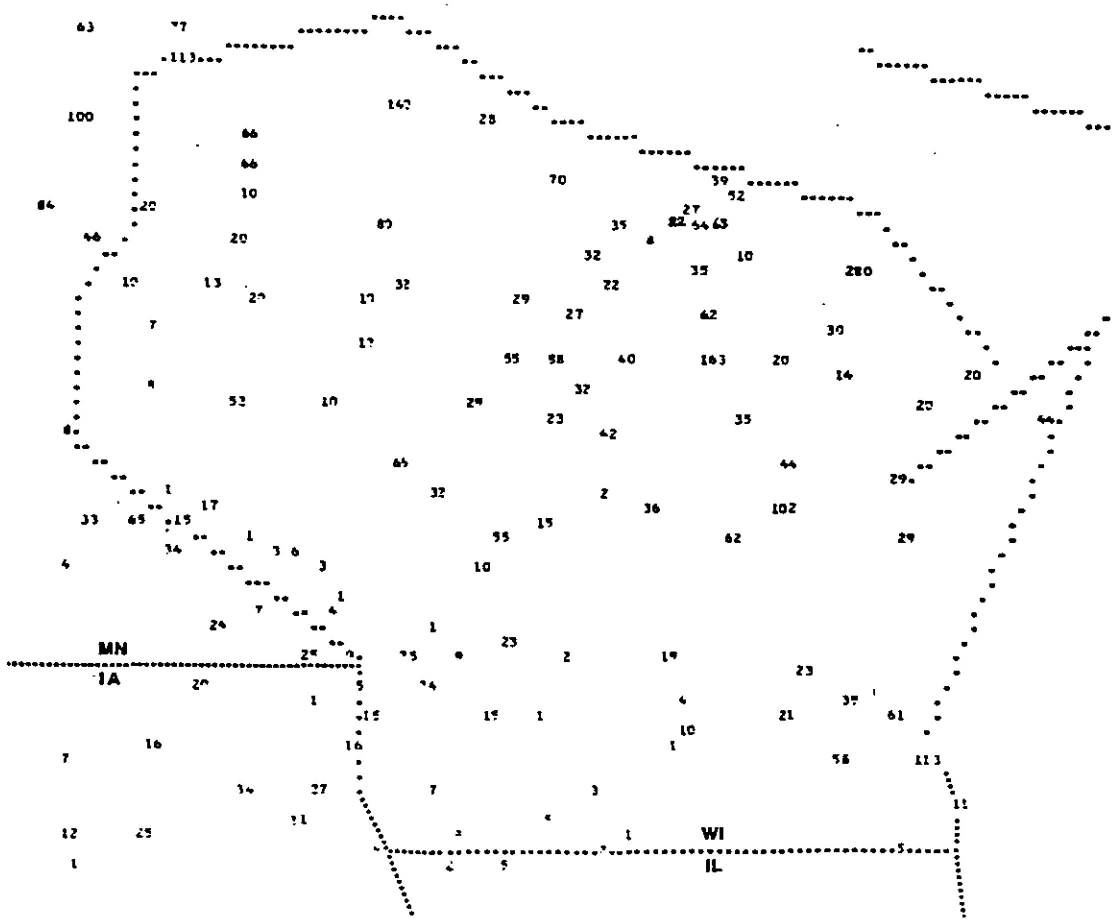
MN
IA
WI
IL